Integrated Simulation Platform Development for Connected and Automated Vehicles and Evaluation of Mixed Traffic Performance

A Dissertation

Presented to

The Faculty of the School of Engineering and Applied Science

University of Virginia

In Partial Fulfillment of the

Requirements for the Degree of

Doctor of Philosophy

By
Lian Cui

December 2018

APPROVAL SHEET

This Dissertation
is submitted in partial fulfillment of the requirements
for the degree of
Doctor of Philosophy

Author Signature: ______________________

This Dissertation has been read and approved by the examining committee:

Advisor: Byungkyu Brian Park

Committee Member: Brian Smith

Committee Member: Michael Fontaine

Committee Member: Lu Feng

Committee Member: Inki Kim

Committee Member: Cody Fleming

Accepted for the School of Engineering and Applied Science:

Craig H. Benson, School of Engineering and Applied Science

December 2018

Acknowledgements

I would like to express the most profound appreciation to my God, who loves me, has mercy on me, and leads me to go through all my studies and life.

I am grateful for my parents for supporting and motivating me for 28 years. My parents and our big family are always waiting for my phone call in a far distance. Though the connections are not frequent, I believe we still feel the love each other. I thank them for their support and care.

I appreciate my advisor, Prof. Byungkyu Brian Park, for supporting me and showing me an excellent example of a scholar. Thank him for being my advisor and guiding me to finish my doctoral program. I also give thanks to my committee, Prof. Brian Smith and Prof. Michael Fontaine in the Department of Civil and Environmental Engineering, Prof. Lu Feng in the Department of Computer Science, Prof. Inki Kim and Prof. Cody Fleming in the Department of Systems and Information Engineering for their help and suggestions on my dissertation research. Thank my collaborator Prof. Jia Hu at Tongji University, Shanghai, China for helping and encouraging me.

In addition, a thank you to dear friends, who are nearby in the US or far away in China and South Korea. I am always missing you and waiting for a chance to meet you all.

Table of Contents

Abstract

With emerging technologies of Connected and Automated Vehicles (CAV), various applications are being developed to help drivers with different driving tasks. Due to the ignorable reaction time and accurate control of CAVs, most of the transportation issues, such as traffic safety, congestion, and energy economy, are expected to be improved. In the meantime, there are public concerns regarding vehicle automation including system liability, deliberate interference, and interaction with human drivers. Therefore, this dissertation aims to assess the impacts of potential risks in CAVs and evaluate the mixed traffic performance.

However, the traditional method of evaluating the mixed traffic uses strong assumptions by simply setting different parameters, such as desired headways, for CAVs from human drivers. Therefore, an integrated simulation platform is developed for realistic modeling of CAVs and mixed traffic. With the simulation platform, this research aims to: (1) provide a realistic platform for CAVs and mixed traffic simulation; (2) quantify the safety impact of cyber-attacks to Cooperative Adaptive Cruise Control (CACC) platoon, which is the prevailing and mature CAV application; (3) improve the traditional CACC algorithm to overcome the potential risks; and (4) provide the impacts of CACC platoons in the mixed traffic flow.

Particularly, the proposed platform explicitly simulates CAVs by considering vehicle dynamics, realistic sensors, communications, and controllers, where CACC is adopted in this research. Extreme cases, i.e., different degree of cyber-attacks that are most likely to happen, are simulated. The crashes are reconstructed to quantify the injury severity using a dedicated mathematical method. Cyber-attacks do not always result in crashes, but they create large

oscillations. Even with Emergency Braking System (EBS) being implemented, some crashes caused by radar attack are avoided, since EBS heavily relies on radar. Besides, mode switches between CACC and EBS cause many control jerks and violent speed oscillations.

Considering the potential risks in the traditional CACC, a robust CACC algorithm against cyber-attack is developed. The proposed algorithm combines the advantages of all-predecessor following (APF) and predecessor-leader following (PLF) control methods to improve the stability and robustness. String stability of the proposed CACC algorithm is theoretically proven, and the performance is validated with simulation. Except for very extreme braking, which rarely happens, the proposed algorithm is capable of ensuring the robustness in various cyber-attacks without control jerk and outperforms the traditional CACC algorithm.

CACC platoons keep a short gap, i.e., 0.6s, to allow CAVs to bind together for efficient movements. However, the long and dense platoons may impede lane changing of human drivers, especially on non-basic freeway segments. Therefore, the mixed traffic on a weaving segment is simulated to explore the impact of platoons. The results reveal that the speed in mixed traffic drops more than in normal traffic (up to 27 km/h), especially with shorter desired gap, lower speed, or higher market penetration rate. Therefore, it is suggested to activate CACC mode at high speed or increase gaps when approaching weaving segments.

This research is expected to provide a powerful and useful tool for mixed traffic simulations. The pros and cons of CAVs in traffic flow-wide can be explored to help the researchers improve the algorithms for traffic system before further implementation. The platform can be enriched by adding various vehicle dynamics models and CAV controllers to be compatible with comprehensive mixed traffic simulation in the future.

List of Figures

List of Tables

Chapter 1. Introduction

1.1 Background

With emerging technologies of Connected and Automated Vehicles (CAVs), bar far, there are various applications, such as adaptive cruise control (ACC), cooperative adaptive cruise control (CACC), lane keeping control, emergency braking system (EBS), automatic parking, have been developed by many car manufacturers (i.e., Google, Toyota, Volvo, Mercedes-Benz, and so on) [1]–[4]. Those applications are designed to help the drivers with some driving tasks.

Due to the ignorable reaction time and accurate controls of CAVs, most of current traffic related issues, such as traffic congestion, motor vehicle crashes, energy economy, are expected to be solved or relieved. For example, in the aspect of traffic safety, efforts have been made to create a crash-free environment by allowing automated vehicles, where the human factors, which are the critical reasons for over 90% of crashes [5], are avoidable. By using communication devices, CAVs can utilize information from near-by vehicles to improve mobility and avoid crashes. The energy efficiency is also supposed to be improved since CAVs can have more stable trajectories and successfully achieve their speed as an energy-optimal value using the information from the infrastructures such as traffic signals and variable speed limit control system.

Therefore, besides the car manufactures, government efforts are also driving the development of CAVs. There are many funding resources, that are supported by the Federal government, for research development, and testing, covering from CAV standards to technologies and application [6]. According to HIS Markit report, more than 26% of new car sales are forecasted to be autonomous vehicles in 2040 [7]. To sum up, CAVs will play key roles in the transportation field.

However, on the other side, when new and significant technology revolutions take place, there always accompany new challenges, issues, and side effect. Therefore, when people are thinking about automated vehicles (AVs) or CAVs, many of them tend to associate with concerns [8]. The public concerns toward vehicle automation include system liability, data privacy, system performance in inclement weathers or deliberate interference, and interacting with human-driven vehicles ([8], [9]). The accidents like Google cars (now as Waymo) [10] or Tesla Model S [11] are also raising the concerns and obstacles of the public toward the automated car commercialization. Therefore, the developers, engineers, and government are trying to be aware of the potential risks, such as cyber-attack, system malfunction, for further implementation. As transportation researchers, we should focus on assessing the impact of those risks on the traffic system. For example, when communication is jammed, whether there will be a crash or not; if there is a crash, how serious is the crash and what is the impact to the upstream. Another concern – interacting with the human-driven vehicle is a timely and important challenge as well in the transportation field. As more and more CAVs travel on the roads, the mixed traffic will dominate the traffic flow in recent decades or longer. Therefore, the performance of the mixed traffic should be learned in advance to understand potential risks and enhance the applications or technologies of CAVs.

As one of the most prevailing CAV applications, CACC or automated platooning technology makes use of sensor and communication to have every vehicle in a platoon follow its preceding vehicles with a pre-defined distance or time headway [12]. The headway between vehicles can be as short as 0.6s to allow the vehicles to bind together for more sufficient movements and improve the safety of freeways ([12]–[14]). However, the long and dense platoons may impede lane changing of human drivers and bring another challenging issue, especially in the weaving, merging, or diverging segments of the freeway. Therefore, it is necessary to evaluate and quantify those mixed traffic performance to find the pros and cons of automated platooning. Even though there are more and more study groups have tested CACC in the field testbed, the scope is still far away from the mixed traffic flow.

1.2 Problem statement

In the transportation field, the most common method of evaluating traffic performance is the simulation. There are kinds of simulation tools available for the traffic flow simulation, where the behavior of each individual vehicle is modeled. The mixed traffic is usually simulated in a similar way, by setting parameters for CAVs differently from human-driven vehicles, such as short time gaps, ignorable perception-reaction time ([15]–[17]). In [18], a car-following model is derived from field test trajectories and used for estimating the capacity of mixed traffic. The behaviors of CAVs for mixed traffic are simplified with strong assumptions in existing research.

Therefore, a realistic and dedicated simulation platform is needed for assessing the mixed traffic performance. In the simulation platform, the sensor, communications, associated errors or delays, and CAV controllers should be covered and modeled properly. Then the mixed traffic flow should be evaluated with the simulation tool to explore the impact of CAVs, provide potential issues of the existing algorithms, and propose an advanced strategy.

1.3 Research objectives

Considering the limitations of existing studies, this research develops an integrated simulation platform that can explicitly simulate CAV by considering the vehicle dynamics, realistic sensors, communications, and controllers. For human-driven vehicles, some general driving behavior models, such as car following model and lane changing model, are used to represent the driving behaviors using PTV VISSIM [19]. Some extreme situations, such as cyber-attack, system malfunctions, and human-driver cut-in, are able to be simulated as well. Then with the simulation platform, the safety impact of cyber-attack to CACC platoon and the mobility of mixed traffic on the weaving segment are evaluated. In summary, the research aims to address the following tasks:

- To develop an integrated simulation platform for mixed traffic and its safety evaluation
- To assess the safety impact of CACC platoon under cyber-attack to sensors and communications
- To develop a robust CACC algorithm against cyber-attack to create a crash-free environment

- To quantitatively evaluate the performance of the mixed traffic (with CACC platoons) on the freeway weaving segment

The contributions and ultimate goals are listed as follows:

- The simulation platform can carry the most prevailing state-of-the-art CAV controllers, not limited to CACC, and any paroxysmal or extreme events, which CAVs may be exposed, to evaluate the safety performance.
- In the case of crash happens due to improper controls in CACC, the crash is reconstructed to quantify crash severity using a dedicated mathematical method. Then a robust CACC is developed to avoid the potential risks.
- The mixed traffic simulation can provide the pros and cons of traditional CAV controllers, help to improve the algorithms and optimize the controllers for mixed traffic flow in different types of freeway segments.

1.4 Dissertation organization

The rest part of this dissertation is organized as follows:

In Chapter 2, an integrated simulation platform for safety impact analysis of CAVs is presented with the case study of cyber-attack in CACC platoon. The simulation platform is proposed which explicitly features: i) vehicle dynamics; ii) sensor errors and communication delays; iii) compatibility with CACC controllers; iv) state-of-the-art predecessor leader following (PLF) based cooperative adaptive cruise control (CACC) controller; and iv) ability to quantify crash severity and CACC stability.

Based on the potential risks in the traditional CACC, Chapter 3 is introducing a robust CACC algorithm development. The proposed algorithm combines the advantage of all-predecessor following (APF) and predecessor-leader following (PLF) control methods to improve the stability and robustness of the CACC platoon under various cyber-attacks. String stability of the proposed CACC algorithm has been theoretically proven, and the performance has been evaluated in simulation.

Chapter 4 expands the focus of CACC platoons to the mixed traffic flow. By integrating the simulation platform in Chapter 2 with a microscopic transportation simulation tool VISSIM, the performance of mixed traffic on the weaving segment is evaluated. The CAVs are traveling with CACC platoons, and the lane changing of the human drivers from the on-ramp and to off-ramp is affected by the automated platoons. The platoon length, desired gap of the platoon, market penetration rate (MPR), traffic volume, and speed are studied as the sensitivity analysis factors.

Overall summary and conclusions of the research are provided in Chapter 5. Contributions and future research are presented at the end.

Chapter 2. Development of a simulation platform for safety impact analysis of CACC

2.1 Introduction

Human factors are critical reasons for over 90% of crashes according to the NHSTA [5]. Efforts have been made to reduce the number of crashes and move towards a crash-free environment. Vehicle automation is one of such efforts. Due to more accurate controls and far lower or almost negligible reaction times compared to human drivers, automated vehicles are expected to have significant contributions to transportation mobility, emissions, and safety. Currently, many auto manufacturers, such as Volvo and Tesla, have already started mass production of automated vehicles ([3], [20]).

Automated vehicles are being further enhanced through communications with infrastructure (V2I communication) and other vehicles (V2V communication). This type of vehicles is referred to as connected and automated vehicles (CAV). It is believed that vehicle automation cannot proceed and survive without connectivity [21]. A large variety of CAV applications have been developed, such as connected automated transit signal priority, eco-cruising, eco approach, and intersection control ([22]–[24]). However, the safety of CAVs is a major concern that has been holding back the wide deployment of CAVs, since communication systems which CAVs rely heavily on are subject to cyber-attacks and system malfunctions/failures. As Ploeg et al. (2011) pointed out, control algorithms of CAVs require highly reliable input information due to the tight spacing among CAV traffic [14]. Hamida et al. (2015) and Dominic et al. (2016) also stressed the vulnerability of ITS applications due to various security threats ([25], [26]). In addition, possible emergency situations should not be overlooked due to unavoidable sensor errors, communication stagnancies, and most importantly, cybersecurity threats. It is necessary to quantitatively evaluate the cybersecurity of CAVs [27]. Nevertheless, the effect of cyber-attack has not been well quantified. In addition, the accuracy of the vehicle dynamics model has been overlooked in the existing studies. It is a common practice to use a simplified driver model to simulate vehicle response. However, driver model is often overly simplified, especially in extreme cases, such as cyber-attack or vehicle malfunctions. It is important to bring in an accurate vehicle dynamics model when evaluating vehicle safety.

Among all CAV applications, CACC is one of the few applications that is closest to its final shape. Hence, a CACC safety evaluation platform is in great need for a potential real-world application. Future users can simply plug in their own vehicle controller to quantify safety under various scenarios. A unified evaluation platform also enables consistent benchmark for inter-application comparisons. To be as realistic as possible, the platform should be capable of modeling the impacts of a number of factors, which include, but not limited to, vehicle dynamics, sensor errors, and communication latencies. The platform should also be able to quantify safety using measurements, such as injury severity. To this end, a simulation platform is needed which can explicitly feature: i) modeling vehicle dynamics; ii) modeling sensor errors and communication delays; iii) compatibility with CACC controllers; and iv) ability to quantify crash severity and platoon stability.

The rest of the paper is organized as follows: Section 2.2 provides a review on existing technologies; Section 2.3 introduces the design of the proposed safety evaluation platform for CACC platoon; Section 2.4 presents a case study with CACC platoon under cyber-attack scenarios; finally, Section 2.5 provides conclusions and future plans.

2.2 Related research

The aforementioned CAV safety evaluation could be realized in two ways: field test and simulation test. Although field test can produce more trustworthy results, simulation test has its own merit. First, it is easier to replicate scenarios in simulation and generate a large sample size. Second, it is more cost-effective and feasible testing under extreme cases, as crashes are costly and dangerous for human participation. As such, all existing studies used simulations to evaluate the risk of CAV systems. Xu et al. (2014, 2015) are the only two studies that quantitatively evaluated the safety of CAV systems ([28], [29]). They both used the simulation. They made the first step in quantifying the effect of communication failure. However, their evaluation did not consider realistic vehicle dynamics model and sensor errors.

A CAV controller relies on sensors and communication devices to obtain information of surrounding vehicles. Sensors detect the relative position and speed of the preceding vehicle, and communication devices acquire other information, such as the position and speed of nearby vehicles and status of control devices. The performance and reliability of sensors and communication devices greatly affect CAV controllers. Therefore, one of the most important requirements in simulating CAV is realistic modeling of sensors and communication devices. Some existing studies have already incorporated communication delay and sensor accuracy into their CAV controller evaluation ([14], [30]–[32]). They all confirmed the necessity of modeling communication delay and sensor error in order to provide a realistic connected vehicle simulation: Naus et al. (2009, 2010) and Ploeg et al. (2011) showed that CACC platoons with communication delays perform differently ([14], [31], [32]); Peters et al. (2014) evaluated the impact of the communication delay on CACC platoons and concluded that transmission delay resulted in an unstable string state [30]; Bleek (2007) demonstrated that sensor error makes a difference in hybrid adaptive cruise control [33].

Incorporating realistic vehicle dynamics allows simulations to be complete and authentic, and is necessary for CAV simulations, as Ward et al. (1999) pointed out [34]. Typically, there are two methods of simulating CAVs: i) using an empirical CAV driver model, or ii) using a combination of a CAV controller and a vehicle dynamics model. The first method is easier in terms of implementation. However, it has limitations when it comes to evaluating abnormal scenarios under which the model has not been calibrated, such as a cyber-attack. Therefore, many studies adopted various vehicle dynamics models to overcome this challenge ([13], [30], [31], [35]–[37]). Most ACC or CACC controls adopt linearized vehicle dynamics model to simplify system analysis [12]. A relatively complete vehicle dynamics model, which is a nonlinear model with the engine, road, tire and slope resistance, was adopted in the simulation conducted by Lu et al. (2002) [37]. Naus et al. (2010) used a generic vehicle dynamics model, and Milanes et al. (2014) applied a second-order vehicle dynamics model. Both of Naus et al. (2010) and Milanes et al. (2014) showed consistency with simulation results and actual field results ([13], [31]). The studies listed above did not provide a general and systematic evaluation platform, and many of them did not consider the effect of sensor and communication failures.

Among many CAV applications, CACC is one of the few applications that is closest to its final shape. Therefore, CACC safety evaluation is selected to be the function of the proposed platform. This platform is the first stage of a series of platform development to come. In recent years, many studies have made efforts to develop various CACC control algorithms, and some were successfully tested in the field. The primary control mechanism of CACC in all studies is having every vehicle in a platoon follow its leading vehicle and preceding vehicle with a certain user predefined distance or time headway [12]. CACC control algorithms can be classified based on vehicle information flow topology and categorized into the following three groups: predecessor following (PF), predecessor-leader following (PLF) and bidirectional (BD) [36]. The PF responds only to its adjacent vehicles using sensor information. Seiler et al. (2004) have demonstrated that PF is weak in string stability. Even small turbulence on one vehicle can be amplified along the platoon and cause large oscillations [38]. Compared to PF, PLF is more stable [12]. On top of the information from the preceding vehicle, PLF also uses information from the leading vehicle. This approach has been validated in the field ([13], [39]). PLF is the control structure used by California PATH [13], which developed the most prevailing state-of-the-art CACC controller. In this study, the PATH model is used.

Measurement of Effectiveness (MOE) of a CACC safety evaluation platform requires further development. In the past, safety assessments in transportation simulations commonly adopt the Surrogate Safety Assessment Model (SSAM) to measure the severity of traffic crashes or conflicts [40]. MOEs, such as time to collision (TTC) and Delta-V (speed difference between two conflict vehicles), can be measured using SSAM. However, the aforementioned MOEs only provide probabilities of crashes, without crash severity. For those MOEs remotely related to severity, their estimation is rough and lacks generality. One good example is TTC. TTC uses time distance to estimate the crash probability, therefore is only applicable for rear-end or head-on crashes, not for angular crashes. Hence, a more advanced and general safety assessment measurements should be adopted which consider the physical characteristics of vehicles and occupants ([41], [42]). Finite element computer solver could be used to acquire more accurate crash severity [43].

In sum, this research proposes an integrated simulation platform for CACC safety evaluation. The simulation platform has the following features:

- Provides a consistent benchmark for various CAV applications
- Models vehicle dynamics
- Incorporates the effect of sensor error and communication delay
- Quantifies crash severity and CACC stability
- Is compatible with any CACC controller types
- Carries the most prevailing State-of-the-art CACC controller

2.3 CACC safety evaluation platform design

In this section, the proposed integrated simulation evaluation platform for CACC is presented. Figure 1 shows the structure of the platform. The entire simulation platform consists of two major parts, Connected Automated Vehicle Simulation and Injury Severity Quantification. The CACC simulation component is in nature a software in the loop simulation. It is designed to fully replicate the real world. It carries multiple software, including sensors and communication simulators, CACC controller, and vehicle dynamics simulator. In this proposed evaluation platform, instead of feeding vehicle state directly into a CACC controller, vehicle state is “collected” by simulated sensors with potential sensor errors/failures and transmitted among vehicles with chances of communication packet drops. The CACC control module can carry any controller of interest. It takes in vehicle state and outputs command to the vehicle dynamics model. Vehicle dynamics model uses real vehicle state together with commands from the CACC controller to produce real vehicle state for the next time step. The incorporation of vehicle dynamics model enables the simulation of response delay and imperfect executions. The injury severity quantification component estimates crash severity based on the crash data extracted from the CAV simulation component. Using the extracted crash data, the vehicle crash trajectory is computed using classic physics and is used as an input into a finite element computer solver in order to acquire crash severity. In addition, a commercially validated human dummy model and vehicle equipment models (e.g., the seatbelt) are adopted to quantify the injury severity of human on board. Details about each component of the proposed platform are discussed in the following subsections. The indices and parameters used in this section are listed in Table 1.

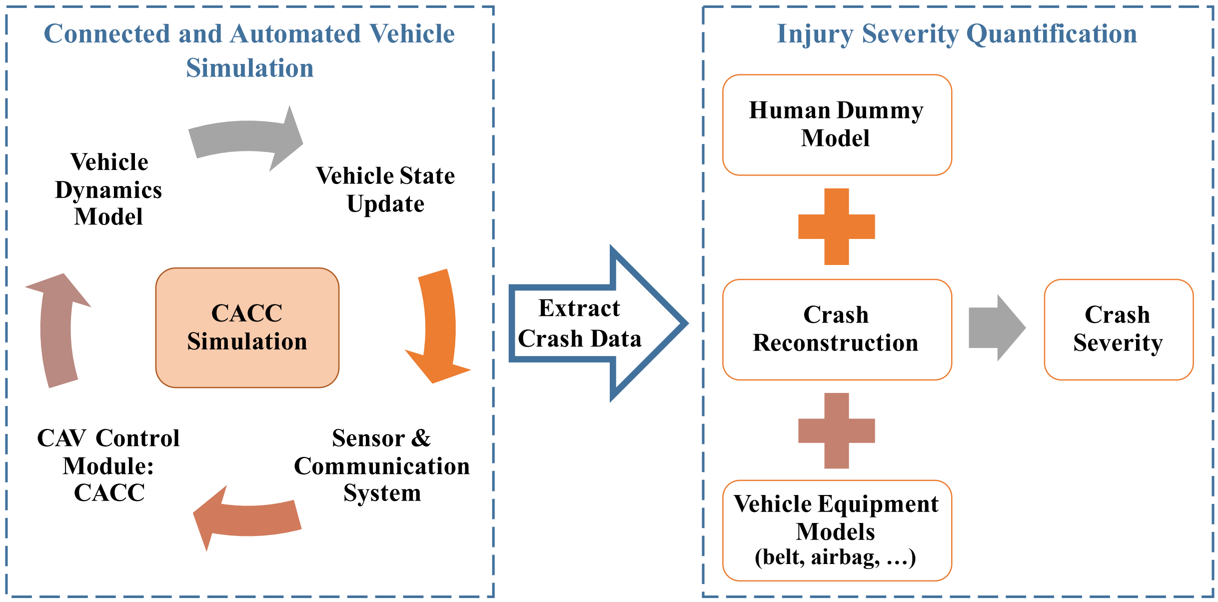

Figure 1 Simulation Platform for CACC Safety Evaluation

Table 1 Indices and Parameters

Name	Explanation
$\boldsymbol{C}$	Constant
$\boldsymbol{C_C}$	Slip factor
$\boldsymbol{D}$	Clutch diameter (unit: m)
$\boldsymbol{D_{max}}$	Maximum deflection during crash
$\boldsymbol{d(t)}$	True distance from the preceding vehicle at time t (unit: m)
$\boldsymbol{d_R(t)}$	Measured distance from the preceding vehicle at time t (unit: m)
$\boldsymbol{d_{braking}(t)}$	Threshold of braking distance in emergency braking system (unit: m)
$\boldsymbol{e(t)_i}$	Total error term
$\boldsymbol{e_P(t)_i}$	Total error of the ego-vehicle relative to the preceding vehicle
$\boldsymbol{e_L(t)_i}$	Total error of the ego-vehicle relative to the leading vehicle

$e_{vP}(t)_i$	Velocity error of the ego-vehicle compared to the preceding vehicle (unit: m/s)
$e_{vL}(t)_i$	Velocity error of the ego-vehicle compared to the leading vehicle (unit: m/s)
$e_{sP}(t)_i$	Spacing error of the ego-vehicle compared to the preceding vehicle (unit: m)
$e_{sL}(t)_i$	Spacing error of the ego-vehicle compared to the leading vehicle (unit: m)
F	Femur force during crash (unit: kN)
F_z, F_{int}	Axial load on the spine and the corresponding tolerance load of the dummies
HIC	Head injury criterion
i	Normal vehicle index (ego-vehicle)
j	Crashed vehicle index
K_P, K_I, K_D	Constant gains for PID control (lower level control)
K_{PP}, K_{IP}	Constant gains for PI control (upper level control) with respect to the preceding vehicle
K_{PL}, K_{IL}	Constant gains for PI control (upper level control) with respect to the leading vehicle
m_j	Vehicle mass of crashed vehicle i (unit: kg)
M_y, M_{int}	Flexion/extension bending moment at the occipital condyles and the corresponding tolerance load of the dummies
n_g	Transmission ratio of gear box
n_d	Transmission ratio of differential
Nij	Neck injury criterion
P_e	Engine power (unit: kW)
P_M	Maximum engine power (unit: kW)
R_g	Geometric tire radius (unit: m)
R_w	Effective tire radius (unit: m)
R_{min}	Minimum distance of emergency braking system (unit: m)

$\boldsymbol{t_1, t_2}$	Two arbitrary times during the duration of the crash, usually $t_2 - t_1 \leq 15ms$
$\boldsymbol{T_e}$	Torque (unit: rpm)
$\boldsymbol{u(t)}$	Control variable (throttle/brake)
$\boldsymbol{v(t)}$	Longitudinal velocity (unit: m/s)
$\boldsymbol{v_D(t)}$	Desired speed (unit: m/s)
$\boldsymbol{v_R(t)}$	Measured speed of the preceding vehicle at time t (unit: m/s)
$\boldsymbol{v_T(t)}$	Target speed of CACC platoon (unit: m/s)
$\boldsymbol{v_j}$	Pre-crash speed of crashed vehicle i (unit: m/s)
$\boldsymbol{v_j'}$	Post-crash speed of crashed vehicle i (unit: m/s)
$\boldsymbol{\Delta v}$	Delta-v, speed change between pre-crash and post-crash (unit: m/s)
$\boldsymbol{\alpha_1, \alpha_2}$	Maximum deceleration rates of preceding vehicle and ego-vehicle (unit: m/s^2)
$\boldsymbol{\rho}$	Oil density (unit: kg/m^3)
$\boldsymbol{\sigma_R}$	Standard deviation of radar error (unit: m)
$\boldsymbol{\sigma_{GPS}}$	Standard deviation of GPS error (unit: m)
$\boldsymbol{\tau}$	Delay time that considered in emergency braking system (unit: s)
$\boldsymbol{\omega_e}$	Engine velocity (unit: rpm)
$\boldsymbol{\omega_M}$	Maximum engine velocity (unit: rpm)
$\boldsymbol{\omega_P}$	Pump angular velocity (unit: rad/s)
$\boldsymbol{\omega_w}$	Angular velocity of tire (unit: rad/s)

2.3.1 Connected automated vehicle simulation

2.3.1.1 Sensors and communication simulator

Sensors and communication system simulates vehicle state to produce input for CACC controller, as shown in Figure 1. The proposed platform is for a typical CACC system, where sensors and communication system incorporated are radar sensors, a global positioning system (GPS) and Dedicated Short Range Communication (DSRC) devices. Radar sensors measure the distance between the subject vehicle and its preceding vehicle; GPS provides the location of other adjacent vehicles while DSRC devices are utilized to pass on the adjacent vehicles' and control devices' information via Basic Safety Message (BSM) [44]. In this proposed simulation platform, sensor errors and communication delays are considered as follows:

Radar error follows the standard normal distribution in distance detection ([14], [31], [32]):

$$\begin{gathered} d_R(t) = d(t) + \varepsilon_R, \qquad \forall\, t \in [0, T] \\ \nu_R(t) = \frac{\partial}{\partial t} d_R(t), \qquad \forall\, t \in [0, T] \\ \varepsilon_R(x) = \frac{1}{\sqrt{2\pi{\sigma_R}^2}} e^{-\frac{x^2}{2{\sigma_R}^2}} \end{gathered} \tag{2.1}$$

where $d_R(t)$ is the measured distance at time *t*, $d(t)$ is the true distance at time *t*, $\nu_R(t)$ is the measured relative speed to the preceding vehicle at time *t*, and σ_R is the standard deviation of radar error. The relative speed is estimated as the derivative of detected distance. Thus, its noise is mainly affected by radar sensor noise.

GPS error follows the standard normal distribution [45]:

$$\varepsilon_{GPS}(x) = \frac{1}{\sqrt{2\pi{\sigma_{GPS}}^2}} e^{-\frac{x^2}{2{\sigma_{GPS}}^2}} \tag{2.2}$$

where σ_{GPS} is the standard deviation of GPS which is a device specified information.

DSRC communication follows the standard set by the Society of Automotive Engineers (J2735) [46]. Constant communication delay in DSRC is adopted [47]:

$$D_C = C \tag{2.3}$$

where C is a user predefined constant.

2.3.1.2 Vehicle dynamics model

In the proposed platform, response delay and imperfect executions of vehicle mechanical system are simulated using the vehicle dynamics model (VDM) developed by [48]. This VDM is extended from a bicycle model with roll dynamics, which is applied for the advanced driver assistant systems research ([49]–[51]). The overall structure of the vehicle dynamics model is shown in Figure 2, which considers the gearshift table, engine model, torque transmission and chassis model. Detailed formulation related to each block in Figure 2 is given in the following:

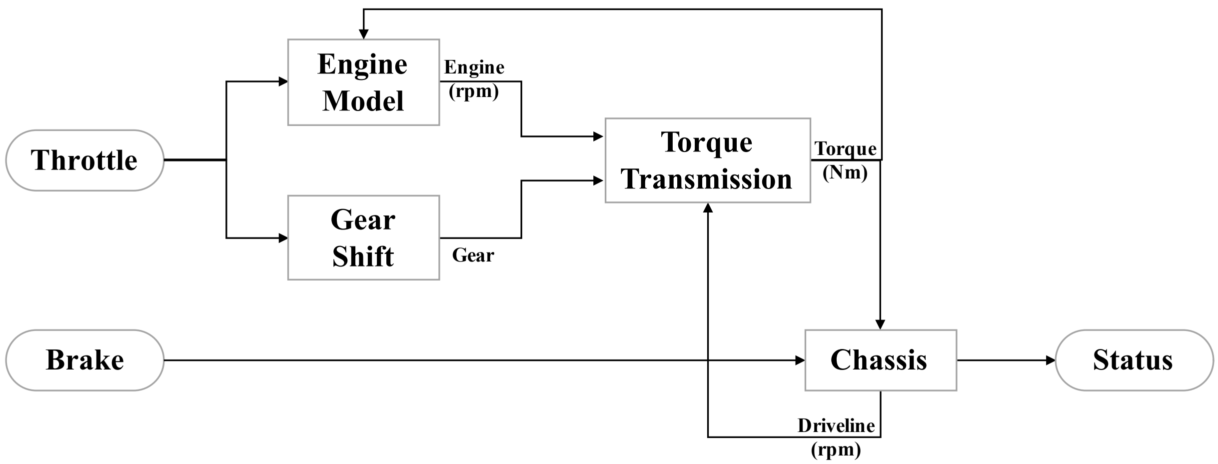

Figure 2 Vehicle Dynamics Model Structure

For gear shift block, a user pre-defined gear shift schedule is used to determine gear position based on speed and throttle level. Shift schedule varies by vehicle.

In the engine model block, a first-order response model is adopted:

$$F(s) = \frac{k}{s + 2\theta\omega_n} e^{-T_d s} \tag{2.4}$$

where, k is the static gain; θ is the damping factor; ω_n is natural frequency; T_d is the time delay.

The angular velocity of the engine may be calculated from the engine power equation:

$$P_e = \frac{P_M}{\omega_M}\omega_e + \frac{P_M}{{\omega_M}^2}{\omega_e}^2 + \frac{P_M}{{\omega_M}^3}{\omega_e}^3 \tag{2.5}$$

where, R_g is the tire's geometric radius; ω_w and ω_e are the angular velocity of tire and engine, respectively; P_M and ω_M are maximum power and maximum engine angular velocity, respectively, when the throttle is wide open. The power is provided by the engine torque:

$$T_e = \frac{P_e}{\omega_e} \tag{2.6}$$

Torque transmission module inputs engine speed and gear position to calculate torque:

$$T_e = C_C \rho \omega_P^2 D^2 \tag{2.7}$$

where, C_C is slip factor, ρ is oil density, ω_P is the pump angular velocity, and D is the clutch diameter.

In the chassis model, the longitudinal velocity of a vehicle is calculated:

$$v = \frac{R_w \omega_e}{n_g n_d} \tag{2.8}$$

where, R_w is the tire's effective radius; ω_e is the angular velocity of the engine; n_g and n_d are the transmission ratios of the gearbox and differential, respectively.

2.3.2 CACC controller formulation

CACC Control Algorithm: As a showcase of CAV controller, CACC is modeled in the proposed simulation platform. A CACC control algorithm utilizing a bi-level control approach (shown in Figure 3) is adopted [13]. The upper-level PD controller is a headway regulator which takes in the information of the preceding vehicle and the leading vehicle to calculate desired speed; the lower level PID controller changes throttle and brake to match vehicle speed to desired speed.

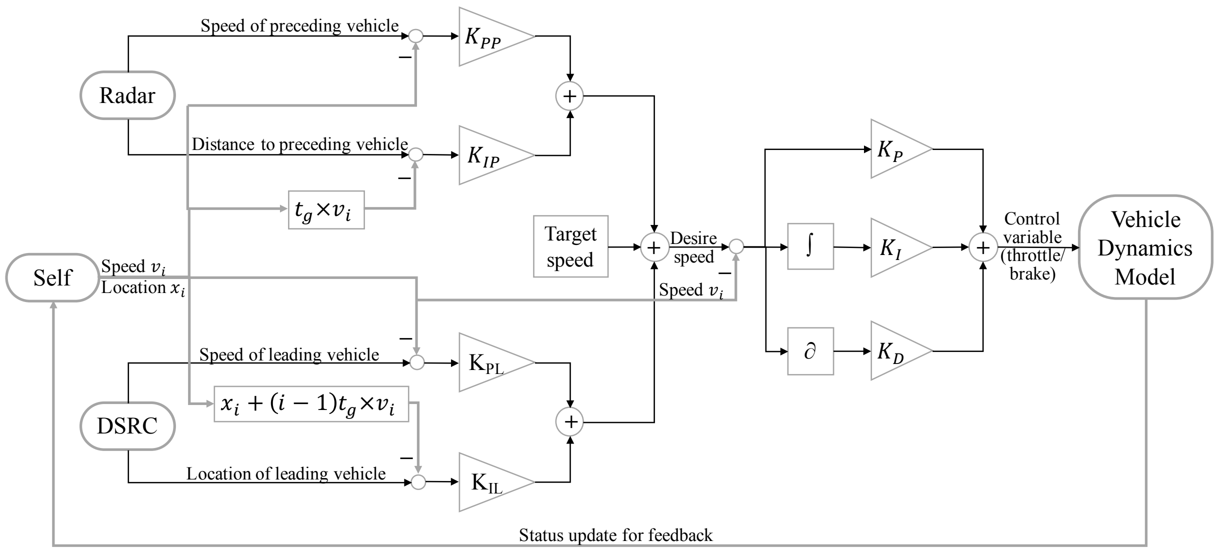

Figure 3 CACC Vehicle Control Structure

The controller can be formulated as follows:

The lower-level control law:

$$u(t)_i = K_P e(t)_i + K_I \int_0^t e(\tau)_i d\tau + K_D \frac{de(t)_i}{dt}, \qquad \forall\, t \in [0, T] \tag{2.9}$$

where $u(t)_i$ is throttle/brake of vehicle i. The error term $e(t)_i$ is the difference between desired speed and actual speed:

$$e(t)_i = v_{D-i}(t) - v_i(t), \qquad \forall\, t \in [0, T] \tag{2.10}$$

The desired speed of vehicle i is:

$$v_{D-i}(t) = \begin{cases} v_T(t), & (i = 1) \\ v_T(t) + e_P(t)_i + e_L(t)_i, & (i > 1) \end{cases}, \qquad \forall\, t \in [0, T] \tag{2.11}$$

The errors relative to the preceding vehicle ($e_P(t)_i$) and the leading vehicle ($e_L(t)_i$)

are composed of spacing errors ($e_{sP}(t)_i, e_{sL}(t)_i$) and velocity errors ($e_{vP}(t)_i, e_{vL}(t)_i$):

$$e_P(t)_i = K_{PP}e_{vP}(t)_i + K_{IP}e_{sP}(t)_i \tag{2.12}$$

$$e_L(t)_i = K_{PL}e_{vL}(t)_i + K_{IL}e_{sL}(t)_i \tag{2.13}$$

The spacing error $e_{sP}(t)_i$ and the velocity error $e_{vP}(t)_i$ relative to the preceding vehicle are:

$$e_{vP}(t)_i = v_{i-1}(t) - v_i(t), \qquad \forall\, t \in [0, T] \tag{2.14}$$

$$e_{sP}(t)_i = x_{i-1}(t) - x_i(t) - t_H \cdot v_i(t), \qquad \forall\, t \in [0, T] \tag{2.15}$$

The spacing error ($e_{sL}(t)_i$) and the velocity error ($e_{vL}(t)_i$) relative to the leading vehicle are:

$$e_{vL}(t)_i = v_1(t) - v_i(t), \qquad \forall\, t \in [0, T] \tag{2.16}$$

$$e_{sL}(t)_i = x_1(t) - (i-1)t_H \cdot v_i(t) - x_i(t), \qquad \forall\, t \in [0, T] \tag{2.17}$$

where, $i \in I = \{1, 2, \ldots\}$ is the index of vehicles in the platoon; $v_k(t)$ is the speed of the k-th vehicle and $v_{D-k}(t)$ is its desired speed; K_P, K_I, K_D are the PID constants of the lower level control; K_{PP} and K_{IP} are the PI constant of the upper level control with respect to the preceding vehicle and K_{PL} and K_{IL} are the PI constant of the upper level control with respect to the leading vehicle; $v_T(t)$ is the target speed of the platoon; $e_{vP}(t)_i$ and $e_{vL}(t)_i$ are the velocity differences of the ego-vehicle compared to preceding vehicle and leading vehicle, respectively; $e_{sP}(t)_i$ and $e_{sL}(t)_i$ are the spacing errors of the ego-vehicle with preceding and leading vehicles, respectively.

Based on the control logic of PLF CACC, the sensor measurements, including their corresponding noises, enter the dynamics as Figure 4. For the preceding vehicle measurement, the speed is computed as the change in distance, as shown in Equation (2.1). Hence, the noise propagates from distances measured by radar into relative speed. For the leading vehicle, the speed information is taken directly from CAN bus via DSRC communication. Therefore, the error from GPS does not propagate into speed signal. These datasets are updated every time interval and fed to the controller.

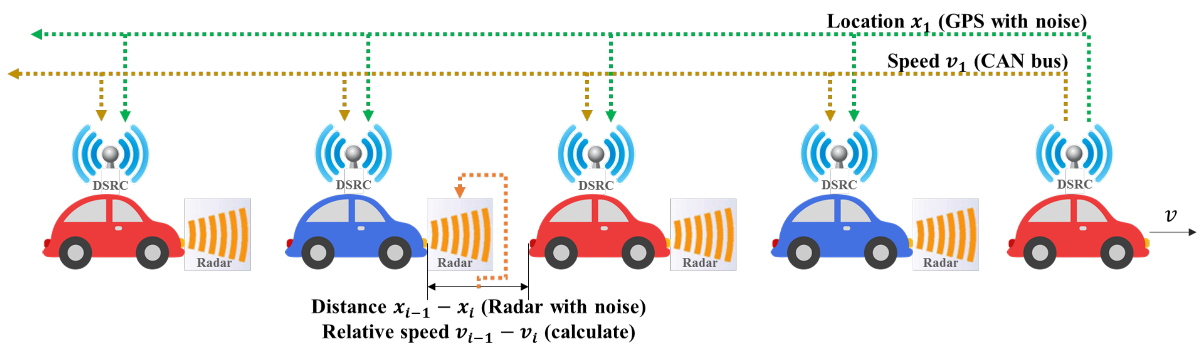

Figure 4 CACC Vehicle Information Flow Structure

Emergency Braking System (EBS): Considering that CACC is designed for non-emergency situations, an emergency braking system is added as an optional controller to the CACC controller so that the vehicles can switch the mode to collision avoidance controller. That is to say, when the actual distance detected by radar sensor (d_R) is smaller than the braking distance ($d_{braking}$), the vehicle will trigger EBS controller. The braking distance is decided based on the fundamental laws of motion with the hypothesis of the deceleration rates and the delay time.

PATH EBS algorithm [52] is used for deciding the braking distance, which adopts the kinematic approach:

$$d_{braking}(t) = \frac{1}{2}\left(\frac{v(t)^2}{\alpha_1} - \frac{v_R(t)^2}{\alpha_2}\right) + v(t)\tau + R_{min} \tag{2.18}$$

where, the maximum deceleration rates $\alpha_1 = \alpha_2 = 6m/s^2$, the delay time τ consists of two parts: the system delay time and the human reaction time, $\tau = \tau_{sys} + \tau_{hum} = 0.2 + 1.0 = 1.2s$, and the minimum distance $R_{min} = 5m$. Considering the needs of this simulation scenario for CAVs, the human reaction time is ignored and only system delay time is considered, i.e. $\tau = \tau_{sys} = 0.2s$. The speed of the preceding vehicle and the distance values are from radar sensor. It is assumed that the preceding vehicle starts to brake with a maximum deceleration rate α_2 until full stop, and the subject vehicle starts to brake after a delay time τ with a maximum deceleration rate α_1 until full stop. Several cruise control or intelligent driving-related studies have adopted this method ([53]–[56]).

2.3.3 Test of homogeneous and heterogeneous CACC platoons

Using the proposed simulation environment, a CACC platoon of four vehicles is simulated to see the impact of VDM in CACC system. The first simulation uses a homogeneous CACC platoon, where all four vehicles have the same vehicle model with the same VDM. The second simulation is conducted with a heterogeneous CACC platoon, where the second vehicle is a different vehicle model with a different VDM. The desired speed is set as 12m/s (27mi/h) and the desired headway is 1s.

A. Homogeneous platoon simulation

A CACC platoon of four vehicles is simulated with the same off-the-shelf VDM of Toyota Yaris provided in PreScan. After calibration efforts, the gain values for the PID controller are set at K_p=20, K_i=1, K_d=0.1. From the speed profile of the platoon (Figure 5), it can be seen that the vehicles start to accelerate from stopping state and stabilize to the desired speed and the desired headway after around 20 seconds. There are some fluctuations but the overall simulation results are reasonable and acceptable.

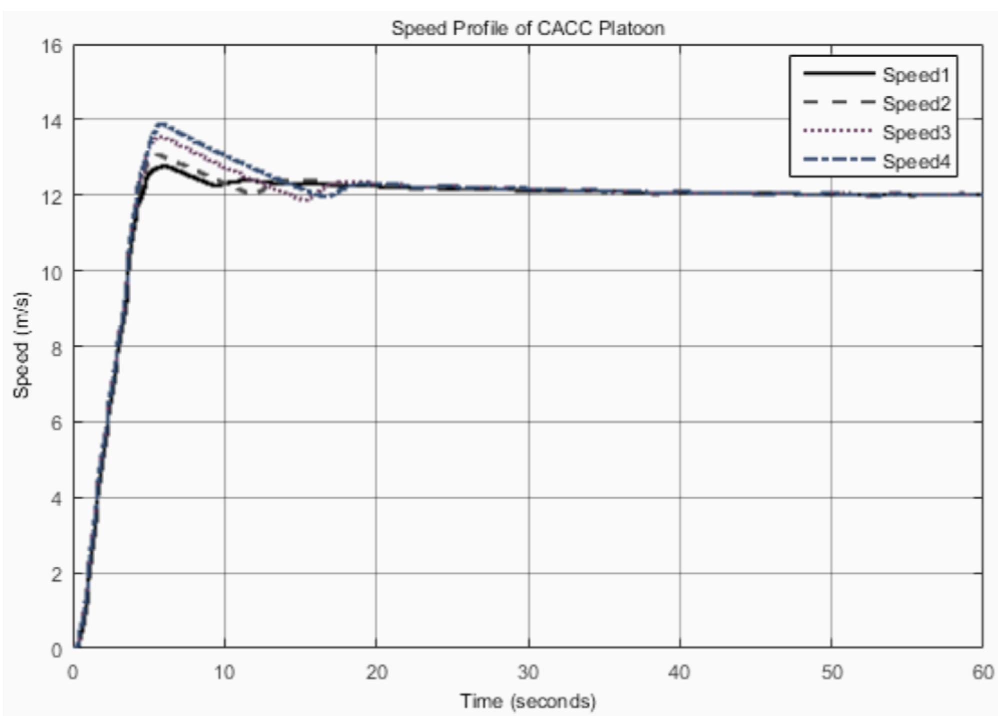

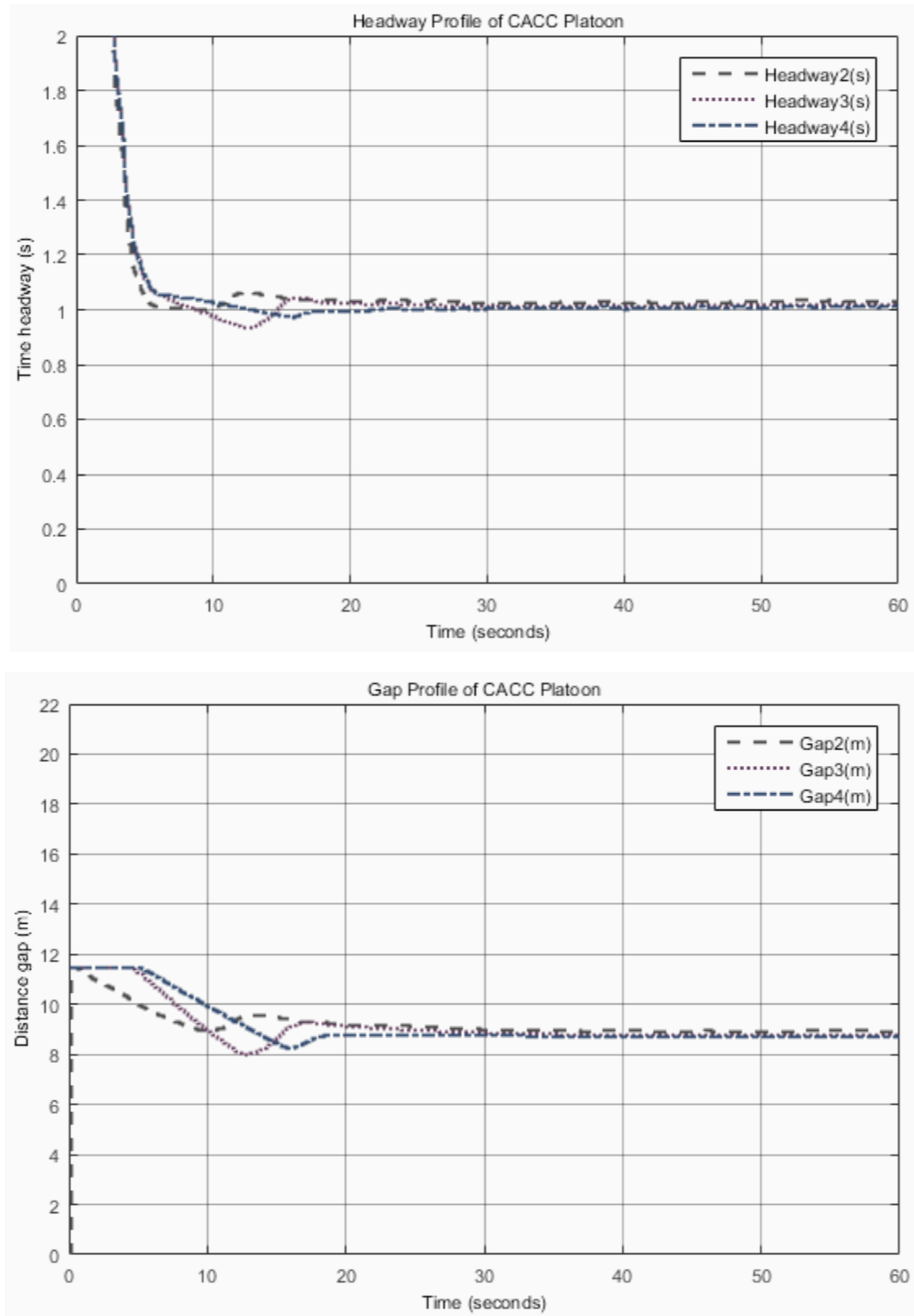

Figure 5 Speed and Headway Profiles of Homogeneous CACC Platoon

B. Heterogeneous platoon simulation

In the this case, the second vehicle is replaced with Nissan Cabstar, a light commercial vehicle. First, a corresponding VDM is used for this second vehicle, with well-tuned gain values in PID control (K_p=6, K_i=0.85, K_d=5). Due to the different characteristic of VDMs, the second vehicle accelerates more rapidly than the leading vehicle, resulting in fluctuations of the distance gaps in the platoon (Figure 6). The closest distance and time headway between the vehicles are less than 7 meters and 0.9 seconds, respectively. The simulation results indicate potential dangers of the heterogeneous platoon because with a vehicle type that has more different VDM than Nissan Cabstar, the fluctuations will be bigger.

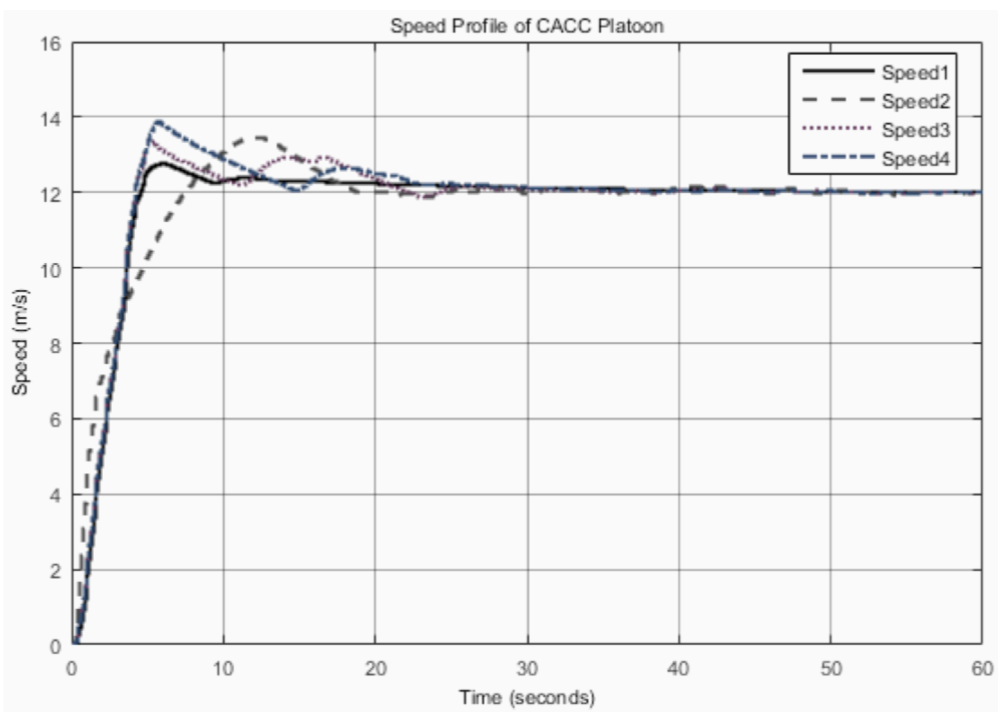

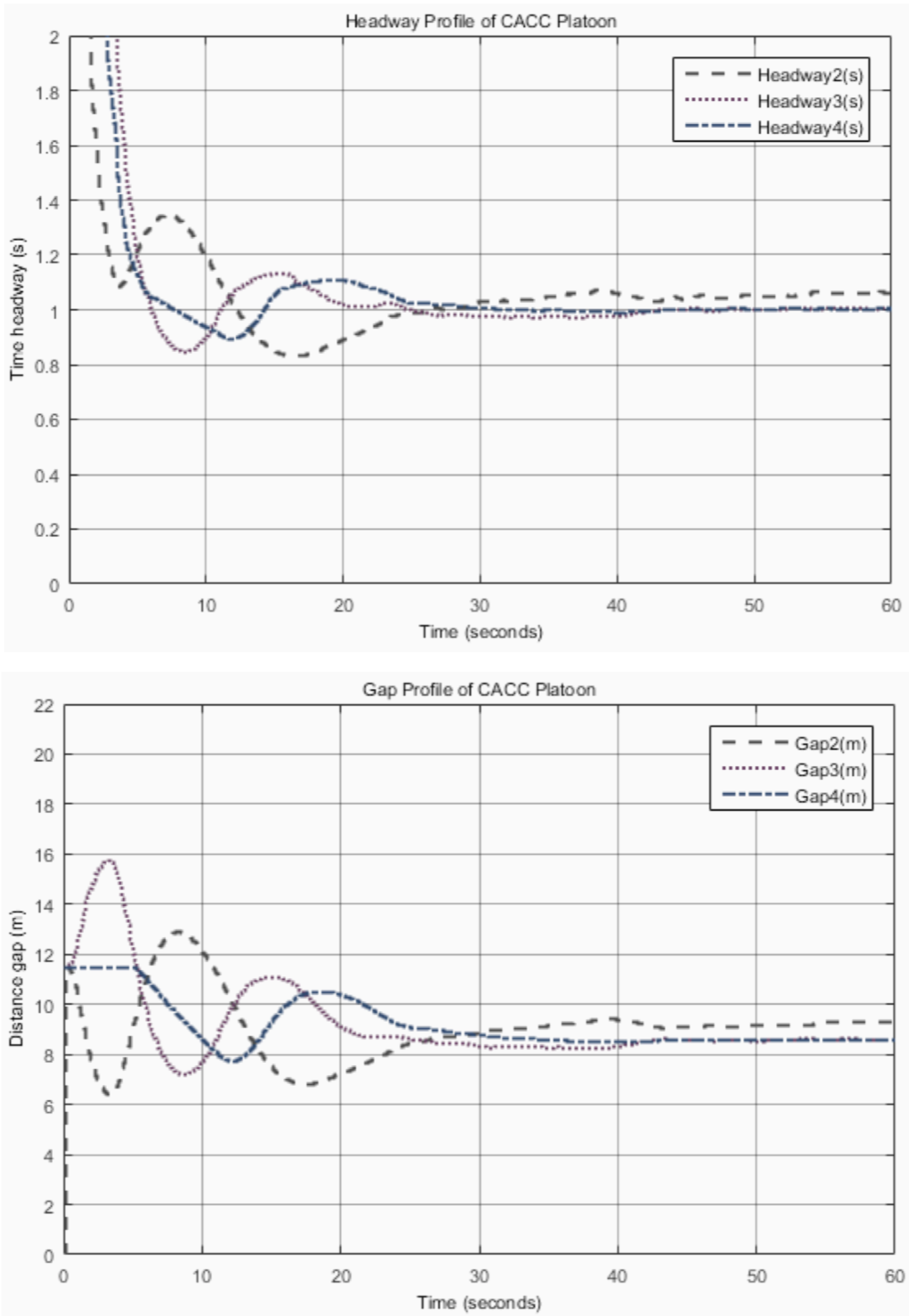

Figure 6 Speed and Headway Profiles of Heterogeneous CACC Platoon

C. Discussions

Based on the simulation results, a couple of important findings were identified. One is that VDM with CACC algorithm can reasonably simulate the behaviors, such as acceleration rates. It is especially important when simulating the heterogeneous platoon since the different characteristic of vehicle dynamics can be well modelled with VDM. Therefore, VDM is necessary and needs to be incorporated into the CAV simulation model for realistic CAV simulations.

2.3.4 Injury severity quantification

The injury severity quantification component estimates crash severity based on the speed data extracted from the CAV simulation component. Using the extracted speed data, the vehicle crash trajectory is computed using classic physics and is used as an input into a finite element computer solver in order to acquire crash severity. In addition, a commercially validated human dummy model and the vehicle equipment (e.g., the seatbelt) is adopted to quantify injury severity on driver/passengers. To generate vehicle crash trajectory, the first step is computing vehicle's Delta-V with pre-crash speed and post-crash speed. The following assumptions are applied:

- The crash is inelastic ([57]–[60]), as shown in Figure 7 (a):

$$v_j' = v_{j+1}' = v' \tag{2.19}$$

- The traffic is homogeneous:

$$m_j = m_{j+1} \quad (2.20)$$

Therefore, the post-crash speed of vehicle j can be estimated:

$$v' = \frac{m_j v_j + m_{j+1} v_{j+1}}{m_j + m_{j+1}} = \frac{v_j + v_{j+1}}{2} \quad (2.21)$$

$$\Delta v = v_i - v' \quad (2.22)$$

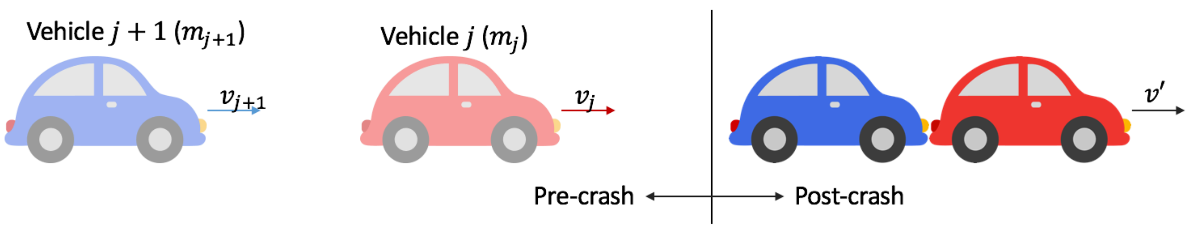

(a) Crash process

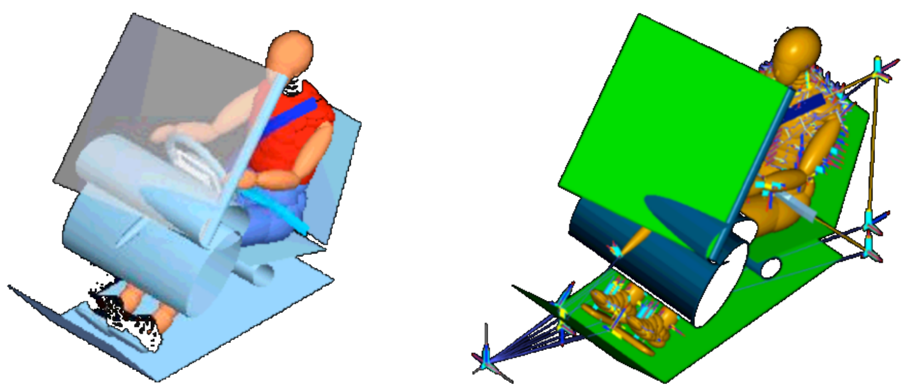

(b) Appearance (Left) and geometry (Right) of dummy and vehicle settings in finite element solver MADYMO

Figure 7 Crash Severity Quantification Diagram

The second step of computing vehicle crash trajectory is to determine the vehicle trajectory in between pre-crash speed and post-crash speed. It is assumed that speed change during crash follows the same pattern. Therefore, field crash data from another study [61] is adopted here to acquire speed change pattern during a collision. The crash trajectory can be calculated using speed pattern together with pre-crash speed and post-crash speed. Finally, the computed crash trajectory is fed into a finite element computer solver [62] in order to acquire crash severity. In the solver, a commercially validated human dummy model and the vehicle equipment (e.g., the seatbelt) (as shown in Figure 7 (b)) is adopted to quantify injury severity on driver or passengers. Injury probability is estimated following the U.S. New Car Assessment Program (US-NCAP) protocol [63].

The injury probability is calculated with a weighted combination of injuries in the head, neck, chest, and legs to represent whole-body injury [64]. For the injury probability of each body part, logistic regression models are used to compute injury level in Abbreviated Injury Scale (AIS) [65]. The injury criteria are developed based on the mechanical responses of human dummies in terms of risk to life or injury to a living human [66]. The criteria are derived from the biomechanics experiments with the human surrogates, where the mechanical parameters and injury consequences are observed. The relationships between the dummy motions or forces and the resulting injuries are obtained with statistical techniques [66].

Taking AIS level 2 as an example, the head injury criterion (HIC) is used for calculating head injury probability [66]:

$$HIC = \max\left[\frac{1}{t_2 - t_1}\int_{t_1}^{t_2} a(t)dt\right]^{2.5} (t_2 - t_1) \tag{2.23}$$

$$p(AIS \geq 2)_{head} = \frac{1}{1 + e^{2.49+200/HIC^{-0.00483HIC}}} \tag{2.24}$$

where, t_1 and t_2 are two arbitrary times during the duration of the crash (in seconds), usually $t_2 - t_1 \leq 15ms$.

For the neck injury probability, the neck injury criterion Nij is as follows:

$$Nij = \frac{F_z}{F_{int}} + \frac{M_y}{M_{int}} \tag{2.25}$$

$$p(AIS \geq 2)_{neck} = \frac{1}{1 + e^{2.054-1.195Nij}} \tag{2.26}$$

where, F_z is the axial load on the spine, M_y is the flexion/extension bending moment at the occipital condyles, and the subscript int means the tolerance line of the dummies.

Thoracic injury uses the maximum deflection D_{max}:

$$p(AIS \geq 2)_{chest} = \frac{1}{1 + e^{1.8706-0.04439D_{max}}} \tag{2.27}$$

Finally, the lower extremity injury probability is calculated with the femur force F (in kN):

$$p(AIS \geq 2)_{leg} = \frac{1}{1 + e^{5.795-0.5196F}} \tag{2.28}$$

This methodology is validated against injury field data and does accurately estimate the injury severity ([67], [68]). Therefore, it is a very well accepted injury evaluation methodology. The method has also been used for a large number of occupant safety analysis

([69], [70]). In addition, this injury evaluation models are continuously being further enhanced and validated by many researchers in detail, including: by human body parts ([71], [72]); by vehicle parts ([73]); and by crash types ([74], [75]). It is proven to be an effective and fairly accurate tool for injury evaluation. Therefore, it is commonly applied to evaluate the safety performance, analyze the occupant injury trend and implement sensitivity studies for the advanced driver assistant systems and active safety ([76]–[80]).

2.4 Assessment of CACC under Cyber Attack

The proposed simulation platform is showcased using a case study of CACC under cyber-attack scenarios.

2.4.1 Simulation setup

The simulation road network is a 2-mile long four-lane freeway (i.e., two lanes in each direction). User-specific parameters of the simulation platform are shown in Table 2. The GPS and radar errors are selected based on reasonable ranges from existing reports and papers ([28], [45], [81]). The gains for PI and PID control are borrowed from [13]. CACC vehicles are assumed to be a fleet of Toyota Yaris, and its vehicle specifications are obtained from software PreScan [82].

Table 2 Simulation Parameter Settings

Parameter	**Value**
Simulation frequency	20 Hz
Simulation time T	260 seconds for Scenario I; 120 seconds for Scenario II
Radar sensor error σ_R	0.05 m
GPS error σ_{GPS}	4.95 m
Communication delay D_C	50 ms
Target speed v_T	30 m/s (67 mph)
Desired time headway t_h	0.6 s
Gains for PI control (upper level)	
K_{PP}	0.45
K_{IP}	0.25
K_{PL}	0.15
K_{IL}	0.10
Gains for PID control (lower level)	
K_P	25
K_I	0.7
K_D	1

2.4.2 Experimental design

The following three scenarios are tested. The first scenario shows the validity of the proposed platform. The second scenario is to estimate the impact of sensor errors. The last scenario is a showcase scenario with cyber-attacks, which is tested with CACC algorithm as well as with the combined algorithm of CACC and EBS.

CACC Platform Validation: In this scenario, a test of target speed change is conducted to validate the proposed test platform. This scenario replicates the field test performed by California PATH [13]. Therefore, the data collected from the field test could serve as ground truth to validate the correctness of the evaluation platform. Measures of effectiveness used are vehicle speed and vehicle gap. In the test, the CACC platoon consists of four vehicles. The test started with all vehicles stopped and spaced randomly at about 7 to 10 meters. The leading vehicle follows a predetermined speed trajectory which is demonstrated in Figure 9 as desired speed.

Sensor Error Impact Evaluation: The crash risk under various GPS error levels have been tested and quantified. Two GPS error levels are tested: 2.48 and 7.43 meters. Measures of effectiveness used are vehicle speed and vehicle time gap.

CACC under Cyber Attack: This scenario shows an example evaluation of the safety impact of cyber-attack on a CACC platoon. The goal is to showcase how the proposed simulation platform could provide a quantitative safety evaluation of CACC control when CAVs are exposed to various paroxysmal or extreme events. This scenario is tested for the CACC platoon with and without EBS controller mode being added. The future user of the platform could and may need to modify or extend the default CACC model to fit their own needs. The potential cyber-attack scenarios are listed below ([26], [27], [83]–[85]). The scenarios are categorized according to the attack surface and the attack method.

Table 3 Potential Cyber-attack Scenarios

Attack surface:	Attack method:
• Electronic Control Unit (ECU) • CAN bus • Sensors • GPS or mapping • V2V/V2I communication	• Spoofing identity • Tampering with data • Repudiation • Information disclosure • Denial of Service (DoS)

According to Heaslip et al. (2018), more than 70 ECUs are interconnected without encryption or authentication and could be hacked through OBD-II or Bluetooth/Cellular [85]. In the cases that ECU or CAN bus is attacked, the controller demands, e.g., throttle, brake, and steer, can be intervened by the hackers. When the sensors (including radar and Lidar) or GPS get attacked, the location or distance, and the relative speed information can be tilted. V2V/V2I communication (such as DSRC) are also vulnerable to cyber-attacks ([26], [27]). In the communication attack cases, the possible disturbing information can be the leading vehicle identity, and the disordered speed or location values. If any other CAV controllers are going to be simulated in the future, the cyber-attack surface can be corresponding controllers or sensors. For example, if the CAV uses camera sensor to detect surrounding objects for parking, the attacks on image processing output can also be modeled.

For the attack methods, there are some different potential errors in the attack surfaces during the communication process, or at the communication conjunctions. The errors or attacks may generate NaN (not a number) or wrong signals as the input of controllers. According to Teixeira et al. (2012), cyber-attack in control system includes the physical attack, data deception attack, and data denial-of-service attack [83]. For example, for a controller formulated as follows:

$$\begin{gathered} x(t+\Delta t) = Ax(t) + Bu(t) + Gw(t) + Ff(t) \\ y(t) = Cx(t) + v(t) \end{gathered} \tag{2.29}$$

where, $x(t)$ is the state variable, $y(t)$ is the measurements from the sensors, $u(t)$ is the control variable, $w(t)\ and\ v(t)$ are the discrepancies between the model and the real process, due to unmodeled dynamics or disturbances, $f(t)$ is the unknown signal representing the effects of anomalies, $A, B, G, F, and\ C$ are constant values/metrics in controller and measurement systems.

A physical attack will disrupt $f(t)$ to modify the control dynamics. DoS attack can be modeled as data jamming or absence of data ($u(t) = \Theta$) since it prevents the actuator or sensor from reaching the destinations. Data deception attack modifies the control variable from the real values $u(t)\ or\ y(t)$ as corrupted signals $\bar{u}(t)\ or\ \bar{y}(t)$ [83].

$$\begin{aligned} \bar{u}(t) &:= u(t) + \Gamma^u b^u(t) \\ \bar{y}(t) &:= y(t) + \Gamma^y b^y(t) \end{aligned} \tag{2.30}$$

where, $b^u(t)\ and\ b^y(t)$ represent the data corruption, $\Gamma^u\ and\ \Gamma^y \in \{0, 1\}$ are the binary matrices, indicating which data channels are accessed and corrupted by the attackers.

In this research, as an example of the potential cyber-attacks, the sensor and GPS are selected as the attack surfaces. Physical attack and the DoS are selected as attack methods. Among the ten CAVs of CACC platoon, the third vehicle is under cyber-attack starting at 60th second. The entire test lasts 120 seconds. Various data corruptions in cyber-attack and their severity levels have been tested, as shown in Table 4. These have been identified by California PATH as some of the most critical conditions [27]. Table 3 provides the deviation of GPS and radar sensors compared to the ground truth. The scenario "Jam" means that the data received via DSRC is frozen (i.e., DSRC data keeps the same values and no updates occur during the cyber-attack). False data in a radar sensor is formulated as follows:

$$d_R(t) = \begin{cases} d(t) + \varepsilon_R, & \forall\, t \in [0, T/2] \\ d(t) + \varepsilon_R + C_R, & \forall\, t \in (T/2, T] \end{cases} \tag{2.31}$$

where $C_R \in \{-20, -15, -10, -5, 0, +5, +10, +15, +20\}$ is the false value collected by the radar sensor under attack.

Similarly, false data in a GPS sensor is as following:

$$d_{GPS}(t) = \begin{cases} d(t) + \varepsilon_{GPS}, & \forall\, t \in [0, T/2] \\ d(t) + \varepsilon_{GPS} + C_{GPS}, & \forall\, t \in (T/2, T] \end{cases} \tag{2.32}$$

where, $C_{GPS} \in \{-34, -17,\ 0, +17, +34\}$ is the false value collected by GPS under attack.

GPS and radar are selected based on the probability of success according to Petit & Shladover (2015). The values are carefully designed to be too small to be easily screened out as outliers. Since the 95% confidence interval of a horizontal GPS error is 17m [45], the change of 17 meters or 34 meters in GPS positioning is unlikely to be screened out as outliers. However, if GPS error is very big, such as several times bigger than GPS noise, it would be easy to be detected. For the radar detection, the relative small false data are considered to possibly happen during CACC due to unexpected cut-in vehicles and is difficult to be filtered out. That is to say, the false data may mislead the CACC platoon to take another fake vehicle into account, but have them control mode switch. Therefore, the relatively small error is tested.

In modeling the attack, only one vehicle, the 3rd vehicle in this scenario, is attacked. It is specifically designed to avoid canceling out effect. The attack took place after the vehicle received data from DSRC (e.g., GPS data of the leading vehicle) and radar (see Figure 8). Please note, applying attack on one single vehicle is just the setting adopted in this study. The proposed platform does allow randomly varying GPS and radar errors. Future users can always adjust error according to their preferences and scenario designs.

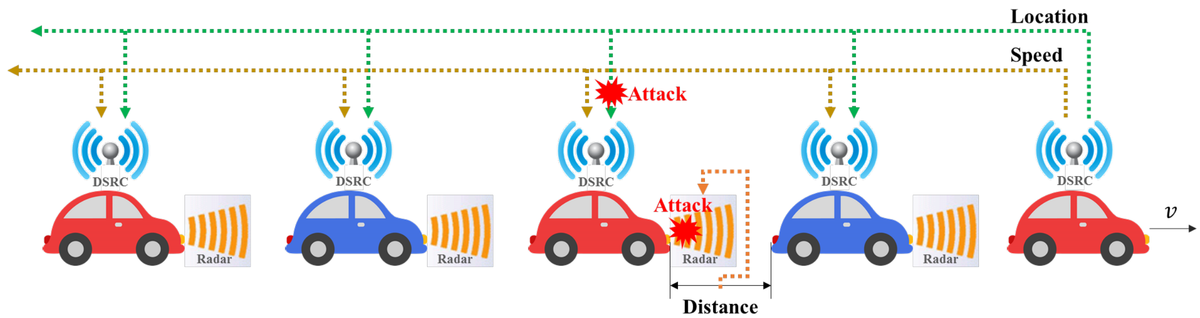

Figure 8 CACC Cyber-attack Scenario

Table 4 Scenario Table of Cyber-attack to the 3rd Vehicle

Scenario series number		**GPS attack (error in meters)**					
		-34	**-17**	**0**	**+17**	**+34**	**Jam**
Radar attack (error in meters)	**-20**	*1-1*	*2-1*	*3-1*	*4-1*	*5-1*	*6-1*
	-15	*1-2*	*2-2*	*3-2*	*4-2*	*5-2*	*6-2*

	-10	*1-3*	*2-3*	*3-3*	*4-3*	*5-3*	*6-3*
	-5	*1-4*	*2-4*	*3-4*	*4-4*	*5-4*	*6-4*
	0	*1-5*	*2-5*	*3-5*	*4-5*	*5-5*	*6-5*
	+5	*1-6*	*2-6*	*3-6*	*4-6*	*5-6*	*6-6*
	+10	*1-7*	*2-7*	*3-7*	*4-7*	*5-7*	*6-7*
	+15	*1-8*	*2-8*	*3-8*	*4-8*	*5-8*	*6-8*
	+20	*1-9*	*2-9*	*3-9*	*4-9*	*5-9*	*6-9*

2.4.3 Measures of Effectiveness

For the scenarios where no crash occurs, safety performance is quantified by the stability of the CACC platoon. The two MOEs adopted are speed variance and headway ratio. Headway ratio is calculated as follows:

$$r_h = \frac{t_H}{t_h} \tag{2.33}$$

where r_h is the headway ratio, t_H is the target time headway, and t_h is minimum actual time headway. A greater headway ratio implies a smaller minimum headway and increased the likelihood of collision.

For the scenarios where a crash occurs, the MOE adopted is injury probability which represents the likelihood and severity of a driver or passenger being injured. A finite element method based computer solver is used to compute the injury probability using speed trajectory data produced from the proposed simulation platform [62]. Within the solver, the injury probability is calculated based on the injury severity of various human parts on a standard crash human dummy model, Hybrid III 50th, as shown in Figure 7 (b).

2.5 Simulation results

2.5.1 CACC Platform Validation

The results of the CACC platform validation scenario are shown in Figure 9. The speed and distance gaps show that the CACC platoon can achieve desired speed and keep desired headway properly at the same time. The results are compared with the results from the PATH's field test [13]. Both stabilization and speed change pattern are consistent with the field results.

Statistical test: the speed profile from the simulation results are validated against the field data. The data points were captured from the original figure in Milanes et al. (2014). Considering the color and clarity of the original figure, the speed profile of the fourth vehicle was selected for the statistical test. A total of 114 data points were captured. Then the speeds of the vehicle in the proposed simulation platform at the corresponding time were extracted and compared. Overall, the statistical analysis confirms the validity of the proposed simulation evaluation platform.

The speed samples are tested with t-test to see if the distribution of speed errors, which is defined as the difference between actual speed and simulation speed, has the true mean of zero. The descriptive statistics of speed error is shown in Table 5. The 95% confidence interval of speed error is (–0.026±0.057) m/s. The t-test result gives the t statistic value as –0.906 with the t critical value 1.981, p-value 0.367, which means the null hypothesis is failed to be rejected, and the true mean of speed errors equals zero. This error can be caused by the uncertainty of sensor noises, and the different vehicle dynamics between the simulation platform, which is the VDM of TOYOTA Yaris, and the field test, where INFINITI M56s is used.

Table 5 Parameters of Speed Error Distribution

Parameters	Values
Maximum	+0.665 m/s
75th Percentile	+0.174 m/s
Median	–0.022 m/s
25th Percentile	–0.261 m/s
Minimum	–0.742 m/s
Mean	–0.026 m/s
Standard deviation	0.312 m/s

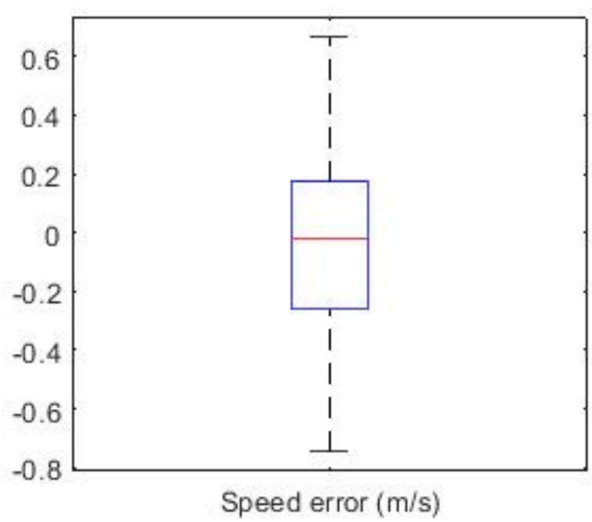

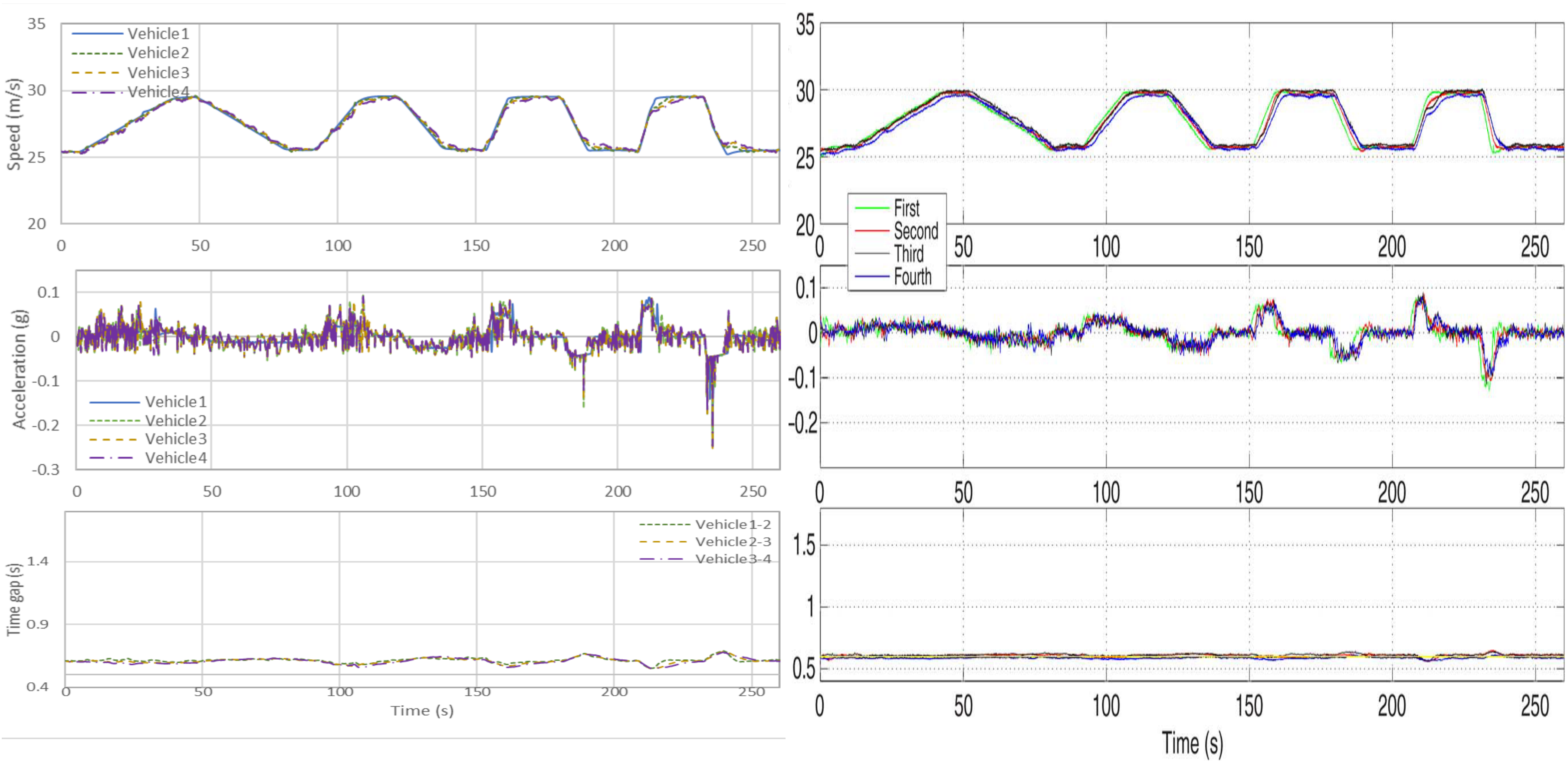

a) Simulation results with proposed simulation platform

b) Field test results from Milanes et al. (2014)

Figure 9 Speed and Distance Gap Trajectory of CACC Platoon with Desired Speed

2.5.2 Sensor Error Impact Evaluation

The crash risk under various GPS error levels has been tested and quantified. As shown in Figure 10, greater GPS noise variance leads to greater fluctuations. However, the fluctuations are not significant enough to raise safety concerns. The platoon was stabilized before any crash happens.

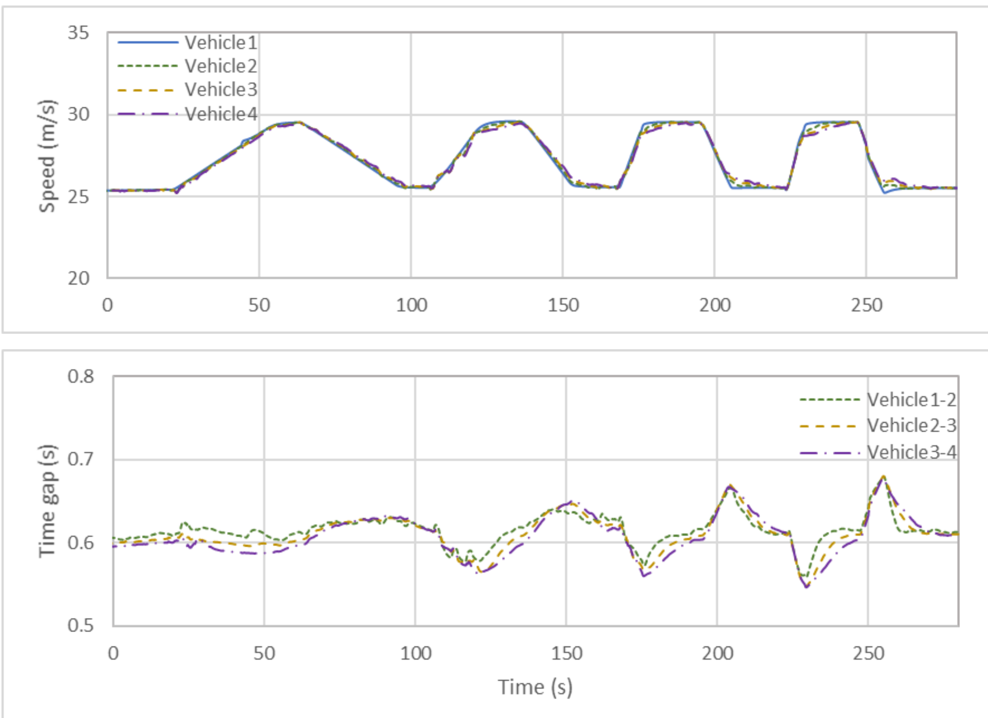

a) GPS noise variance – 2.48 m

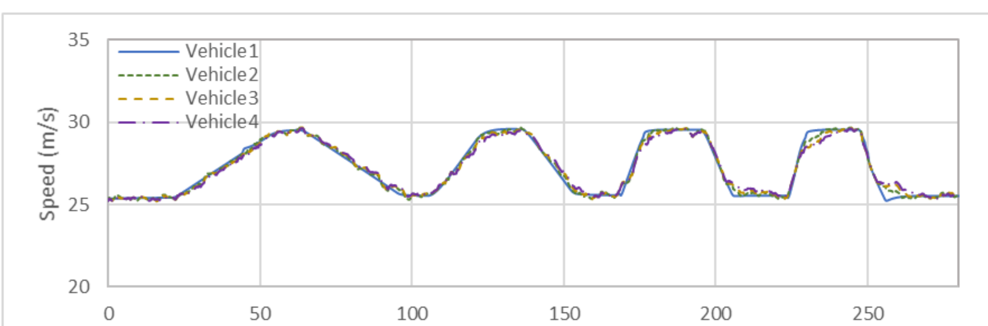

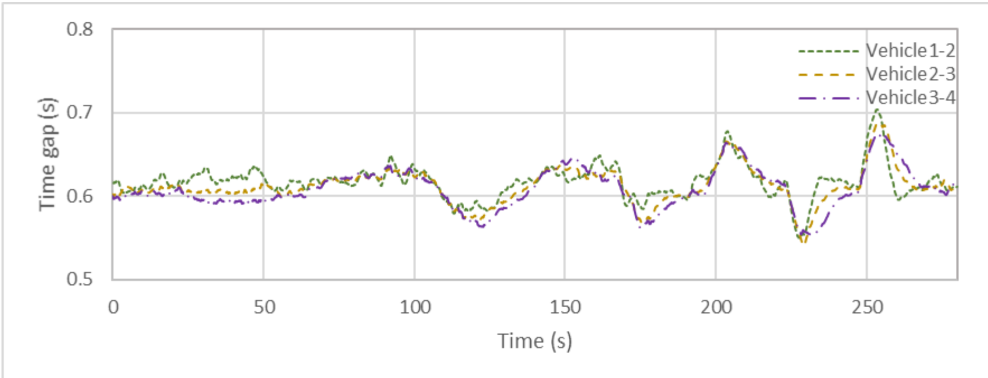

b) GPS noise variance – 7.43 m

Figure 10 Speed and Time Gap Trajectory of CACC Platoon with Different GPS noises

2.5.3 CACC under Cyber Attacks

The proposed CACC safety evaluation platform is showcased using a case study of CACC under the cyber-attack scenario. The simulation results show that non-crash scenarios are Scenario 1-1~9, 2-1~9, 3-1~9, 4-1~7, and 5-1~6; crash scenarios are Scenario 4-8~9, 5-7~9, and Jam-1~9. The details are discussed in the following subsections.

Stability evaluation For no crash scenarios, there are still fluctuations in the speed of the attacked vehicle (3rd vehicle). The unstable movements of the 3rd vehicle also cause fluctuations on its following vehicles. Two scenarios are chosen as examples to show the stability of platoon. Figure 11 shows the speed and headway profile of the platoon under Scenario 2-3 (GPS -17, Radar -10) and 6-6 (GPS jam, Radar +5), respectively. The 3rd vehicle starts a sudden deceleration as soon as the incorrect information is received due to the cyber-attack. Then, in the Scenario 2-3, the 3rd vehicle adjusts its speed and headway to a new stabilized state. As a result, the following vehicles also have a sudden acceleration or deceleration but are stabilized within 30 seconds. In the Scenario 6-6, the 3rd vehicle kept hard braking until the following 4th vehicle crashed into it. This also happens between the 4th vehicle and its following vehicles since the vehicles are trying to find a new stabilized state with the information from the preceding vehicle and leading vehicle.

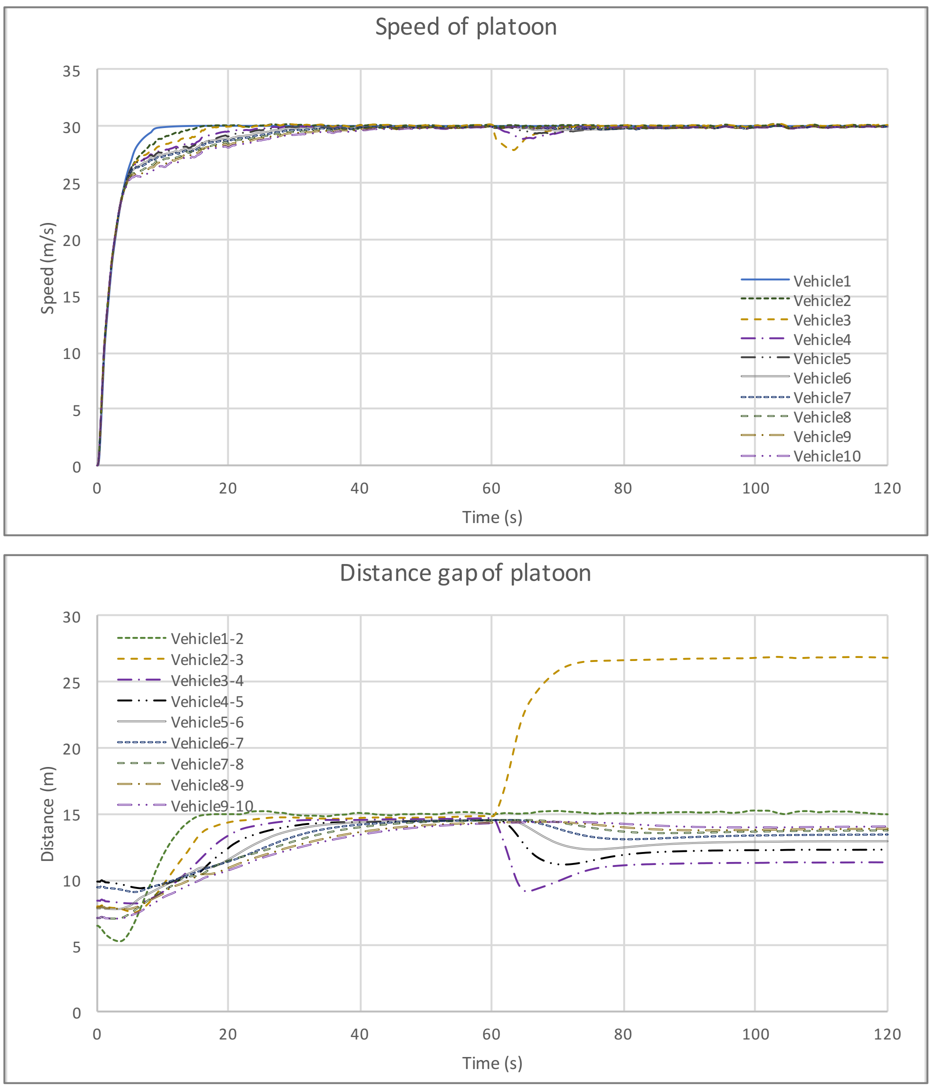

(a) Scenario 2-3 (GPS -17, Radar -10)

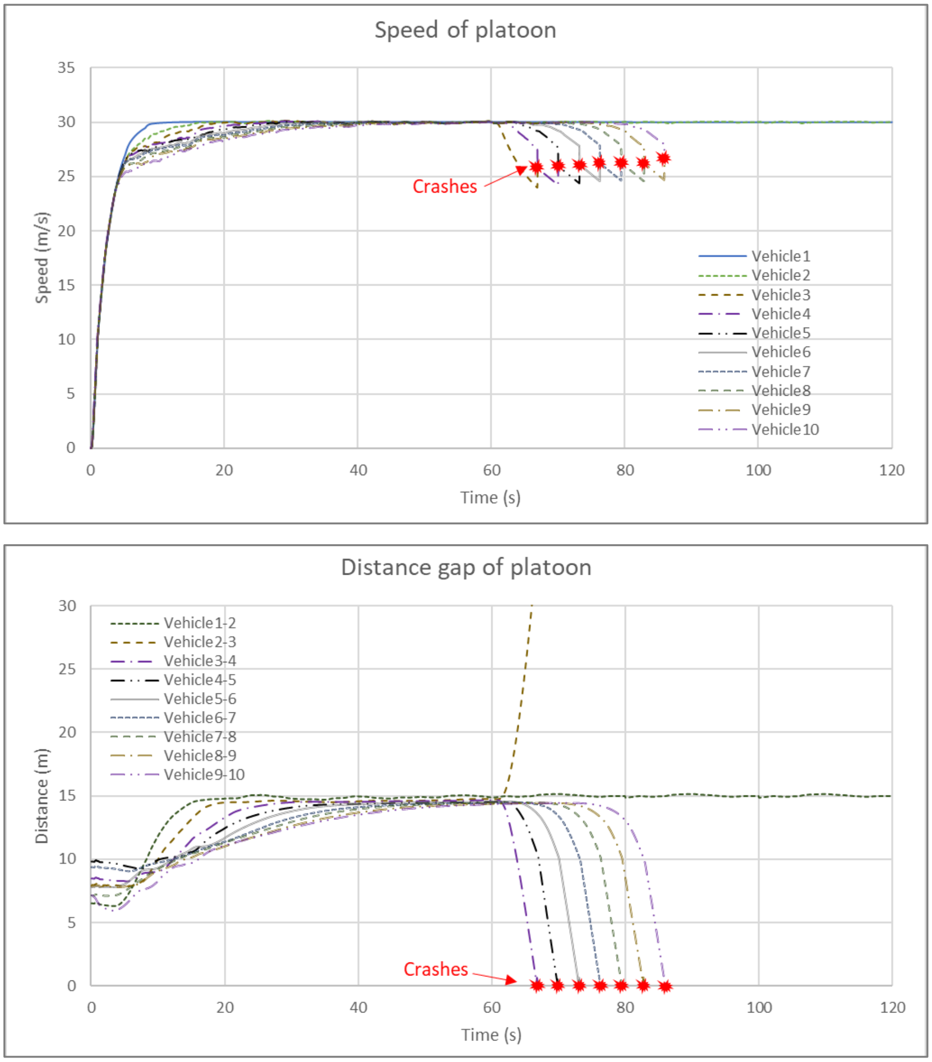

(b) Scenario 6-6 (GPS jam, Radar +5)

Figure 11 Speed and Distance Gap Profile of Example Scenarios

The stabilization assessment table of the maximum headway ratio and the speed variance for every vehicle (3rd to the 10th vehicle) is shown in Table 6. The results of the 4th vehicle are visualized in Figure 12 as an example. Table 6 and Figure 12 demonstrate that the platoon is most stable when the sum of the errors in GPS and Radar is near zero. It is because the two errors can be canceled out in the upper level of the CACC control (i.e., PI control). The platoon is much less stable when errors on GPS and Radar are the same sign (i.e., positive/negative).

When GPS is jammed, crashes occur regardless of the error value in radar. The speed variances for GPS jam scenarios are less than, in some scenarios, without a crash. This is because analysis period stops at the time of the crash, as speed variance after the crash is zero, total speed variance during the entire simulation is brought down by zero variance after the crash. The results (headway ratio and speed variance) for stabilization during 60~90s are as follows (where cyber-attack happens at the 60th second, Veh 3 represents the 3rd vehicle):

Table 6 Platoon Stability Analysis for Each Vehicle

GPS attack / Radar attack		Headway ratio						Speed variance					
		-34	-17	0	+17	+34	Jam	-34	-17	0	+17	+34	Jam
VEH 3	-20	0.99	0.99	0.99	0.99	0.99	0.99	1.49	0.96	0.55	0.26	0.06	2.38
	-15	0.99	0.99	0.99	0.99	0.99	0.99	1.09	0.64	0.33	0.11	0.00	2.63
	-10	0.99	0.99	0.99	0.99	1.15	0.99	0.75	0.39	0.16	0.02	0.01	2.88
	-5	0.99	0.99	0.99	1.06	1.48	0.99	0.47	0.22	0.04	0.00	0.09	3.30
	0	0.99	0.99	0.99	1.34	2.11	0.99	0.27	0.07	0.00	0.06	0.21	3.71
	+5	0.99	0.99	1.22	1.83	3.64	0.99	0.12	0.01	0.03	0.16	0.38	4.16
	+10	0.99	1.13	1.62	2.90	5.00	0.99	0.02	0.01	0.12	0.32	0.63	4.33
	+15	1.04	1.45	2.39	4.94	5.18	1.01	0.00	0.08	0.25	0.57	0.93	4.84
	+20	1.31	2.04	4.57	5.08	5.32	1.04	0.05	0.20	0.44	0.80	1.44	5.20
VEH 4	-20	2.33	1.78	1.48	1.29	1.11	4.55	0.44	0.26	0.15	0.07	0.02	0.55
	-15	1.90	1.55	1.33	1.15	1.01	4.62	0.30	0.17	0.09	0.03	0.00	0.59
	-10	1.63	1.38	1.20	1.04	0.99	4.62	0.20	0.11	0.05	0.01	0.00	0.54

	-5	1.43	1.25	1.08	0.99	0.99	4.58	0.13	0.06	0.01	0.00	0.02	0.56
	0	1.29	1.12	0.99	0.99	0.99	4.54	0.07	0.02	0.00	0.01	0.06	0.58
	+5	1.16	1.02	0.99	0.99	0.99	4.58	0.03	0.00	0.01	0.04	0.11	0.65
	+10	1.05	0.99	0.99	0.99	4.44	4.59	0.01	0.00	0.03	0.09	1.27	0.60
	+15	0.99	0.99	0.99	4.55	4.55	4.58	0.00	0.02	0.07	1.14	1.54	0.64
	+20	0.99	0.99	0.99	4.56	4.49	4.59	0.01	0.05	0.12	1.46	1.62	0.61
VEH 5	**-20**	1.60	1.41	1.27	1.17	1.07	4.53	0.12	0.07	0.04	0.02	0.01	0.56
	-15	1.46	1.30	1.19	1.10	1.01	4.57	0.09	0.05	0.02	0.01	0.00	0.49
	-10	1.34	1.22	1.12	1.03	1.00	4.62	0.06	0.03	0.01	0.00	0.00	0.46
	-5	1.24	1.15	1.05	1.00	1.00	4.54	0.04	0.02	0.00	0.00	0.01	0.46
	0	1.17	1.08	1.00	1.00	1.00	4.54	0.02	0.01	0.00	0.01	0.02	0.51
	+5	1.10	1.02	1.00	1.00	1.00	4.52	0.01	0.00	0.00	0.01	0.03	0.48
	+10	1.04	1.00	1.00	1.00	4.53	4.58	0.00	0.00	0.01	0.03	0.56	0.44
	+15	1.00	1.00	1.00	4.50	4.48	4.53	0.00	0.01	0.02	0.54	0.69	0.44
	+20	1.00	1.00	1.00	4.49	4.54	4.61	0.01	0.02	0.04	0.63	0.69	0.45
VEH 6	**-20**	1.33	1.24	1.17	1.10	1.05	4.53	0.03	0.02	0.01	0.01	0.00	0.41
	-15	1.26	1.18	1.12	1.06	1.01	4.57	0.02	0.01	0.01	0.00	0.00	0.44
	-10	1.20	1.13	1.08	1.02	1.00	4.64	0.02	0.01	0.00	0.00	0.00	0.39
	-5	1.15	1.09	1.03	1.00	1.00	4.56	0.01	0.00	0.00	0.00	0.00	0.39
	0	1.11	1.05	1.00	1.00	1.00	4.55	0.01	0.00	0.00	0.00	0.01	0.37
	+5	1.06	1.01	1.00	1.00	1.00	4.60	0.00	0.00	0.00	0.01	0.01	0.38
	+10	1.02	1.00	1.00	1.00	4.52	4.59	0.00	0.00	0.01	0.01	0.37	0.39
	+15	1.00	1.00	1.00	2.68	4.62	4.60	0.00	0.00	0.01	0.24	0.36	0.36
	+20	1.00	1.00	1.00	4.63	4.62	4.57	0.00	0.01	0.02	0.36	0.38	0.31
VEH 7	**-20**	1.20	1.15	1.11	1.07	1.03	4.56	0.01	0.01	0.00	0.00	0.00	0.32
	-15	1.16	1.12	1.08	1.04	1.01	4.60	0.01	0.00	0.00	0.00	0.00	0.33
	-10	1.13	1.09	1.05	1.02	1.00	4.58	0.00	0.00	0.00	0.00	0.00	0.30
	-5	1.10	1.06	1.02	1.00	1.00	4.56	0.00	0.00	0.00	0.00	0.00	0.29
	0	1.07	1.03	1.00	1.00	1.00	4.56	0.00	0.00	0.00	0.00	0.01	0.32
	+5	1.04	1.01	1.00	1.00	1.00	4.64	0.00	0.00	0.00	0.00	0.01	0.29
	+10	1.02	1.00	1.00	1.00	2.06	4.58	0.00	0.00	0.00	0.01	0.11	0.30

	+15	1.00	1.00	1.00	1.16	4.58	4.59	0.00	0.00	0.01	0.03	0.28	0.30
	+20	1.00	1.00	1.00	4.55	4.55	4.54	0.00	0.01	0.01	0.28	0.29	0.34
VEH8	**-20**	1.13	1.10	1.07	1.04	1.02	4.66	0.01	0.00	0.00	0.00	0.00	0.29
	-15	1.10	1.08	1.05	1.03	1.00	4.60	0.00	0.00	0.00	0.00	0.00	0.28
	-10	1.08	1.06	1.03	1.01	1.00	4.61	0.00	0.00	0.00	0.00	0.00	0.28
	-5	1.06	1.04	1.02	1.00	1.00	4.55	0.00	0.00	0.00	0.00	0.00	0.28
	0	1.05	1.02	1.00	1.00	1.00	4.65	0.00	0.00	0.00	0.00	0.00	0.26
	+5	1.03	1.01	1.00	1.00	1.00	4.66	0.00	0.00	0.00	0.00	0.00	0.27
	+10	1.01	1.00	1.00	1.00	1.11	4.66	0.00	0.00	0.00	0.00	0.01	0.27
	+15	1.00	1.00	1.00	1.01	1.46	4.57	0.00	0.00	0.00	0.01	0.04	0.25
	+20	1.00	1.00	1.00	1.31	1.53	4.59	0.00	0.00	0.00	0.03	0.05	0.25
VEH 9	**-20**	1.08	1.07	1.05	1.03	1.01	4.56	0.00	0.00	0.00	0.00	0.00	0.24
	-15	1.07	1.05	1.03	1.02	1.01	4.60	0.00	0.00	0.00	0.00	0.00	0.25
	-10	1.06	1.04	1.02	1.01	1.01	4.59	0.00	0.00	0.00	0.00	0.00	0.24
	-5	1.04	1.03	1.01	1.01	1.01	4.60	0.00	0.00	0.00	0.00	0.00	0.24
	0	1.03	1.02	1.01	1.01	1.01	4.54	0.00	0.00	0.00	0.00	0.00	0.28
	+5	1.02	1.01	1.01	1.01	1.01	4.55	0.00	0.00	0.00	0.00	0.00	0.28
	+10	1.01	1.01	1.01	1.01	1.01	4.58	0.00	0.00	0.00	0.00	0.00	0.28
	+15	1.01	1.01	1.01	1.01	1.07	4.58	0.00	0.00	0.00	0.00	0.00	0.25
	+20	1.01	1.01	1.01	1.05	1.07	4.56	0.00	0.00	0.00	0.00	0.00	0.24
VEH 10	**-20**	1.05	1.04	1.03	1.02	1.01	4.46	0.00	0.00	0.00	0.00	0.00	0.22
	-15	1.04	1.03	1.02	1.01	1.01	4.41	0.00	0.00	0.00	0.00	0.00	0.22
	-10	1.04	1.02	1.01	1.01	1.01	4.44	0.00	0.00	0.00	0.00	0.00	0.21
	-5	1.03	1.02	1.01	1.01	1.01	4.43	0.00	0.00	0.00	0.00	0.00	0.19
	0	1.02	1.01	1.01	1.01	1.01	4.43	0.00	0.00	0.00	0.00	0.00	0.19
	+5	1.01	1.01	1.01	1.01	1.01	4.47	0.00	0.00	0.00	0.00	0.00	0.20
	+10	1.01	1.01	1.01	1.01	1.01	4.52	0.00	0.00	0.00	0.00	0.00	0.21
	+15	1.01	1.01	1.01	1.01	1.01	4.40	0.00	0.00	0.00	0.00	0.00	0.19
	+20	1.01	1.01	1.01	1.01	1.01	4.46	0.00	0.00	0.00	0.00	0.00	0.19

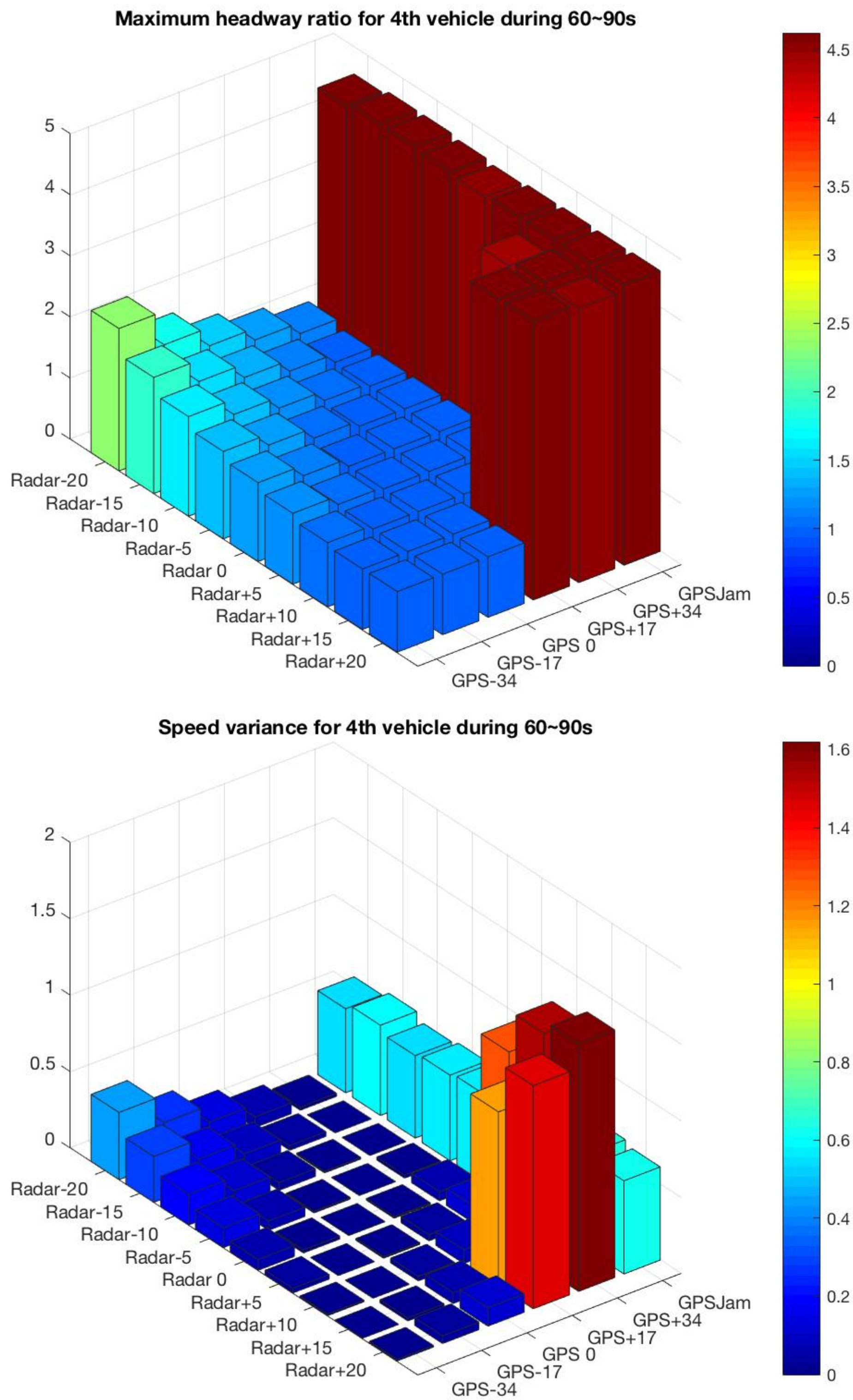

Figure 12 Stabilization of 4th Vehicle's Movement in Scenario Table

Crash severity evaluation The injury probabilities of drivers and passengers in the crashed vehicle pair are presented in Table 7. The resulting injury probabilities range from 4.7% to 40.2%. According to NHTSA, injury probabilities greater than 46% are defined as severe crashes [86]. Therefore, the crashes observed in this study are quite serious already. The crashes occurred when the attacked vehicle suddenly accelerated to crashing into its preceding vehicle, or when it had a rapid deceleration, and its following vehicle could not avoid crashing. In some scenarios, multiple pile-up crashes occurred because multiple vehicles did not have enough time to stop. The results demonstrate that the proposed CACC evaluation platform is capable of quantifying crash severity level. In addition, the severity output is sensitive to test scenario settings.

Table 7 Injury Probability in Preceding and Following Vehicles

Injury probability of drivers (%)		**GPS attack**								
		-34	**-17**	**0**	**+17**		**+34**		**Jam**	
Crash Related Vehicle					Preceding	Following	Preceding	Following	Preceding	Following
Radar attack	**-20**	-	-	-	-		-		*12.6*	*24.9*
	-15	-	-	-	-		-		*9.3*	*16.7*
	-10	-	-	-	-		-		*8.0*	*18.5*
	-5	-	-	-	-		-		*7.9*	*16.2*
	0	-	-	-	-		-		*7.1*	*16.3*
	+5	-	-	-	-		-		*7.9*	*15.8*
	+10	-	-	-	-		*6.9*	*5.4*	*8.9*	*16.6*
	+15	-	-	-	*5.0*	*4.7*	*6.3*	*6.4*	*8.0*	*20.6*
	+20	-	-	-	*6.7*	*6.1*	*8.4*	*7.9*	*8.5*	*16.3*

Injury probability of passengers (%)		GPS attack								
		-34	-17	0	+17		+34		Jam	
Crash Related Vehicle					Preceding	Following	Preceding	Following	Preceding	Following
Radar attack	**-20**	-	-	-	-		-		*14.5*	*40.2*
	-15	-	-	-	-		-		*10.1*	*24.8*
	-10	-	-	-	-		-		*8.2*	*28.5*
	-5	-	-	-	-		-		*8.2*	*22.8*
	0	-	-	-	-		-		*7.2*	*25.0*
	+5	-	-	-	-		-		*8.1*	*23.0*
	+10	-	-	-	-		*7.1*	*5.7*	*9.5*	*24.6*
	+15	-	-	-	*5.1*	*4.8*	*6.5*	*7.0*	*8.4*	*33.0*
	+20	-	-	-	*6.9*	*7.0*	*8.6*	*9.7*	*9.7*	*24.6*

2.5.4 CACC with EBS under Cyber Attacks

This CACC controller with EBS is tested with the same cyber-attack scenarios, and the results are as follows. With EBS added to CAVs, the simulation results show less crashes under extreme cases. The Scenario 5-7 and Jam-1~9, where crashes happened without EBS, exempted from crashes. The main changes in the safety impact of cyber-attack on the CACC platoon are going to be discussed in this part.

Stability evaluation The evaluation demonstrates that EBS has is pros and cons. On the positive side, EBS can help avoid most of the crashes caused by the 3rd vehicle due to the cyber-attack. However, when the radar is attacked, EBS cannot work effectively since the braking distance is calculated with the wrong radar information. That is why the Scenarios 4-8~9 and 5-8~9 still cause crashes when the 3rd vehicle accelerates and strike into its preceding vehicle without proper braking actions. In the GPS jam scenarios, sudden decelerations of the 3rd vehicle triggered EBS in its following vehicles, and the crash is avoided. The speed and headway profile under Scenario 6-6 (GPS jam, Radar +5), which caused a crash without EBS, in Figure 13 present how the CACC platoon with EBS reacts to the cyber-attack. When the 3rd vehicle brakes suddenly, the following vehicles start to decelerate successively and maintain the speed similar to the 3rd vehicle and the distance at 10 meters.

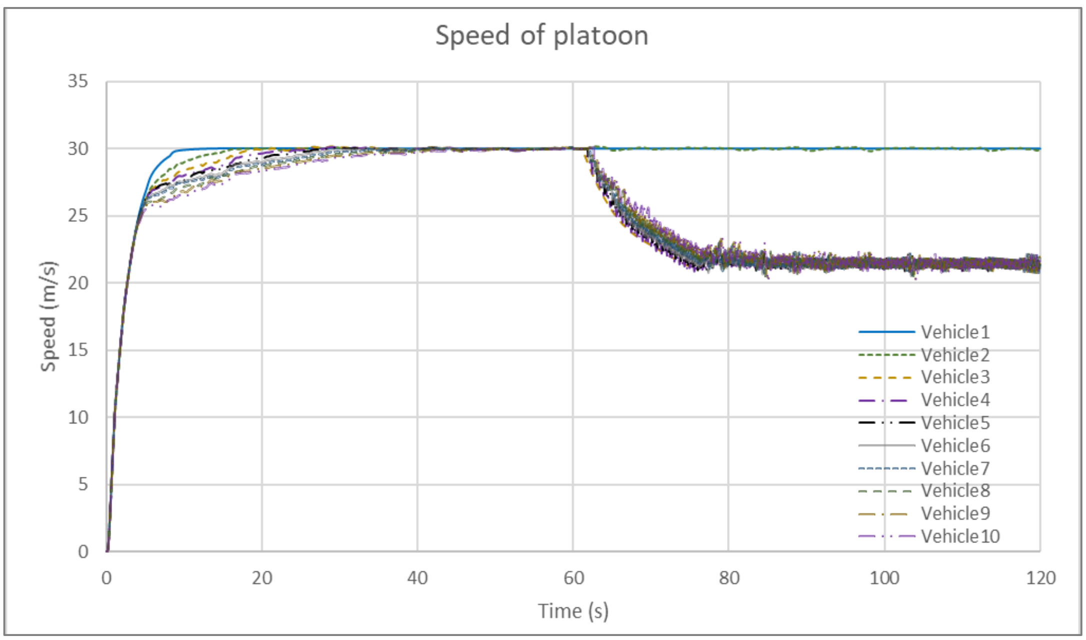

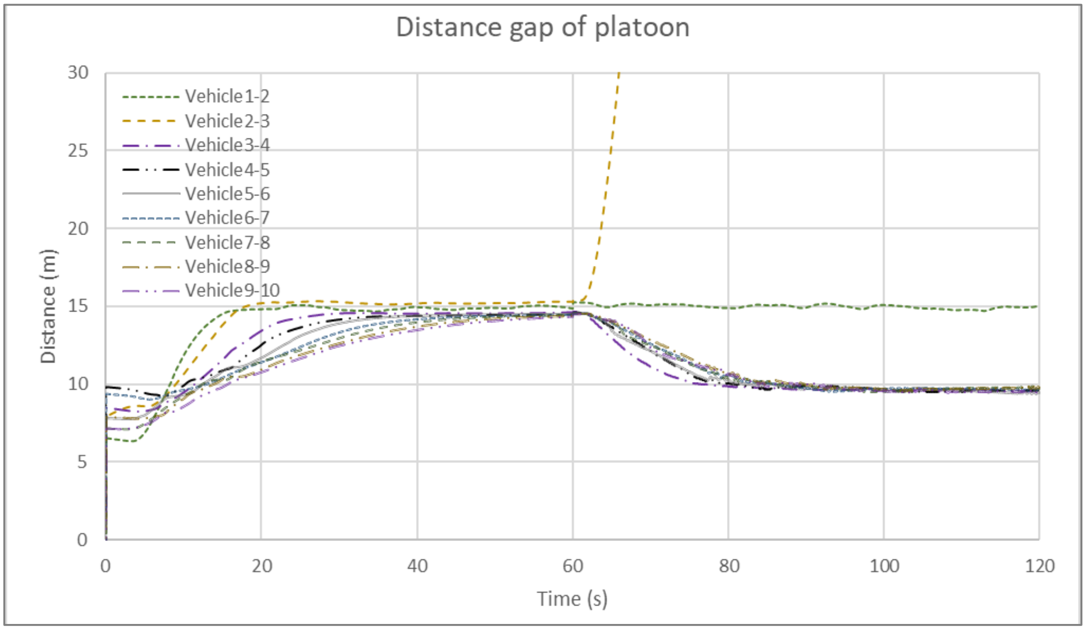

Figure 13 Speed and Distance Gap Profile of Scenario 6-6 (GPS jam, Radar +5) with EBS

However, on the negative side, more speed fluctuations are caused. This is because the vehicles are staggering between trying to maintain the CACC platoon and activating EBS. The speed variances in Figure 14 also support this phenomenon. Take the 4th vehicle as an example, although the maximum headway ratios are all below 1s due to EBS, the speed variances in GPS jam scenarios and the crash scenarios (4-8~9 and 5-8~9) are much higher than the other scenarios. The findings prove the importance of designing the switching threshold of EBS.

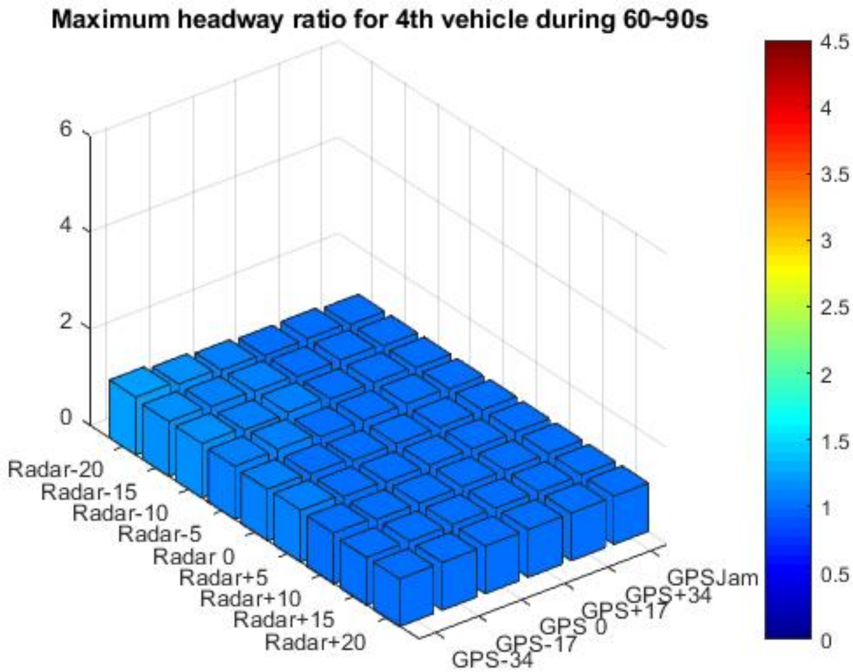

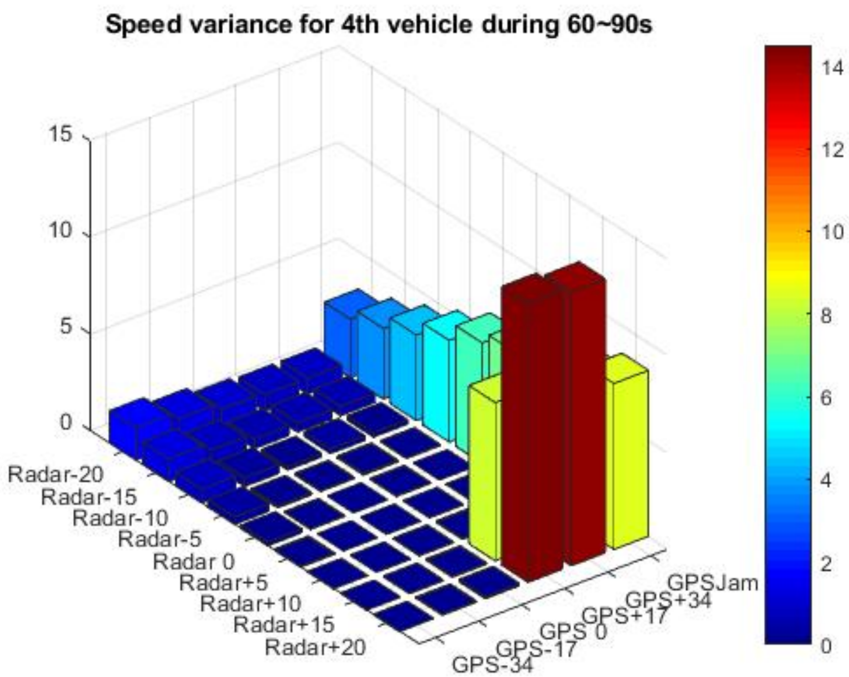

Figure 14 Stabilization of 4th Vehicle's Movement with EBS

Crash severity comparisons To compare the severity of the crashes, Delta-V values are listed in Table 8. All of the crashes can be avoided or mitigated with EBS embedded to CACC controller. However, EBS relies heavily on radar sensor. Once radar is attacked, EBS cannot be properly triggered.

Table 8 Delta-V of Crashed Vehicles without EBS vs. with EBS

Delta-V (m/s)		**GPS attack**								
		-34	**-17**	**0**	**+17**		**+34**		**Jam**	
With/Without EBS					w/o	w/	w/o	w/	w/o	w/
Radar attack	**-20**	-	-	-	-		-		*1.844*	-
	-15	-	-	-	-		-		*1.832*	-
	-10	-	-	-	-		-		*1.825*	-
	-5	-	-	-	-		-		*1.767*	-
	0	-	-	-	-		-		*1.779*	-
	+5	-	-	-	-		-		*1.797*	-
	+10	-	-	-	-		*0.278*	-	*1.799*	-
	+15	-	-	-	*0.138*	*0.118*	*0.704*	*0.362*	*1.822*	-
	+20	-	-	-	*0.551*	*0.514*	*1.228*	*0.812*	*1.842*	-

Discussion Application of EBS with CACC requires further study. Although EBS can avoid most of the crashes, it is still vulnerable when there is incorrect information in radar sensor, which EBS highly relies on. Sensor fusion technology, such as Kalman Filter, may be adopted to reduce the risk of the system. Furthermore, to decide the threshold of braking distance is another issue with EBS. To avoid the frequent mode switches and violent vehicle oscillations, the method to compute the trigger of EBS should be developed.

2.6 Concluding remarks

In this paper, an integrated simulation platform is developed and evaluated for CACC safety under cyber attacks. The developed evaluation platform i) simulates vehicle dynamics; ii) simulates sensor errors and communication delays; iii) is compatible with any CACC controllers; iv) implements state-of-the-art predecessor leader following (PLF) based CACC controller; and v) is capable to quantify crash severity and CACC stability. The output of the platform includes speed variation, headway ratio, and injury probability. The first two MOEs represent the stability of CACC platoons when no crashes happen. The injury probability quantifies the severity of a crash. The proposed evaluation platform can be used to evaluate the safety performance of different CAV controllers under various paroxysmal or extreme events. It is particularly useful when traditional empirical driver models no longer apply. Such situations include, but are not limited to, cyber-attack, sensor failure, and heterogeneous traffic. The proposed platform is validated against data collected from real field tests and evaluated under various cyber-attack scenario. The validation and evaluation results reveal that:

- The vehicle behavior is accurate compared to CACC field data. It ensures that stability and severity measurements output from the platform are accurate.

- The proposed CACC evaluation platform is capable of quantifying the crash severity level. In addition, the severity output is sensitive to test scenario settings.
- Cyber-attacks do not always result in crashes, but they do create larger oscillations.
- It is relatively more dangerous and unstable when both GPS and Radar have errors with the same sign (positive/negative).
- GPS jamming is the most dangerous cyber-attack. Crashes always happen when the GPS is jammed.
- Emergency braking system (EBS) embedded to CACC platoon can effectively avoid most of crashes. But when the radar sensor is attacked with inappropriate information, the crash may not be prevented since EBS relies on radar.
- EBS trigger determination is a critical issue with CACC. To avoid the frequent mode switches and violent vehicle oscillations, the method to compute the trigger of EBS should be developed.

This study only focuses on CACC platoon-wide performance and enables safety evaluation under the setting of 100% CAV market penetration. The next step is to incorporate the proposed evaluation platform with a microscopic traffic simulation software, such as VISSIM, to assess the impact of CAVs in the mixed traffic with various CAV penetration rates tested. For example, the impact of CAV abnormal behavior on nearby human-driven vehicles can be evaluated. Both safety and mobility performance can be quantified. A robust CAV controller is to be developed by considering the sensor fusion under cyber-attack, the reasonable threshold for the mode switch, the trigger of control to human-driven mode. In addition, more CAV modules other than CACC should be developed to enrich application library to enable various CAV test and evaluations.

Chapter 3. Development of a robust CACC algorithm against cyber-attacks

3.1 Introduction

CAVs are being developed at a rapid speed. Some lower level CAV applications are already on the road and fully automated CAVs are expected to be commercialized in a short future. To realize the automation of CAVs, various kinds of controllers are embedded to assist the drivers. CACC is one of the CAV applications that are expected to play an important role, especially on freeways.

As an extension of adaptive cruise control, CACC uses sensors and communication technologies to enable a shorter time headway within vehicle platoons, e.g., as short as 0.6s ([13], [14], [87]). Therefore, it can potentially bring significant road capacity improvement (over 4200 veh/h/lane) and congestion reduction ([13], [15], [31]). Various CACC algorithms have been developed and verified to meet the basic demand on effective platoon movements with string stability maintained ([13]–[15], [31], [32], [35], [88], [89]). However, there are potential risks that existing CACC algorithms cannot deal with and may lead to collisions [90]. For example, when there is a deliberate cyber-attack in communication and sensors or an aggressive cut-in of the human driver, a standard CACC would fail to avoid crashes.

The countermeasure to cyber-attack, as one of the major public concerns toward CAVs, is still not well developed yet and needs to be explored ([25], [27]). The cyber-attack, as a deliberative offensive disturbance, can spoof the identity, tamper with data, repudiate, and disclose the information, and the attack surface can range from ECU, CAN bus, sensors, GPS or mapping, to V2X communications ([26], [27], [83]–[85]). The cyber-attack may lead to wrong decisions of CAVs and severe crashes due to the short gaps between CAVs [90].

On the aspect of traffic flow, when CAVs are on the road, the mixed traffic will be the dominance for a long time. The potential risks in CACC platoons would also affect the surrounding human-driven vehicles. Besides, it is unavoidable for human drivers to cut in front of CAVs unexpectedly, which also leads to some hazardous behaviors with existing CACC algorithms.

An emergency brake assist system can be a solution to dangerous situations, especially to the rear-end crashes [90]. However, the control mode switch between cruise control and braking system is another issue in vehicle automation since there can be a lot of control noises happening ([91]–[93]). That is to say, if triggering EBA is not successful with an improper threshold, there are another potential safety problems in the switch between CACC and EBA. Then those jags in CAV control may interfere with and be magnified along the traffic flow. Furthermore, the jags can result in shockwaves due to the long reaction time of the human drivers [94].

Therefore, whether from the view of CAV controller or the perspective of the influence on the mixed traffic, a more advanced robust CACC algorithm is necessary to be developed. The proposed CACC algorithm in this paper is not only capable of basic functions of CACC, but also able to deal with even extreme or unexpected situations. The rest of this chapter is organized as follows: next section reviews existing CACC algorithms; the third section proposes the CACC algorithm, and its stability is proven in the following section; then simulation-based case studies are presented in the fifth section; finally, the discussions and conclusions are provided in the last section.

3.2 CACC algorithm review

CACC algorithms can be categorized depending on the communication flow topology: predecessor following (PF), predecessor-leader following (PLF), bidirectional (BD), and n-preceding following (including the all-predecessor following (APF)) ([12], [36], [89]). It should be noted that the communication flow is based on the communication connections between the ego-vehicle, or the subject vehicle, and the other vehicles. The predecessor represents the vehicle immediately preceding vehicle, and the leader represents the leading vehicle of the platoon. Since each CACC algorithm collects the information differently, their performances also vary based on their topologies.

As the most prevailing control method, PLF requires the leading vehicle to broadcast its information, such as the location, speed, and the control input. The following vehicles can respond to the leading vehicle with less delay and more stability by sharing the control information. This method has already been proven feasible with field tests ([13], [39]). Compared to PLF, PF controller is less stable since the vehicles only response to their immediate processor ([12], [38]). As a result, fluctuations from downstream cannot be anticipated, and precautions cannot be taken beforehand. BD controller has a similar problem with PF since the algorithm only looks at one vehicle in front. However, since PLF controller only takes the preceding vehicle and leading vehicle into consideration, there are delays in the response of ego-vehicle when one vehicle between those two vehicles has abnormal behavior ([28], [29], [90]).

To improve the safety of the aforementioned CACC algorithms, rear-end collision warning/avoidance (CW/CA) systems are introduced. According to Seiler et al. (1998), CW/CA system design should meet several criteria: should not interfere with the normal driving operation; should perform well in various driving environments; and need to minimize load on the driver attention [52]. However, it is difficult to come up with perfect thresholds on switching mode between CACC and CW/CA controls ([92], [93]). Therefore, some fluctuations, i.e., jerks or control noises, unavoidably happen during mode switches ([91], [95]). That is to say, the ideal scenario would be to have a CACC algorithm embedded with collision avoidance mechanism to ensure a continuous and smooth control without mode switches. Geiger et al. (2012) adopted a method of switching the leading vehicle in their CACC algorithm to have the following vehicles react to any abnormal vehicle immediately and avoid crashes ([96]). The vehicle who deviates from its optimum position most (out of a certain threshold) is targeted as the leading vehicle. However, due to the mode switch is discrete, some fluctuations or noises are also unavoidable in the control process.

N-preceding following controller takes in the status of more than one vehicle to complement the above shortcomings of the PLF controller ([89], [97], [98]). Ge and Orosz (2014) showed that the multiple-vehicle look-ahead strategy reduced the fluctuations in the speed of ego-vehicle even when the leading vehicle was following a human-driven vehicle with an unstable trajectory [98]. APF controller is a special case of the N-preceding following.

In the APF controller platoon, all the vehicles need to broadcast their information through communication and collect the information from other vehicles at the same time. Every ego-vehicle responds to the behaviors of all vehicles that are ahead of it. Therefore, the benefit of APF over PLF is to improve safety during intra-platoon error events [99]. However, the shortcoming of APF is that the stability is not necessarily improved when comparing with PLF. Ploeg et al. (2014) theoretically proved that the two-vehicle look-ahead strategy in CACC did not improve the string stability properties of one-vehicle look-ahead strategy [97]. More information is not always better. More importantly, tuning gains or weights in the algorithm is always a big problem with APF controller.

In sum, the existing CACC algorithms have their pros and cons. Without interference from the outside world, PLF is the most stable controller. However, PLF is not safe enough under cyber-attacks, cut-in of an unconnected vehicle, or other sudden abnormal interferences. N-preceding following is robust against abnormal impact but is not always stable. Therefore, this research aims to overcome the shortcomings of traditional CACC algorithms by using the combination of N-preceding following and PLF controls. The proposed CACC algorithm is expected to have the following features:

- String stable and safe under normal cruising scenario, i.e., without inference from the outside world
- Capable of covering the full range of cruising speed
- Ensuring the stability and safety under sudden interferences, such as cyber-attack

- Equivalent to embedding collision avoidance without control jerks and keeping smoothness in the vehicle behaviors

3.3 Algorithm development

3.3.1 Control architecture

The primary sensor equipment and communication structure of the proposed CACC is shown in Figure 15. Every CAV uses a radar sensor to detect its preceding objectives and a dedicated short range communication (DSRC) device to share (send & receive) the data through basic safety message (BSM) protocol ([44], [46]).

The CACC algorithm makes driving decisions, with a bi-level controller – high-level and low-level, based on the data from sensors. The sensed data include the distance to the other vehicles, speed, and control variable of the other vehicles. The sequences of the vehicles are assumed to be known to all. The output of the high-level controller is the target speed of ego-vehicle. With the target speed and the actual speed as feedback, a low-level controller calculates the throttle or brake actions as the input of vehicle dynamics so as to update the acceleration and speed.

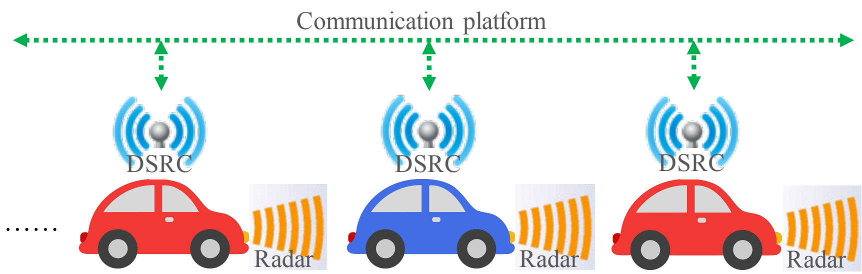

Figure 15 Sensor and Communication Structure of CACC Platoon

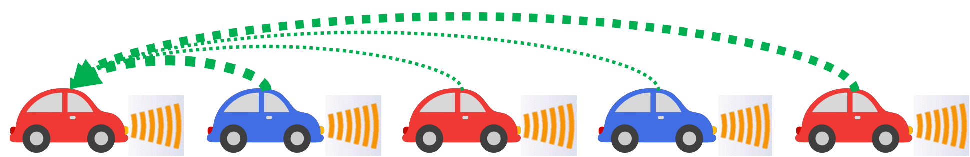

a. Focusing on the leading vehicle and the preceding vehicle in normal cruise

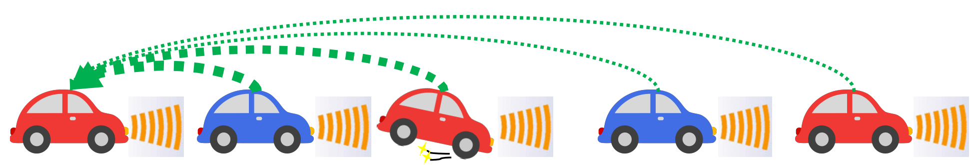

b. Focusing on the abnormal vehicles in an emergency situation

* Widths of the connections represent the weights of preceding vehicles to the ego-vehicle

Figure 16 Mechanism of Robust CACC

3.3.2 Algorithm design

The proposed CACC mechanism is as Figure 16. The goal is to maintain the desired time gap to the preceding vehicles in any conditions. The algorithm can be explained with two cases. One is the case when the system works well, and the platoon is normally cruising (Figure

16(a)). In this case, the CACC algorithm focuses on the leading vehicle and the corresponding preceding vehicle of ego-vehicle, which is close to the PLF controller. That means the weight of the leading vehicle and the preceding vehicle is relatively high compared to the other vehicles to make sure the string stability. The other case is when some unexpected interference happens, such as cyber-attacks (Figure 16 (b)). The ego-vehicle will gradually turn the focus to the abnormal vehicles with dynamic weight mechanism in CACC algorithm and tend to implement APL controller. Therefore, the vehicles can take actions in time to avoid crashes. It should be noted that the control mode switch between these two cases is smooth and continuous.

The structure block diagram of proposed CACC is shown in Figure 17. The fundamental purpose of this algorithm is to let the CACC platoon cruise in the desired speed and maintain a constant time gap at the same time. The string stability of the platoon should also be guaranteed. This algorithm relies on the radar detection data and the information being shared by the other vehicles through communications.

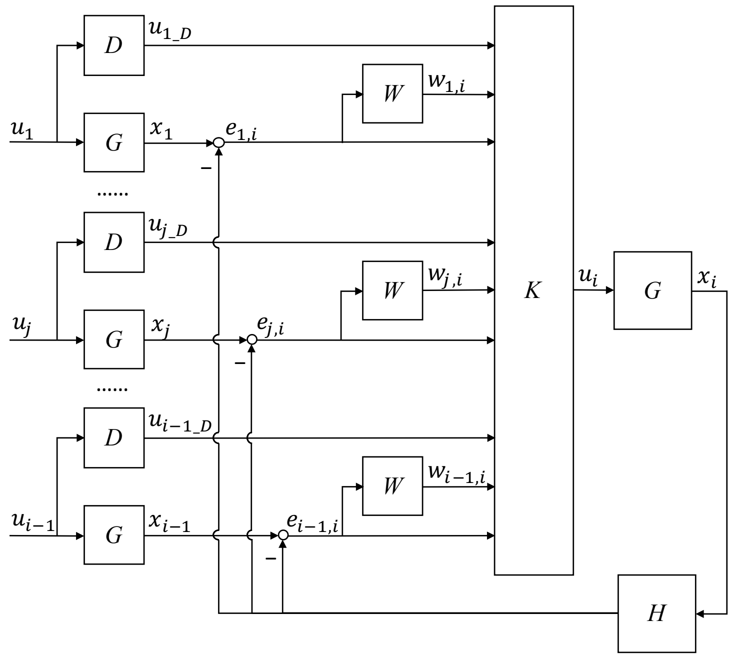

Figure 17 CACC Structure Block Diagram

The time gap is adopted here instead of the time headway, which is adopted in most traditional CACC algorithms, in consideration of the low-speed cruise. To make the CACC platoons being capable of any speed range, especially the low speed, maintaining a constant time gap would be safer since the corresponding desired distance headway can be smaller than a vehicle length. On the other hand, if a vehicle without communicable connection cuts in mandatorily, to keep a constant gap is more conservative because the vehicle length is unknown.

A. High-level controller

In the high-level controller, the control action of ego-vehicle is the sum of a feedback term

$u_i(t)$ and a feedforward term $v_{i_T}(t)$:

$$v_{i_D}(t) = u_i(t) + v_{i_T}(t) \tag{3.1}$$

where $v_{i_D}(t)$ is the desired speed (i.e., control action); $u_i(t)$ is the output of a proportional-derivative (PD) controller. The goal of the PD feedback control is to maintain the desired time gaps to the preceding vehicles:

$$u_i(t) = \sum_{j=1}^{i-1} ({w_{j,i}}^T \cdot \begin{bmatrix} e_{j,i}(t) \\ \dot{e}_{j,i}(t) \end{bmatrix}), \qquad i \geq 2 \tag{3.2}$$

where $i\ or\ j \in I = \{1, 2, \dots\}$ indexes vehicle in the platoon when $j = 1$ is the leading vehicle; vehicle i represents the ego-vehicle; t is time; "·" denotes the derivative respect to time; $w_{j,i}(t)$ is the dynamic control weights of the ego-vehicle in regard to the vehicle j; $e_{j,i}(t)$ is the spacing error to the vehicle j from the ego-vehicle:

$$e_{j,i}(t) = x_j(t) - x_i(t) - (i - j)g_d \cdot \dot{x}_\imath(t) - (i - j) \cdot L_j \tag{3.3}$$

where $x_j(t)$ is the location of the vehicle j; g_d means the desired inter-vehicle time gap; and L_j is the length of the vehicle j.

The weights $w_{j,i}(t)$ are made dynamically change according to the spacing error, in order to enable the CACC platoon to be responsive to any abnormal behavior of the vehicles within a platoon. That is to say, if a vehicle is out of the range where it should be because of any reason, such as a cyber-attack, the weights for its following vehicles in regard to this vehicle will increase and force the following vehicles to respond to that abnormal vehicle to avoid the collision. Otherwise, if there is nothing abnormal, the weights are mainly distributed on the leading vehicle and the preceding vehicle. For the other vehicles, the weights are almost evenly distributed. The dynamic weights are calculated by dividing constant total weights $w = \begin{bmatrix} w_1 \\ w_2 \end{bmatrix}$ as follows.

$$w_{j,i}(t) = \begin{cases} \dfrac{\alpha_{j,i}(t)}{\sum_{j=1}^{i-1} \alpha_{j,i}(t)} \cdot w + w_p, & for\ j = i-1 \\ \dfrac{\alpha_{j,i}(t)}{\sum_{j=1}^{i-1} \alpha_{j,i}(t)} \cdot w, & for\ j \neq i-1 \end{cases} \tag{3.4}$$

where additional constant weight $w_p = \begin{bmatrix} w_3 \\ w_4 \end{bmatrix}$ is added to the preceding vehicle since it is most critical for the safety of ego-vehicle. The intermediate term $\alpha_{j,i}$ is introduced to calculate the dynamic weights with the information from the vehicle j:

$$\alpha_{j,i}(t) = 10^{-e_{j,i}} + \beta \tag{3.5}$$

where β is used to give more weight on leading vehicle when normal cruise case, and is defined as:

$$\beta = \begin{cases} 10, & for\ j = 1 \\ 0, & for\ j > 1 \end{cases} \tag{3.6}$$

Therefore, if the platoon is stably cruising with insignificant spacing errors, then $\alpha_{j,i}(t) = 1 + \beta$, yielding:

$$w_{j,i}(t) \approx \begin{cases} \dfrac{11}{i+9}w, & for\ j = 1 \\ \dfrac{1}{i+9}w, & for\ 1 < j < i-1 \\ \dfrac{1}{i+9}\mathrm{w} + w_p, & for\ j = i-1 \end{cases} \tag{3.7}$$

In addition, connectivity is taken advantage of by having the control actions of preceding vehicles shared among the platoon to help ego-vehicle responds faster to the speed change of preceding vehicles. Target speed v_{i_T} is calculated as the weighted average of all preceding vehicles' desired speed and serves as the feedforward term:

$$v_{i_T}(t) = \frac{1}{w_1 + w_3} \times \sum_{j=1}^{i-1} ({w_{j,i}}^T \cdot \begin{bmatrix} 1 \\ 0 \end{bmatrix} \cdot v_{j_D}(t - \theta)) \tag{3.8}$$

where $v_{i_T}(t)$ is the target speed of the ego-vehicle; v_{j_D} is the desired speed of vehicle j; θ is communication delay.

B. Low-level controller

Due to the nonlinearity of vehicle dynamics, a low-level controller is needed to determine the throttle and brake inputs so that the desired speed from the high-level controller can be accurately achieved. A well-accepted version of the low-level controller is adopted which utilizes the inverse engine map and a set of feedforward signals (e.g., vehicle speed, engine speed, transmission ratio) to pre-compensate the nonlinear behaviors of the engine and transmission system, leading to a first-order linear relationship between desired acceleration a_{i_d} and actual acceleration a_i [100]:

$$\tau_i \dot{a}_i(t) = a_{i_d}(t) - a_i(t) \tag{3.9}$$

where τ_i is the system lag.

In this study, however, the command from the high-level controller is desired speed instead of desired acceleration. To decide the desired acceleration, speed feedback is added, yielding a second-order system:

$$\begin{gathered} a_i(t) = \ddot{x}_i(t) \\ a_{i\_d}(t) = k_{i_l}\left(v_{i_D}(t - \emptyset_i) - \dot{x}_i(t)\right) \\ \tau_i \dot{a}_i(t) = a_{i\_d}(t) - a_i(t) \end{gathered} \tag{3.10}$$

where k_{i_l} is the low-level control gain, and $\emptyset_i$ is the actuator delay.

Taking the Laplace transfer of (3.10), the vehicle dynamics with low-level control can be described by the transfer function in s domain:

$$F(s) = \frac{L\left(\dot{x}_i(t)\right)}{L(v_{i_D}(t))} = \frac{k_{i_l}}{\tau_i s^2 + s + k_{i_l}} e^{-\emptyset_i s} \tag{3.11}$$

where $F(s)$ is the transfer function of vehicle (speed) dynamics, and $L(\cdot)$ denotes Laplace transfer.

The coefficients in (3.10) can be fitted from the vehicle's step response using MATLAB system identification tool. For the Yaris vehicle model provided by PreScan, the fitting results are:

$$F(s) = \frac{1}{1.72s^2 + 2s + 1} e^{-0.74s} \tag{3.12}$$

for accelerating and

$$F(s) = \frac{1}{0.42s^2 + 1.26s + 1} e^{-0.31s} \tag{3.13}$$

for braking.

3.4 String stability analysis

The *String Stability* property is widely used to study the stability performance of a CACC system. It indicates the capability of attenuating the disturbance from downstream. Based on the definition in [82], a CACC vehicle is string-stable if:

$$|SS(\imath\omega)| = \left|\frac{X_i(\imath\omega)}{X_{i-1}(\imath\omega)}\right| \leq 1, \quad i \geq 2, \omega > 0 \tag{3.14}$$

where $SS(\imath\omega)$ is the transfer function between the position of vehicle i-1 and vehicle i, with s substituted by $\imath\omega$; ω is the frequency of perturbation, $\imath$ is the imaginary unit that $\imath^2 = -1$, and $X_i(s)$ and $X_{i-1}(s)$ are the Laplace transfer of $x_i(t)$ and $x_{i-1}(t)$.

In the proposed CACC algorithm, the ego-vehicle makes a decision based on the states of all the preceding vehicles. At the same time, behaviors of the preceding vehicles are coupled, i.e., a preceding vehicle's behavior is further decided by its own preceding vehicle(s). The string stability analysis would be too complicated when explicitly considering the states of all the preceding vehicles and couplings between them. In addition, the preceding vehicles may or may not use the same CACC algorithm with ego-vehicle. Thus, the coupling effects between preceding vehicles are unknown in the real world. For these reasons, a virtual leading vehicle is introduced to represent the weighted average position of all the preceding vehicles:

$$x_v = \sum_{j=1}^{i-1} \frac{\alpha_{j,i}(t)}{\sum_{j=1}^{i-1} \alpha_{j,i}(t)} x_j \tag{3.15}$$

where x_v is the position of that virtual leading vehicle. Using (3.15), the perturbation on any single or multiple preceding vehicles can be reflected as a corresponding perturbation on the virtual leading vehicle. In this case, the string stability of ego-vehicle is guaranteed if (3.14) holds for any perturbation on the virtual leading vehicle.

Inserting (3.3), (3.4), (3.15) into (3.2) and taking the Laplace transfer, we have:

$$U_i = w_p \begin{bmatrix} 1 \\ s \end{bmatrix} \left(X_{i-1} - H_p X_i\right) + w \begin{bmatrix} 1 \\ s \end{bmatrix} (X_v - H_v X_i) \tag{3.16}$$

where $U_i(\mathrm{s}) = L(u_i(\mathrm{t}))$, $X_v(\mathrm{s}) = L(x_v(\mathrm{t}))$, $K_p = {w_p}^T \begin{bmatrix} 1 \\ s \end{bmatrix}$ and $K_v = w^T \begin{bmatrix} 1 \\ s \end{bmatrix}$; H_p is the spacing policy respect to the nearest preceding vehicle:

$$H_p = sg_d + 1 \tag{3.17}$$

H_v is a non-linear spacing policy with respect to the virtual leading vehicle:

$$H_v = sg_v + 1 \tag{3.18}$$

where g_v is the weighted average desired gap to the preceding vehicles and $g_v = \sum_{j=1}^{i-1} \left(\frac{\alpha_{j,i}(t)}{\sum_{j=1}^{i-1} \alpha_{j,i}(t)} (i-j) g_d\right)$.

Based on (3.7), we have (3.18) in the vicinity of steady status:

$$H_v \approx s\frac{i^2 + 19i - 20}{2(i+9)} g_d + 1 \tag{3.19}$$

To present the non-significant changes in the spacing error relative to the virtual leading vehicle and the validity of the assumption in (3.7), g_v in (3.18) is drawn with the simulation results similarly in 3.5.1. In this case, the platoon is cruising under a pre-determined speed profile, which changes between 25.5 m/s and 29.5 m/s with the acc/deceleration rate of (1/80)g. The acceleration happens during 10-40s, and the deceleration happens during 50-80s. From Figure 18, it can be observed that g_v does not have significant changes, and varies around 3.5s, which is $5.8g_d$ that can be derived from (3.19) by replacing i with 8. Therefore, the assumption of (3.7) is acceptable.

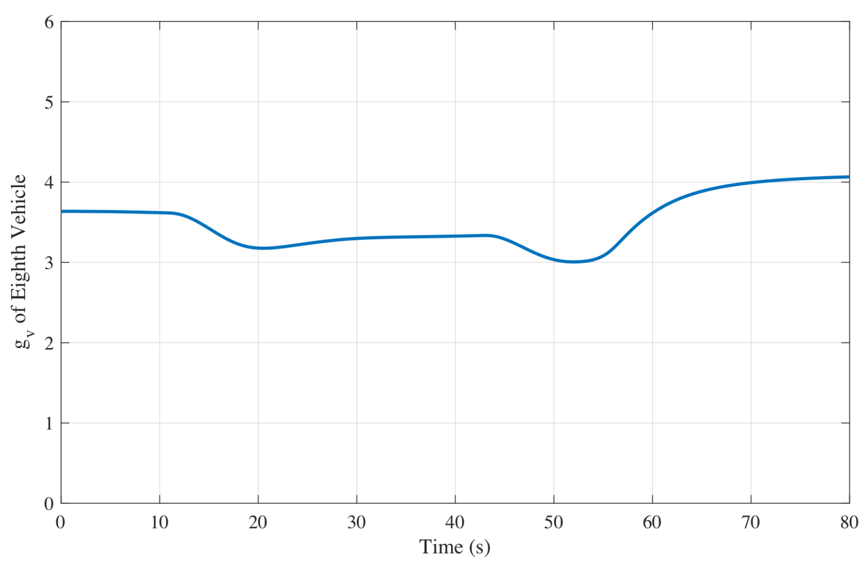

Figure 18 g_v of Fifth Vehicle when Cruising under Pre-determined Speed Profile

Furthermore, taking Laplace transfer of (3.8) and combining it with (3.11) yield:

$$V_{i_T} = \frac{1}{G}\frac{D}{w_1 + w_3}(w_1 X_v + w_3 X_{i-1}) \tag{3.20}$$

where $V_{i_T}(s) = L(v_{i_T}(t))$, $G(s) = F(s)/s$ and $D(s) = e^{-\theta s}$.

Assuming the vehicles start from rest and using (3.1), (3.16), and (3.20), the relationship between the ego-vehicle and the preceding one is given by:

$$SS(s) = \frac{X_i}{X_{i-1}} = \frac{GK_p + \frac{w_p}{w + w_p}D}{1 + G(K_v H_v + K_p H_p)} \tag{3.21}$$

where $K_p = w_p{}^T \begin{bmatrix} 1 \\ s \end{bmatrix}$ and $K_v = w^T \begin{bmatrix} 1 \\ s \end{bmatrix}$. Note that (3.21) has the same form with $SS(s)$ of PLF CACC [101] due to the introduction of the virtual leading vehicle.

To fulfill (3.14), the control weights and desired gap need to be properly chosen so that the Bode magnitude of (3.21) is below one at any frequency and for both accelerating and braking phases. Assuming an average communication delay of 0.05s (which is also adopted in the previous part, corresponding to an update frequency of 20Hz with zero-order hold approach) and the platoon size of 10 vehicles, the Bode diagrams for the 10th vehicle with $g_v \approx 7.1 g_d$ are shown in Figure 19. The control weights used are $w_1 = 0.1, w_2 = 0.15, w_3 = 0.15, w_4 = 0.45$, and the desired gap g_d is 0.6s.

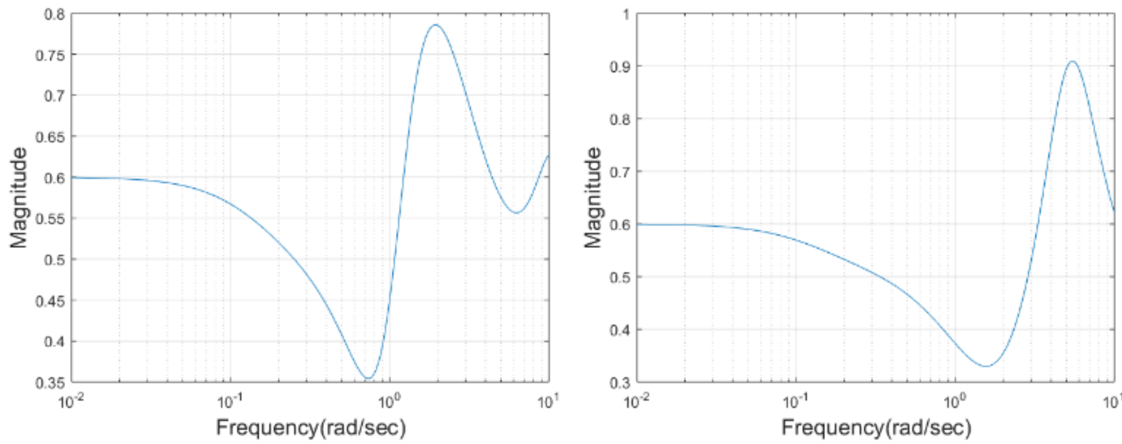

(a) Accelerating (b) Braking

Figure 19 Bode Diagram of (3.21) for both Accelerating and Braking

Similarly, it can be proven that the Bode magnitude is below 1 for the 2^{th}~9^{th} vehicle by assuming different g_v. It is found that the string stability is automatically fulfilled as long as $g_v \leq 8g_d$. Considering that in an emergency condition the actual leading vehicle can have an increased weight up to w, leading to a $g_v = (i-1)g_d$ for vehicle i, a maximum platoon size of 8+1=9 vehicles is recommended.

3.5 Simulation tests

On top of the theoretical proof, the algorithm is also implemented in several scenarios to verify its robustness and stability. A dedicated simulation platform developed by [90] is adopted. The basic settings are as follows:

- The platoon consists of five vehicles, assuming a homogeneous TOYOTA

Yaris CACC platoon;

- Vehicle specifications are obtained from TASS PreScan [82];
- The radar sensor is used to detect the relative distance and speed of the preceding vehicle;
- DSRC transmitters and receivers are used to share vehicle information;
- Sensor errors and communication delay follow the settings in [90], which include the radar sensor error as 5% and the DSRC communication delay as 50ms;
- The desired gap g_d is 0.6s;
- Total weights are $w_1 = 0.1\ and\ w_2 = 0.15$ for all (w) and $w_3 = 0.15\ and\ w_4 = 0.45$ for the preceding vehicle (w_p);

3.5.1 Normal cruise with varying desired speed

As the first step, the base function of the proposed CACC algorithm is tested (as Figure 20).

A. Scenario design

A pre-determined speed profile from [13] is used as the desired speed of the leading vehicle. The speed profile consists of several cycles of speed changing between 25.5 m/s (57.0 mi/h) and 29.5 m/s (66.0 mi/h) with different acc/deceleration rates, i.e. (1/80) g, (1/40) g, (1/20) g, and (1/10) g. This speed pattern is expected to appear in a real driving environment when the leading vehicle follows a moderately congested traffic flow [90].

Besides, a lower speed profile is also tested to show the proposed algorithm is capable of dealing with low cruise speed range. The lower speed profile has the same patterns as the one above, but the speed magnitude changes between 3.5 m/s (7.8 mi/h) and 7.5 m/s (16.8 mi/h). It mimics the speed pattern of the congested traffic condition.

The goal of this scenario is to demonstrate: i) the proposed algorithm functions proper and stable under various normal traffic conditions; secondly, to compare with the field test results in [13] as ground truth to validate the capability of the algorithm in the aspect of the normal cruise.

B. Simulation results

From Figure 20, the speed and distance gap trajectories present that the CACC platoon can closely follow the pre-defined desired speed on the whole under both high and low-speed ranges.

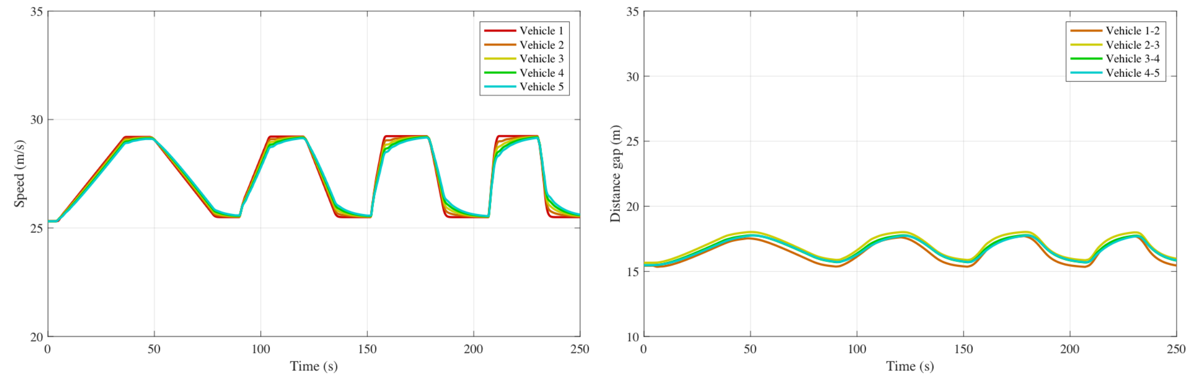

a) High-speed range

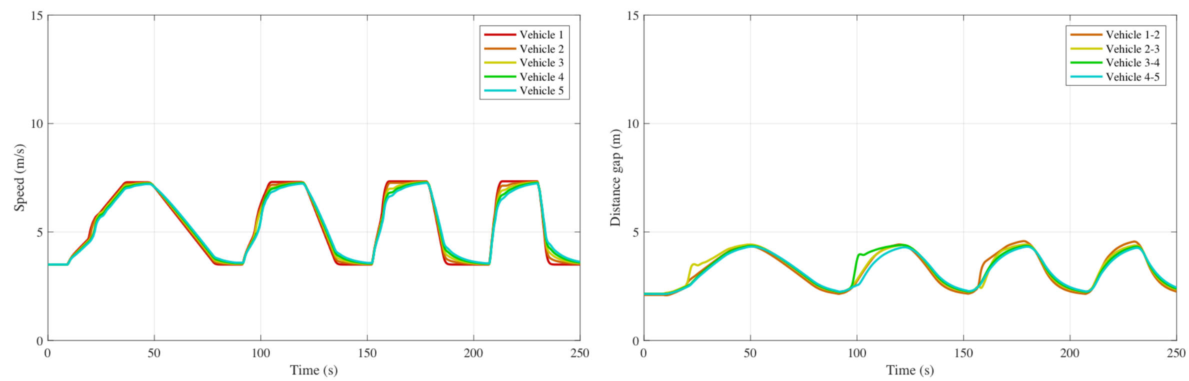

b) Low-speed range

Figure 20 Test Results of CACC Platoon under Varying Desired Speed

However, when there is acc/deceleration of the desired speed, some fluctuations are observed. The following vehicles tend to have more fluctuations compared to their preceding vehicles, but they return to the stable status after a while. The delay in the response of the following vehicles is considered as the result of the vehicle dynamics delay, which also exists in other research ([13], [14], [87]). Some relatively high-frequency fluctuations are observed under low-speed profile. This is mainly due to the gear shift during acc/deceleration.

3.5.2 Abnormal behaviors caused by cyber-attack in the middle of the platoon

This scenario is simulated to validate the robustness of the algorithm against the cyber-attack of a vehicle in CACC platoon. For this purpose, several scenarios are tested where the abnormal behaviors are caused by cyber-attack in the middle of the platoon. The scenarios are categorized into two – one is minor and the other one is severe cyber-attack. The minor cyber-attack means the case that caused only turbulences in the platoon movement but no crashes, and the severe cyber-attack means that the hacked vehicle has extreme behaviors and it may result in crashes. More details are provided in the scenario descriptions.

In the simulation scenarios, five vehicles cruise at the desired speed of 30m/s. The total simulation time for presentation is 50s (90s in the second case of the minor cyber-attack scenario). Then cyber-attack happens to one of the vehicles from a certain time point, i.e., to the 3rd vehicle from the 20s (10s in the second case of the minor cyber-attack scenario). That is to say, the sensor or the command on the 3rd vehicle get hacked, and the given data are false values. The false values would mislead the vehicle with a fake acceleration or deceleration of its preceding vehicles so that the vehicle would have abnormal behaviors. This is a dangerous situation because if the following vehicles (i.e., 4th and 5th) do not respond properly or delay in responding, they will fluctuate or even crash.

In addition, for the comparison purpose, an existing PLF algorithm with fixed weights is tested in the same situation. A field-verified algorithm in [13] is selected in this scenario. Considering that traditional CACC is used for safe cruises but not for dangerous situations, two solutions are provided to make fair comparisons. Firstly, an EBS is attached to this CACC algorithm. This allows the vehicles to switch the control mode between CACC and EBS according to the actual distance vs. safety distance to the preceding vehicle. PATH EBS algorithm is adopted for this use ([52]). In the second solution, the leading vehicle is transferable, as the similar mechanism in [96]. The vehicle with the biggest spacing error, by an amount greater than a threshold, is targeted as the leading vehicle to the following vehicles. The threshold is needed for the steady leading vehicle lock and the corresponding stable platoon behaviors in the steady state ([96]).

The MOE – gap ratio – is adopted as in previous chapter for a quantitative evaluation. The gap ratio is calculated as follows, which replaces the headway with the gap in (2.33):

$$r_g = \frac{t_G}{t_g} \tag{3.22}$$

where r_g is the gap ratio, t_G is the target time gap, and t_g is minimum actual time gap. A greater gap ratio implies a smaller minimum gap and increased the likelihood of collision.

3.5.2.1 Minor cyber-attack

A. Case 1 – short braking

In this case, Scenario 1-2 in [90], the fake data −34m and −15m are added to the GPS value and the radar sensor, respectively. False data are formulated as follows, where the notations are the same as in Chapter 2:

$$d_R(t) = \begin{cases} d(t) + \varepsilon_R, & \forall\, t \in [0,20] \\ d(t) + \varepsilon_R - 15, & \forall\, t \in (20,50] \end{cases} \tag{3.23}$$

$$d_{GPS}(t) = \begin{cases} d(t) + \varepsilon_{GPS}, & t < 20 \\ d(t) + \varepsilon_{GPS} - 34, & t \geq 20 \end{cases}$$

where $d_R(t)$ or $d_{GPS}(t)$ is the measured distance at time t, $d(t)$ is the true distance at time t, $\varepsilon_R(t)$ or $\varepsilon_{GPS}(t)$ is the sensor noise at time t.

The speed, acceleration trajectories of the vehicles, the time and distance gaps between adjacent vehicles are drawn in Figure 21. The cyber-attack causes a short and hard brake to the 3rd vehicle and then the vehicle accelerates back to the desired speed. The following vehicles react to the abnormal behavior, but with different level of fluctuations using different algorithms.

The behaviors, including the accelerations and the gaps, in the proposed robust CACC algorithm are reacting properly and smoothly until the platoon recover to the steady state.

However, with the traditional PLF algorithm with EBS, severe fluctuations in the speed and acceleration are observed (in red circles). The distance gap descends to 2m, which indicates dangers and may cause discomfort to the occupants. From the figures, it can be observed that the EBS is not properly triggered due to the issues of the mode switch – proper threshold selection and harsh transition.

For the traditional PLF algorithm with transferable leading vehicle, the overall performance is good but a control jerk in the acceleration profile (in red circle), between the steep slopes. The 4th and 5th vehicles decelerate almost as hard as the 3rd vehicle at first, since the radar sensors are playing main roles at this time. However, before the 3rd vehicle become new leading vehicle, the original leading vehicle (1st vehicle), which is far ahead of them, drags the vehicles to move forward. Therefore, increases in the accelerations are observed in the 4th and 5th vehicles even though the 3rd vehicle keeps decelerating hard. When the spacing error of the 3rd vehicle increases enough to be the new leading vehicle, the deceleration rates of the 4th and 5th vehicles drops again to follow the 3rd vehicle. The same issue, the control noise, exists in this leading vehicle transfer as EBS. However, the proposed algorithm can avoid this issues with dynamic weights so that the platoon was controlled smoothly.

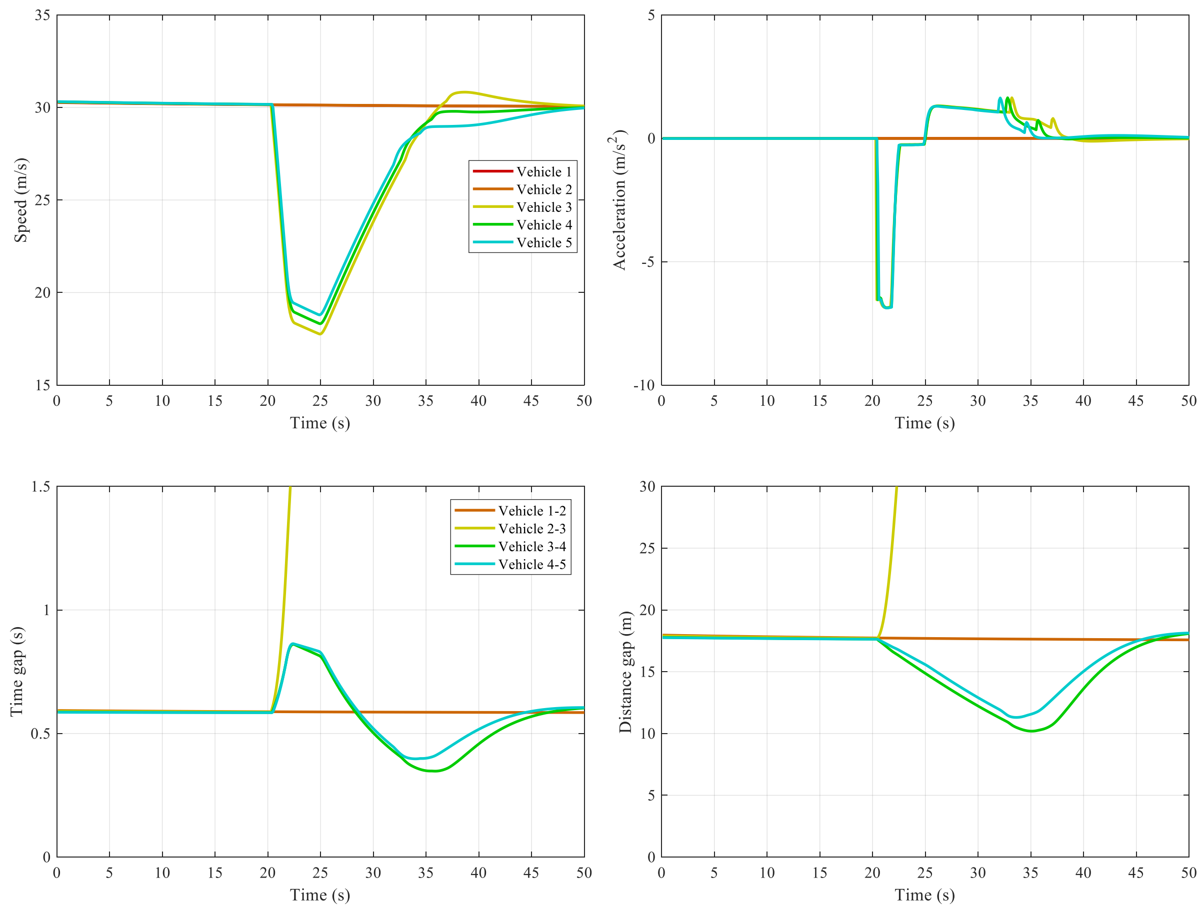

(a) Robust CACC algorithm

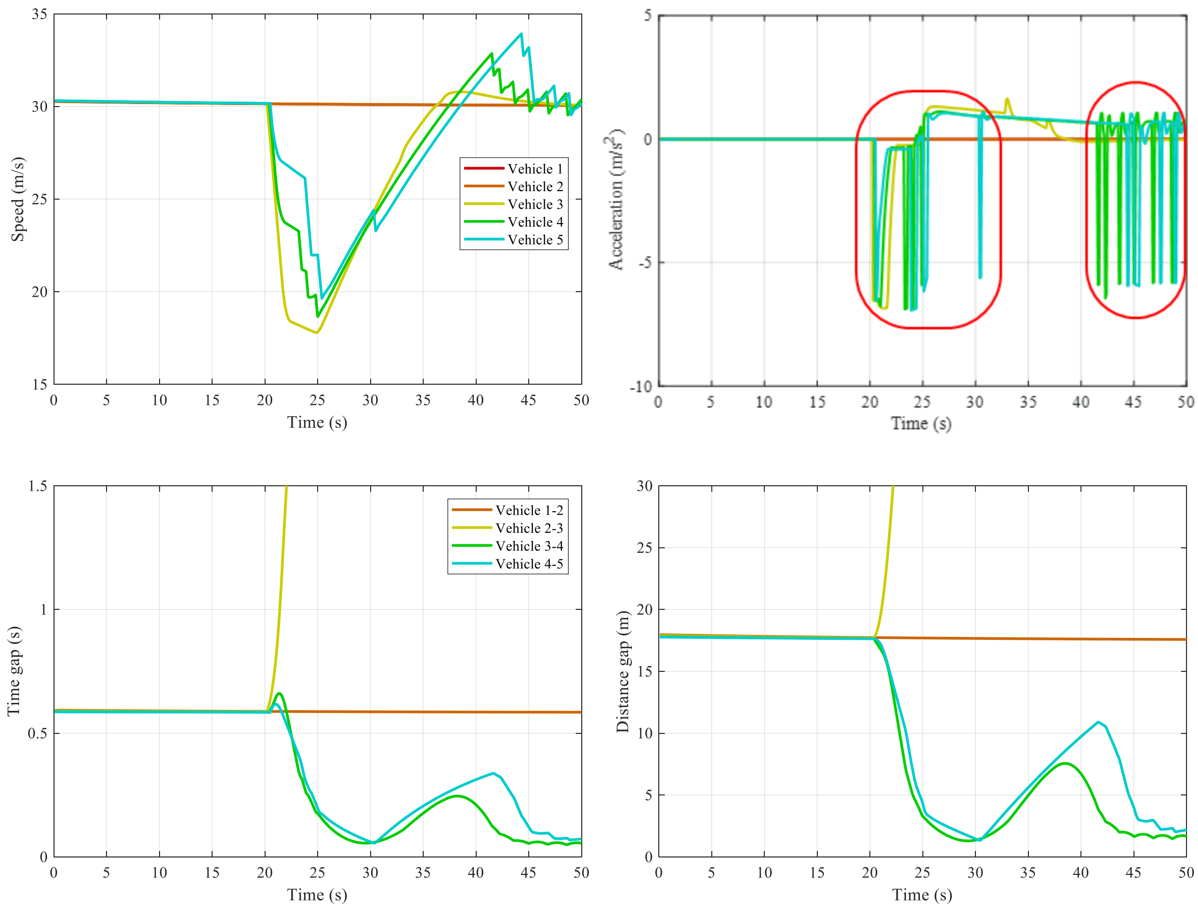

(b) Traditional PLF algorithm with EBS

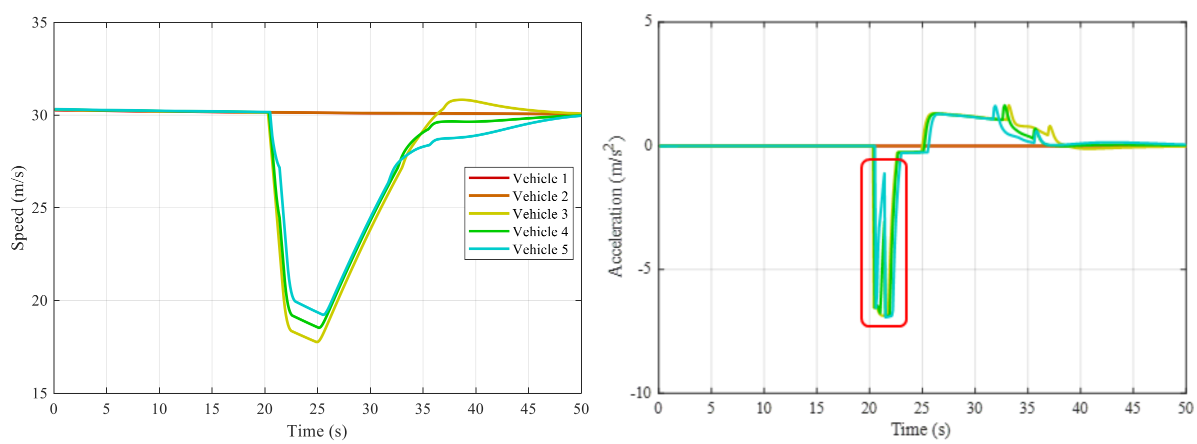

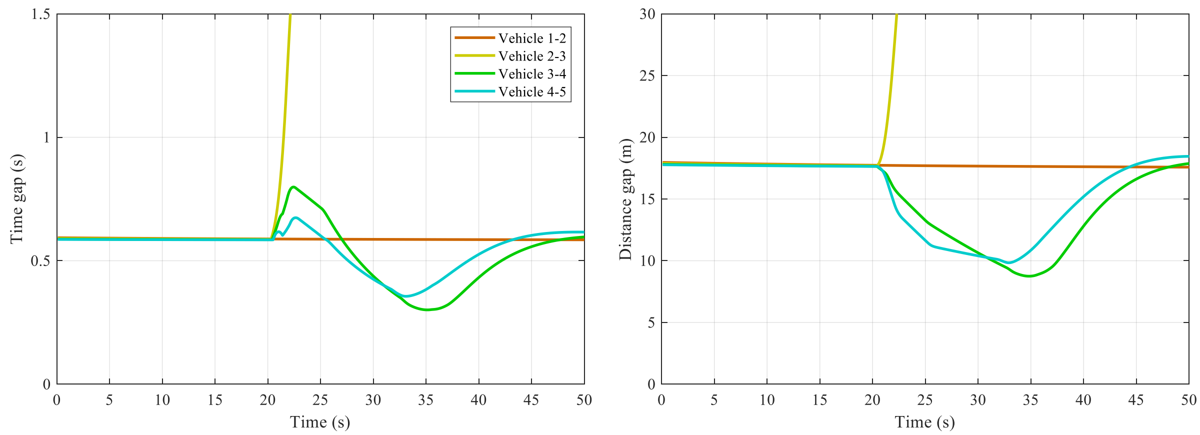

(c) Traditional PLF algorithm with transferable leading vehicle

Figure 21 Test Results of Minor Cyber-attack (GPS −34 Radar −15)

The gap ratio results are listed in Table 9 for a quantitative evaluation. The gap ratios of the 4th vehicle with the robust CACC is 1.72, while with the traditional PLF algorithm with EBS and with transferable leading vehicle, the values are 12.37 and 1.99. This indicates that the robust CACC controls the platoon most safely, or robustly. The platoon controlled by the traditional PLF algorithm with EBS is the most dangerous one.

Table 9 Platoon Stability Analysis of Minor Cyber-attack Case 1

Vehicle	Robust CACC algorithm	Traditional PLF with EBS	Traditional PLF with transferable leading vehicle
VEH 3	1.02	1.02	1.02
VEH 4	1.72	12.37	1.99
VEH 5	1.51	10.75	1.69

B. Case 2 – speed fluctuation

This case is assuming the desired gap of the third vehicle is changing suddenly as (3.24). Under this cyber-attack, the 3rd vehicle goes back and forth between acceleration and deceleration.

$$g_d(t) = \begin{cases} 0.6s, & t < 10 \\ 1.1s, & 10 \le t < 30 \\ 0.6s, & 30 \le t < 50 \\ 0.9s, & 50 \le t < 70 \\ 0.6s, & 70 \le t \end{cases} \tag{3.24}$$

where $g_d(t)$ is the desired gap of the third vehicle at time *t*.

The behaviors in the proposed robust CACC algorithm (Figure 22 (a)) and in the traditional PLF algorithm with EBS (Figure 22 (b)) are reacting properly and smoothly until the platoon recover to the steady state. The fluctuations of the 3rd vehicle speed are too small to trigger EBS. For the 4th vehicle, the errors from the preceding 3rd vehicle and the leading 1st vehicle cancelled out and a new state with shorter distance gap is achieved without EBS. This shows that though the control of the traditional PLF with EBS is smooth, the safety is not assured.

For the algorithm with transferable leading vehicle, the overall performance is good but with unnecessary control jerks in the acceleration profile (in red circles, Figure 22 (c)). The control noises happen, when the 3rd vehicle become new leading vehicle by replacing the original leading vehicle (1st vehicle). The reason is the abrupt change in the leading vehicle.

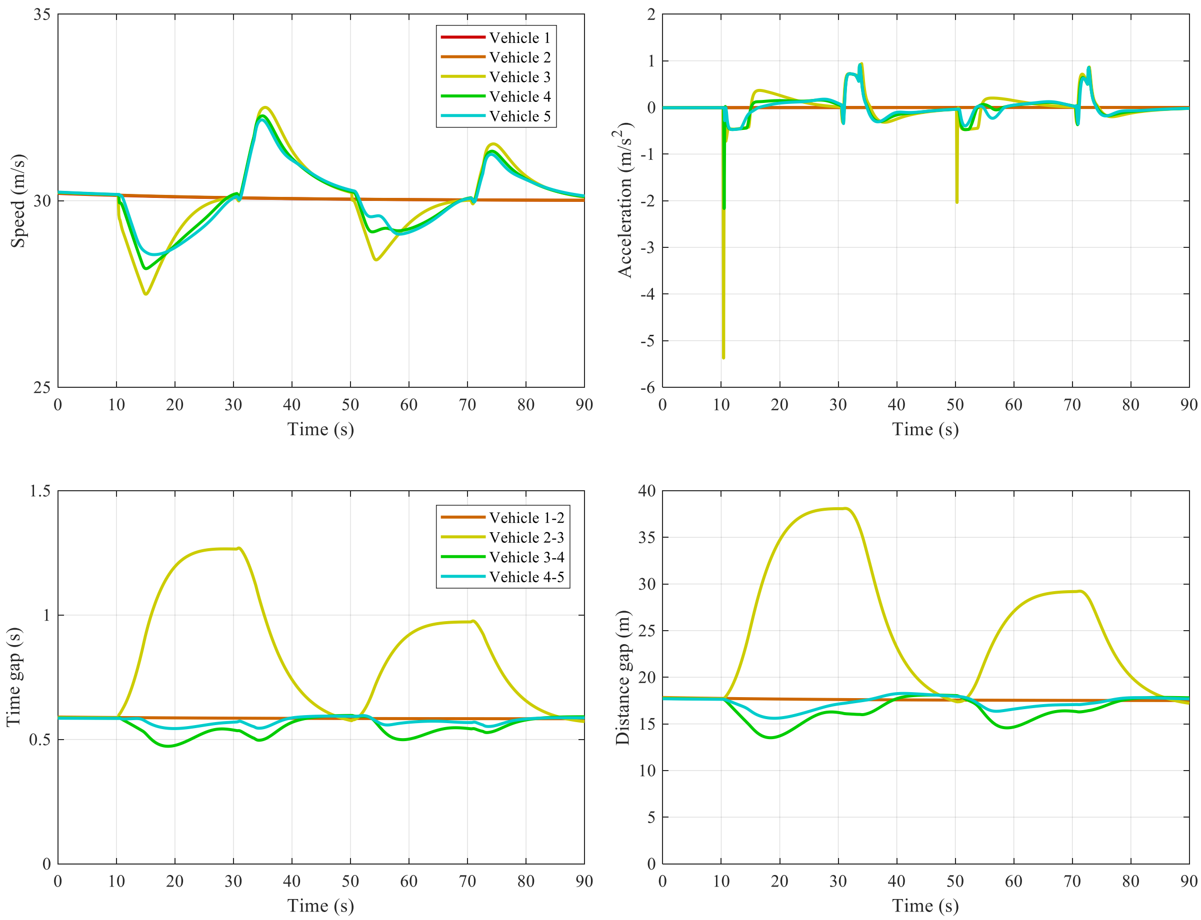

(a) Robust CACC algorithm

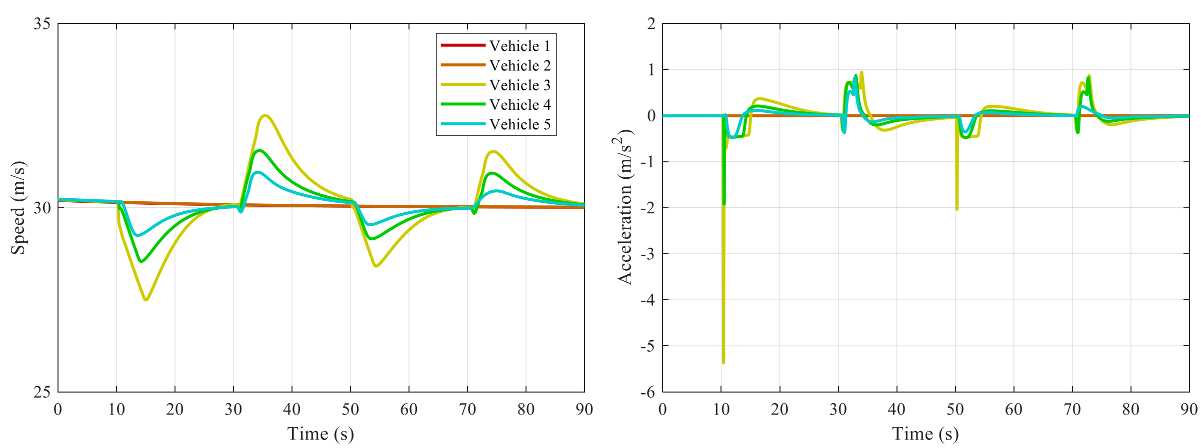

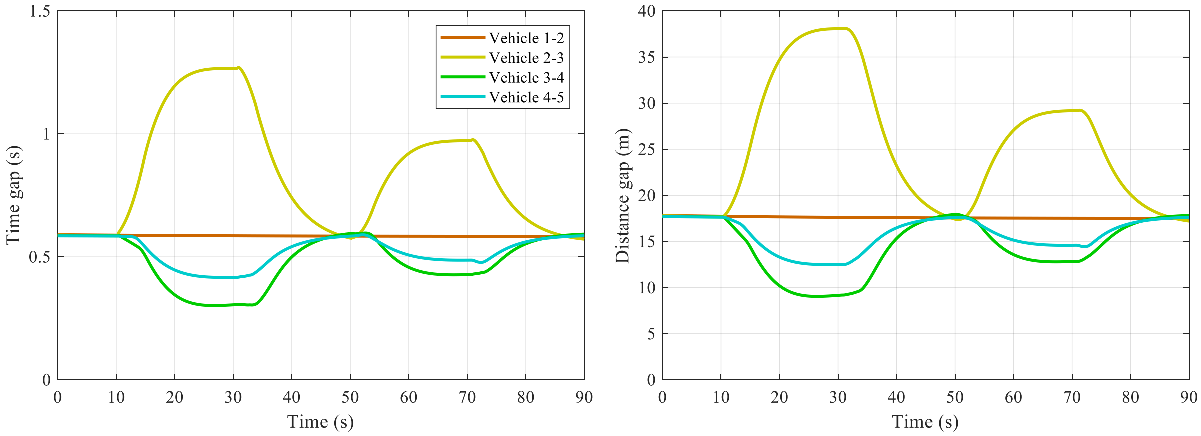

(b) Traditional PLF algorithm with EBS

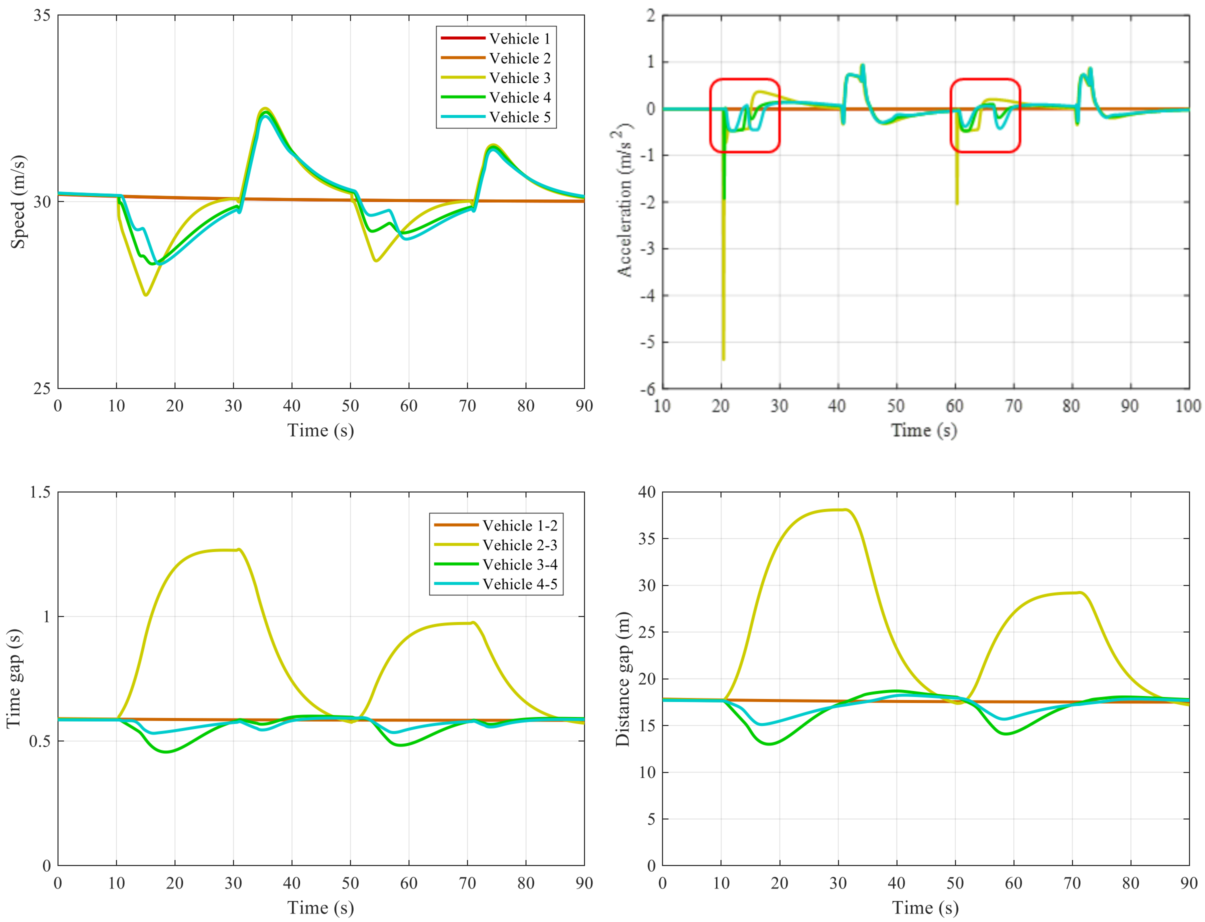

(c) Traditional PLF algorithm with transferable leading vehicle

Figure 22 Test Results of Minor Cyber-attack (varying desired gap)

The gap ratios in Table 10 show that the robust CACC controls the platoon most safely. The problem of the traditional PLF algorithm with EBS is reflected with high values of gap ratios. Besides, the gap ratio of the 5th vehicle is smaller than the 4th vehicle, which means the string is still stable.

To sum up, the robust CACC satisfies the safety and the smooth control better than the other two algorithms in this case.

Table 10 Platoon Stability Analysis of Minor Cyber-attack Case 2

Vehicle	Robust CACC algorithm	Traditional PLF with EBS	Traditional PLF with transferable leading vehicle
VEH 3	1.05	1.05	1.05
VEH 4	1.27	1.99	1.32
VEH 5	1.10	1.44	1.13

3.5.2.2 Severe cyber-attack

A. Case 1 – communication jam

For the severe cyber-attack, GPS jam condition is selected, which is Scenario 6-5 in [90]. It is one of the worst scenarios, which lead to severe crashes with high probabilities of occupants' injuries with the traditional algorithm or result in control jerks with Emergency Braking System (EBS) embedded. (More details can be seen in 2.5.3 – 2.5.4.)

The hacked vehicle has a sudden brake for a while (Figure 23). Its following vehicles start to brake similarly to the abnormal vehicle almost at the same time. In the end, they still maintain proper distance gaps to ensure the safety.

The following vehicles can successfully avoid the crash due to immediate response to the abnormal behaviors. When the hacked vehicle starts to decelerate suddenly, the spacing error grows up, leading to a rapid increase on the intermediate term ($\alpha_{3,i}$) and the dynamic weight ($w_{3,i}$). In some sense, the vehicles behind the 3rd vehicle take the 3rd vehicle as their new leading vehicle and thus decelerate with it.

In the traditional algorithm, though the platoon could avoid the crash with EBS, the braking action was not properly implemented, and severe fluctuations in the speed of platoon were observed. The proper threshold selection and harsh transition issues still play critical roles. The PLF with transferable leading vehicle also shows the same issue as in the previous case. The control jerk in the acceleration profile here has longer lag and is more obvious than in minor cyber-attack (marked with the red circle in Figure 23 (c)). This is caused by the different deceleration rate of the 3rd vehicle. In this case, the 3rd vehicle decelerates less hard, which means the spacing error increase more slowly, and thus, it takes longer to be a new leading vehicle. This results in latency in the responses.

Therefore, the advantage of the proposed robust CACC algorithm is concluded as the immediate reactions, smooth controls and transitions without noises or jerks. It satisfies the stability and robustness requirements of CACC algorithm.

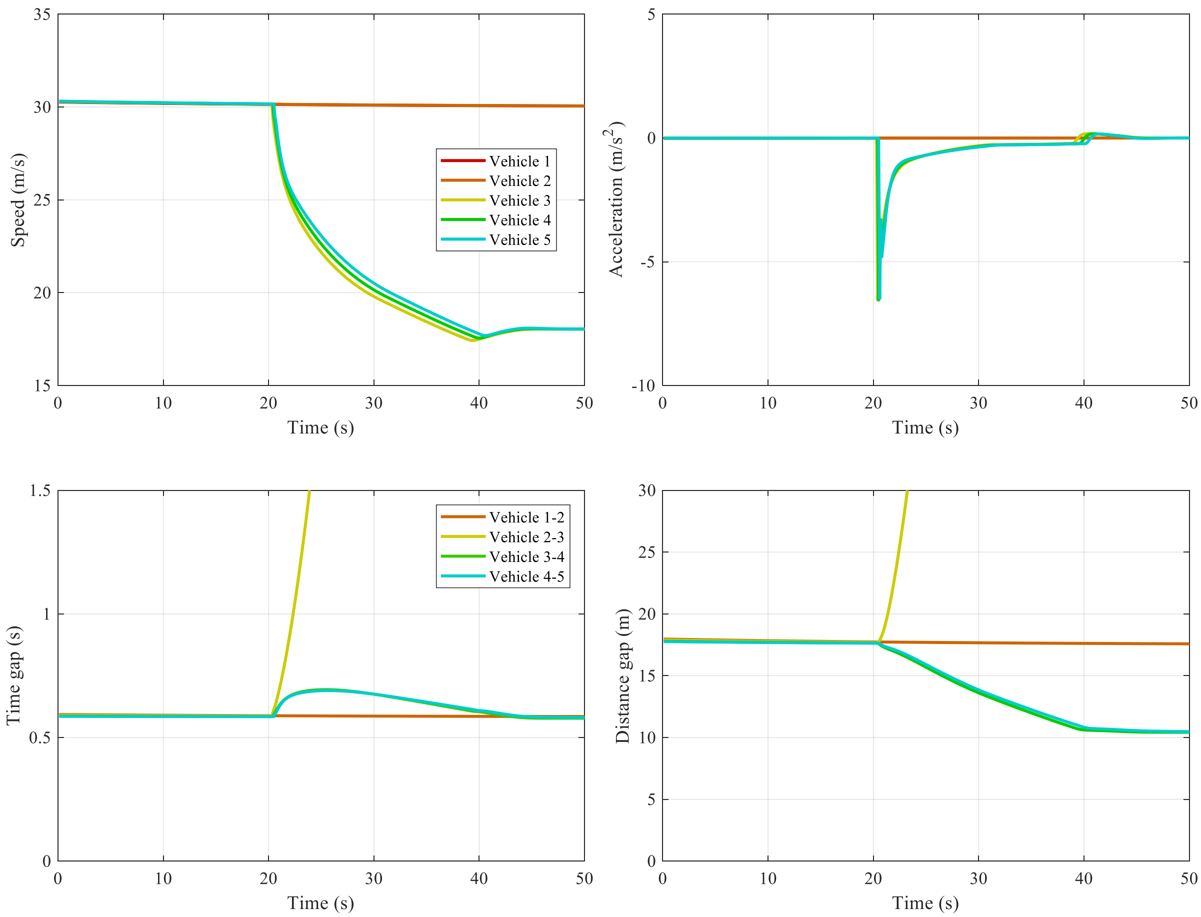

(a) Robust CACC algorithm

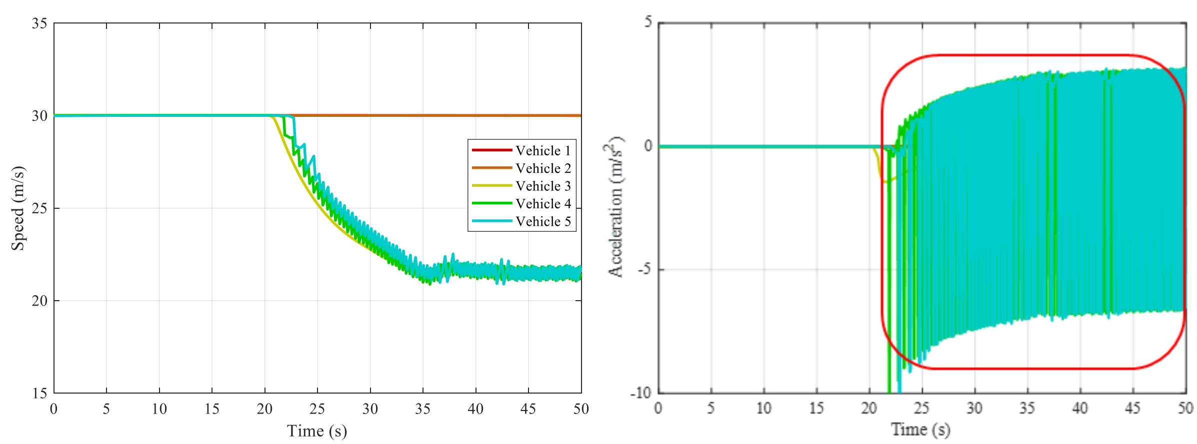

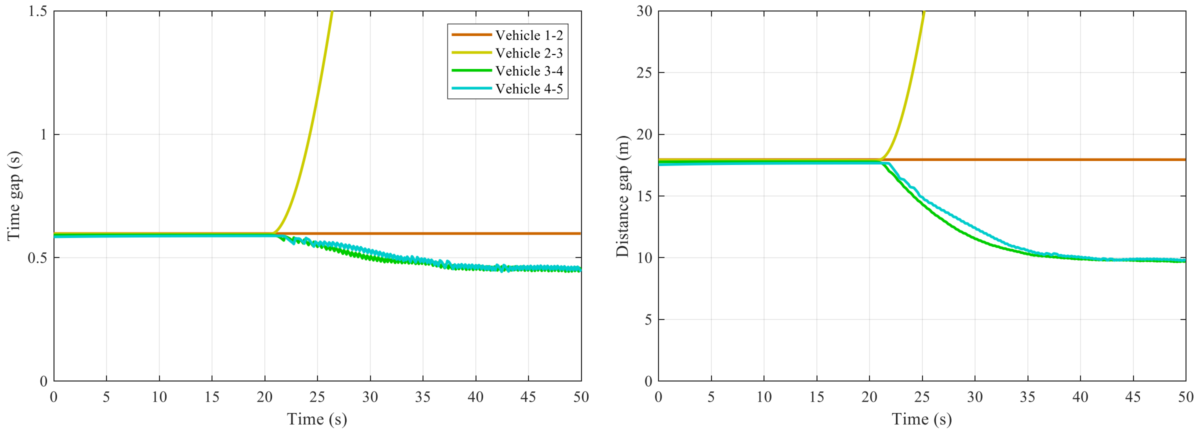

(b) Traditional PLF algorithm with EBS

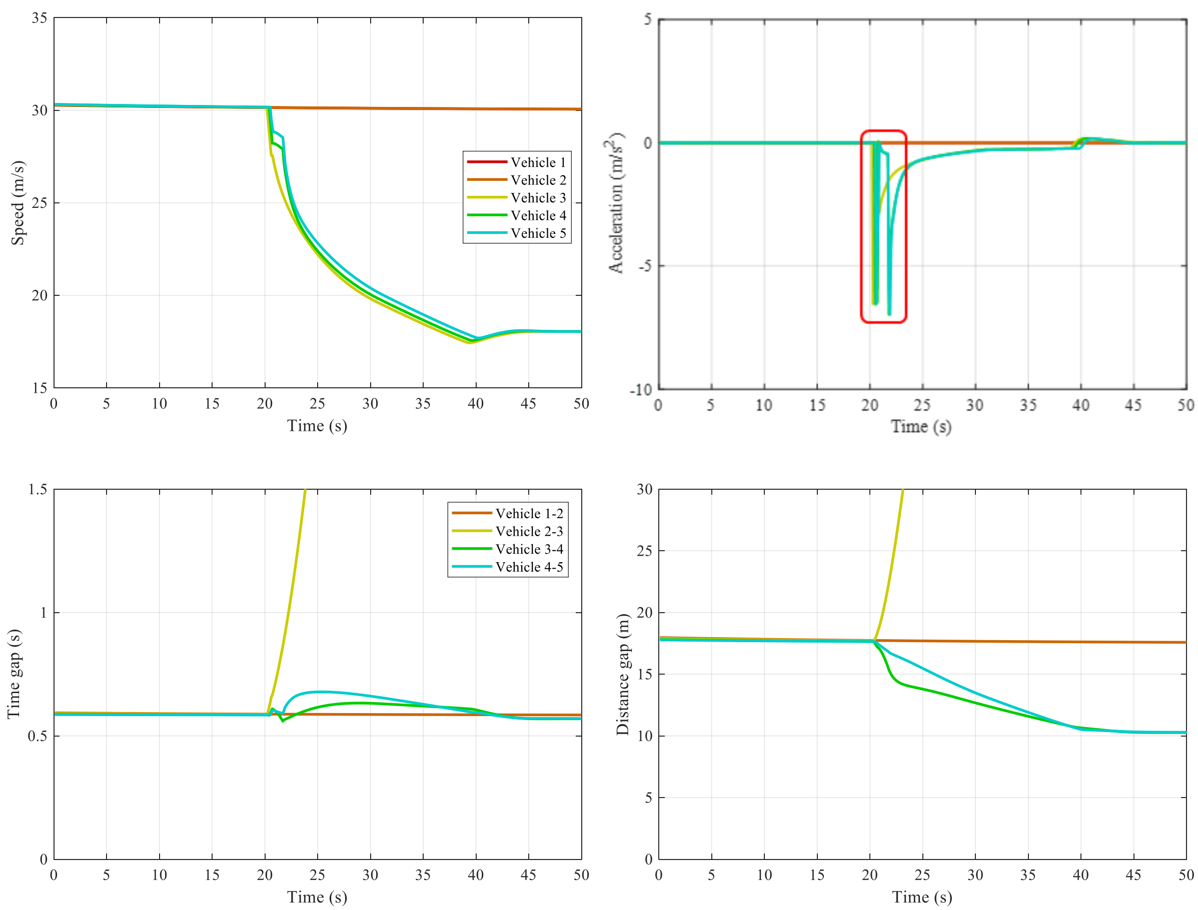

(c) Traditional PLF algorithm with transferable leading vehicle

Figure 23 Test Results of Cyber-attack under GPS Jam Condition

In this case, the gap ratio values are pretty small (Table 11). Therefore, the overall safety does not have severe problem. The robust CACC resulted in the smallest gap ratios (as of 1.03 for both the 4th and 5th vehicles), while the traditional PLF algorithm with EBS caused the largest gap ratios 1.35. The traditional PLF with transferable leading vehicle has the gap ratios of 1.07 for the 4th vehicle and 1.05 for the 5th vehicle, which happened right before the vehicle transferring the leading vehicle. However, compared to the control noise, the safety is not affected too much.

Table 11 Platoon Stability Analysis of Severt Cyber-attack Case 1

Vehicle	**Robust CACC algorithm**	**Traditional PLF with EBS**	**Traditional PLF with transferable leading vehicle**
VEH 3	1.02	1.02	1.02
VEH 4	1.03	1.35	1.07
VEH 5	1.03	1.35	1.05

B. Case 2 – long hard braking

As an extreme case, a long hard braking of the 3rd vehicle is generated by a false value intervened to the target speed. It is formulated as follows, where the target speed of the 3rd vehicle $v_{3_T}(t)$ is updated with (3.8) as expected before the cyber-attack ($t < 20s$), but it starts to give a low value of 7.5 m/s (25% of the desired speed) from the time 20s.

$$v_{3_T}(t) = \begin{cases} \dfrac{1}{w_1 + w_3} \times \displaystyle\sum_{j=1}^{2} (w_{j,3}{}^T \cdot \begin{bmatrix} 1 \\ 0 \end{bmatrix} \cdot v_{j_D}(t - \theta)), & t < 20s \\ 7.5m/s, & t \geq 20s \end{cases} \quad (3.25)$$

The braking rate the 3rd vehicle caused by cyber-attack is over –6 m/s^2 in the first 2.5s and then decreases gradually until the speed reaches the false target speed of 7.5 m/s (Figure 24). Its following vehicles start to brake similarly to the abnormal vehicle almost at the same time and avoid the crash, except in the traditional PLF with EBS.

In the robust CACC algorithm, the following 4th and 5th vehicles decelerate with the 3rd vehicle at very beginning moment, but later (in the left red circle) and when the platoon is stabilized (in the right red circle), the oscillations are observed. It is due to the weight for the first vehicle $w_{1,4}\ or\ w_{1,5}$ remains as a value, not zero, and the spacing error $e_{1,4}\ or\ e_{1,5}$ is very large due to the cumulative deceleration. Thus, the first vehicle is affecting the 4th and 5th vehicles. The influence also includes the safety. The distance gap between the 3rd and 4th vehicles reduces to almost zero at around 47s. Therefore, in this case, the following vehicles need to discard the 1st and 2nd vehicles. This indicate the robust CACC is good for transition process when there is change in the platoon from steady state and the change is not extreme.

The traditional PLF with EBS generates severe oscillations as in previous cases. The control even could not avoid the crash, which happens on the 5th vehicle during the hard braking caused by tardy response (in the left red circle). However, the 4th vehicle is the safest under the help of EBS, when comparing the gap distance with the other algorithms.

The best performance is observed in the PLF algorithm with transferable leading vehicle. Though the control jerks are generated in the acceleration profile during the transfer of the leading vehicle, the 4th vehicle could confine the time gap above 0.25s.

The positive aspect of the robust CACC and the PLF with transferrable leading vehicle is that the performance of the 5th vehicle is more stable than the 4th vehicle, which indicates the string stability. Considering the comfortable maximum deceleration rate lies on –2.5~3 m/s^2 ([102], [103]), this is extreme and rare case. For this kind of situations, the cyber-security should be enhanced and more advanced algorithms are needed.

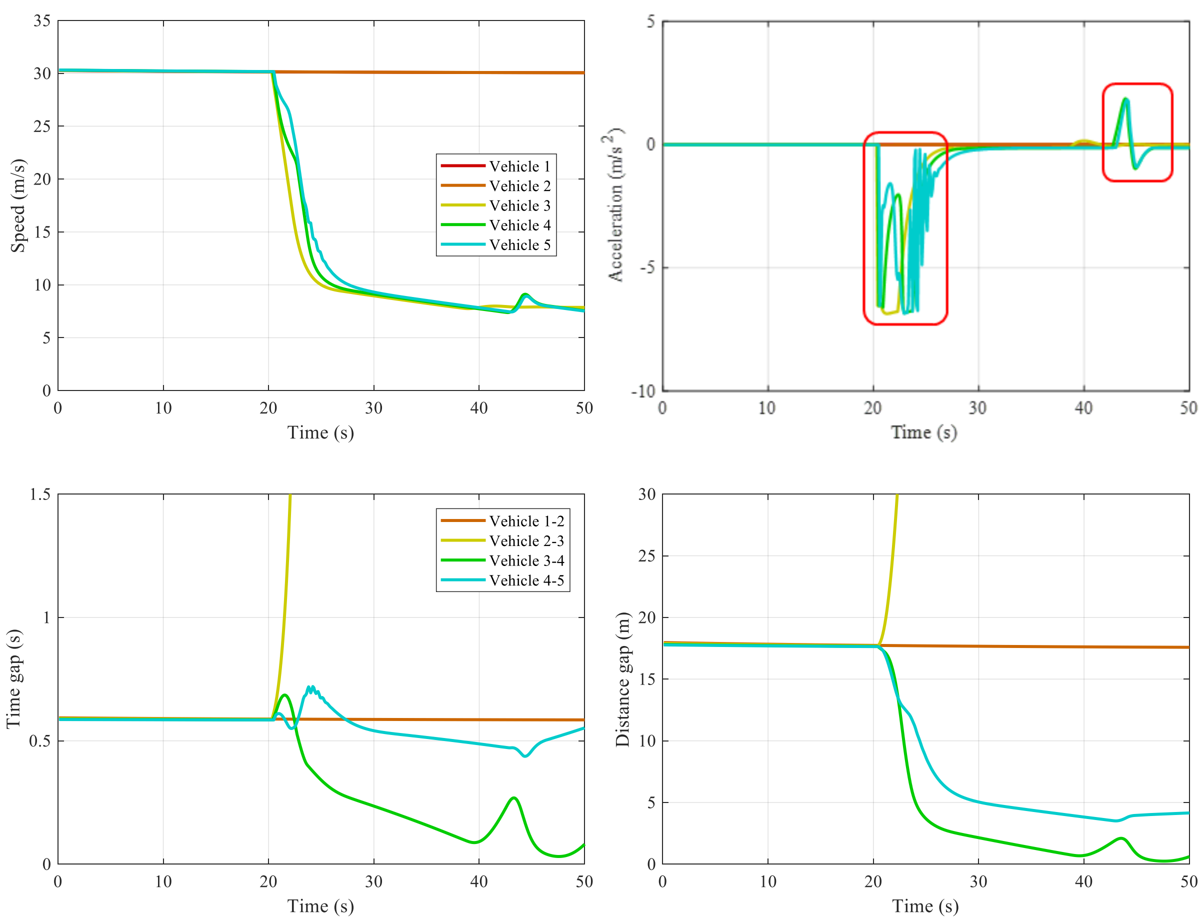

(a) Robust CACC algorithm

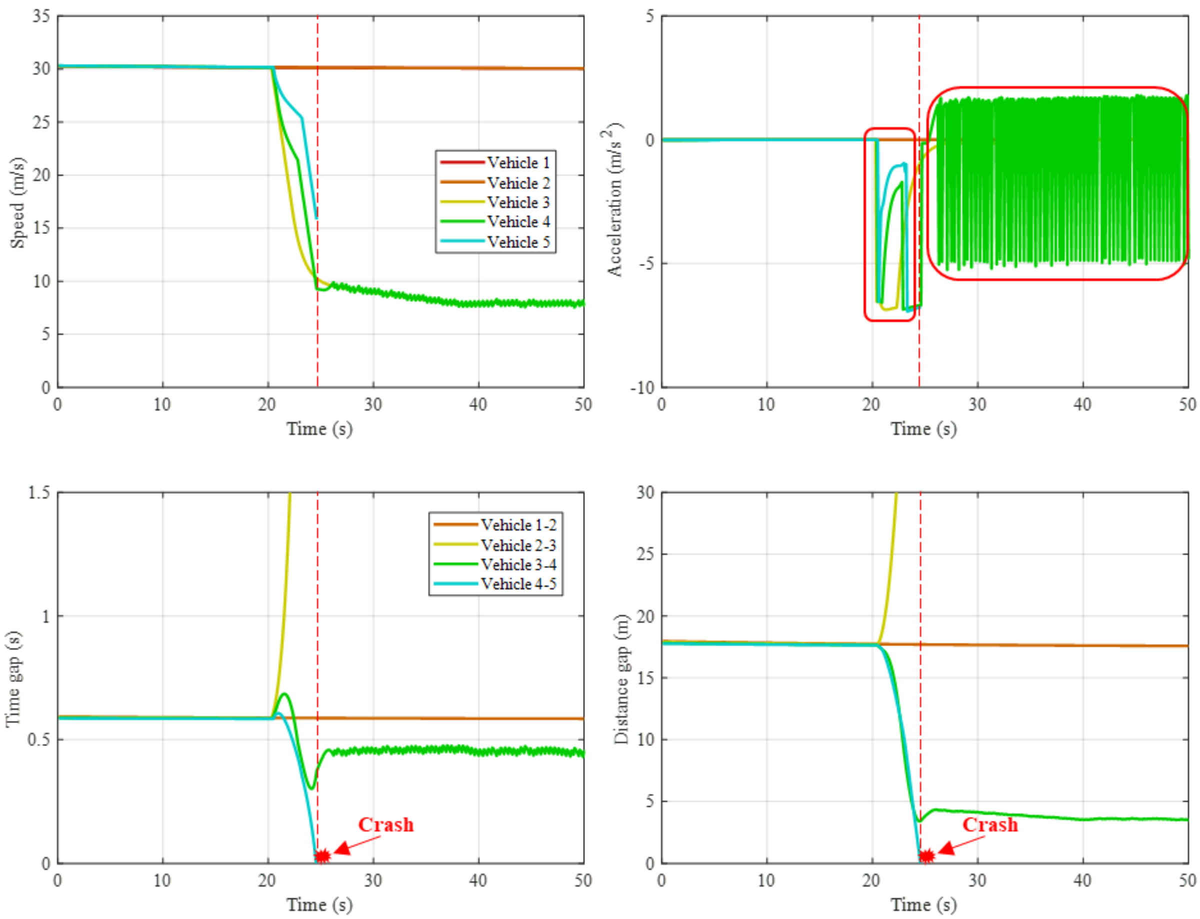

(b) Traditional PLF algorithm with EBS

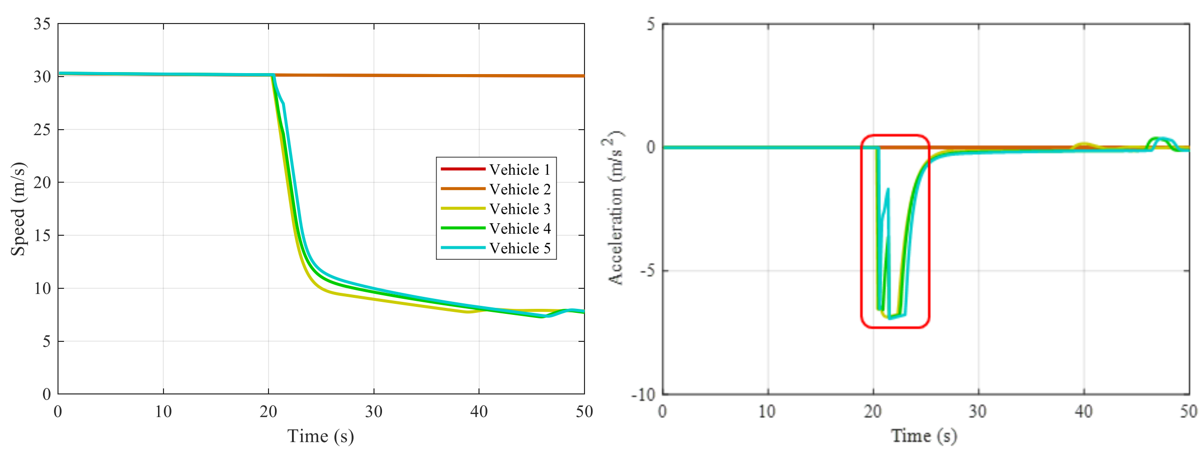

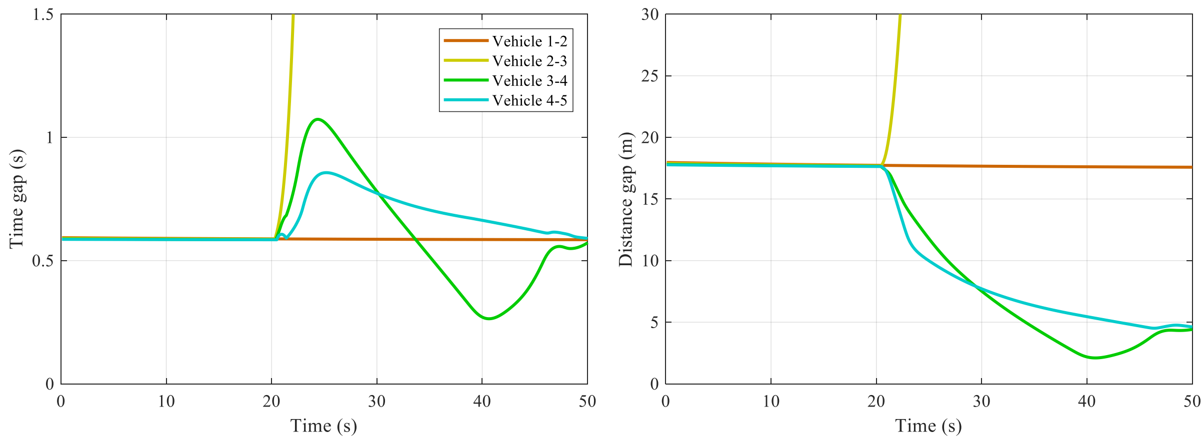

(c) Traditional PLF algorithm with transferable leading vehicle

Figure 24 Test Results of Cyber-attack causing long hard braking

The large gap ratios in Table 12 quantify the dangers that are described above. The traditional PLF with EBS controls the 4th vehicle most safely but the 5th vehicle resulted in a crash. The robust CACC generates a poor gap ratio of 19.25 in the 4th vehicle but a not bad gap ratio in the 5th vehicle. The traditional PLF with transferable leading vehicle has the best performance overall, with gap ratios of 2.27 and 1.03 for the 4th and 5th vehicles, respectively.

Table 12 Platoon Stability Analysis of Severt Cyber-attack Case 2

Vehicle	Robust CACC algorithm	Traditional PLF with EBS	Traditional PLF with transferable leading vehicle
VEH 3	1.02	1.02	1.02
VEH 4	19.25	1.99	2.27
VEH 5	1.37	+∞	1.03

3.5.3 Discussions

Based on the simulation results, the proposed CACC algorithm is string stable and capable of dealing with the cyber-attack situations robustly. Its capabilities and limitations can be highlighted as follows.

A. Capabilities

In normal situations, the platoon can follow the leading vehicle with stability ensured. Some small fluctuations are observed when the target speed changes, but can quickly settle down. Therefore, the CACC platoon is expected to survive in the real traffic circumstance, including different traffic volumes, different speed limits, or speed fluctuations in the traffic flow. It should be noted that some realistic sensor errors and communication delays have already been considered.

The other important attribute of the algorithm is its robustness against the cyber-attacks. If the robustness is not guaranteed, some other controllers, e.g., braking assistance system or emergency brake assist, should be associated with the CACC algorithm to ensure the safety. The proposed CACC can use dynamic weight according to the spacing error. Therefore, if the radar sensor or DSRC detect any abnormal behavior, the following platoon will give more focus on it so as to response immediately and avoid the crashes. Though the communication is hacked in one of the vehicles in the platoon and leads it to a sudden brake or speed fluctuations, the platoon can still maintain the safety without speed fluctuations. However, it cannot handle the extreme case.

B. Limitations

Several limitations are existing in the proposed algorithm, which needs to be solved and improved in the future. The communication topology is relatively complicated, where the number of directional communication links is A_n^2 (n is the number of vehicles in the platoon). However, if the central broadcast is used, i.e., one collects information from all vehicles, and then pack and send to the vehicles (number of communication links to be $2n$), the communication structure is not problematic. For the small fluctuations on the speed, the algorithm can perform better with more accurate sensors and communication technologies being available or being fused with more data sources such as the camera.

In extreme case, the robust CACC cannot control the platoon well when it is split due to the braking of the vehicle in the middle and the two sub-platoons are far apart. The control noises are generated on the following vehicles and the safety is not guaranteed, though the string is still stable. Therefore, the following vehicles need to discard the vehicles in the front sub-platoon, which can be dealt with a future algorithm advancement.

3.6 Concluding remarks

This research proposed a robust CACC algorithm which overcomes the shortcoming of the state-of-the-art CACC in dealing with unexpected cyber-attacks. The stability and robustness of the CACC platoon are aimed to improve under all range of cruising speed. The proposed algorithm combined the advantages of APF and PLF control methods and implemented dynamics weights to improve the stability and robustness of the CACC platoon. In addition, the proposed algorithm was theoretically proven to be maintaining string stability.

To evaluate the proposed algorithm, it was tested with the simulation in the cases of normal cruising and cyber-attacks, including slight fluctuation on the speed, communication jam, and extreme situation. An integrated simulation evaluation platform was utilized that considers sensor errors, communication delay, and vehicle dynamics. The platoon with the proposed algorithm was able to closely follow the pre-defined desired speed under various cruising speeds, which were similar to speed fluctuations in the real world. In the case of cyber-attacks, the proposed robust algorithm could quickly detect the platoon member having abnormal following speed using dynamic weights and coordinated other platoon members accordingly, except in the extreme case, to avoid the collision. The evaluation results confirmed the robustness and stability of the proposed robust CACC algorithm.

Furthermore, the proposed algorithm was compared to a traditional CACC algorithm embedded with EBS and with transferrable leading vehicle. The results confirmed that in general, the proposed algorithm produced much smoother speed trajectories than conventional CACC, where mode switches between EBS and CACC or transfer of the leading vehicles cause severe oscillations. However, in the extreme case, the robust CACC cannot control the platoon well and control noises are generated on the following vehicles with potential safety risks. Considering the comfortable maximum deceleration rate lies on –2.5~3 m/s^2, this extreme case (–6 m/s^2) rarely happens in the real world. Therefore, the robust CACC outperforms the traditional algorithm in most of the cases.

On the other hand, the proposed CACC algorithm is only applicable to homogeneous fleets (i.e., vehicles with the same vehicle dynamics model) in this study. The future study could consider upgrading the current algorithm to be compatible with heterogeneous vehicle platoons by adopting different vehicle dynamic models. In addition, given the low market penetration of CAV in the near future, the algorithm should be tested to optimize the CACC algorithm for the mixed traffic flow, e.g., to decide the maximum platoon lengths, or to enhance for the case of CAV merging with a platoon.

Chapter 4. Evaluations of the mixed traffic flow on multi-lane weaving segment

4.1 Introduction

As higher and higher automated levels being available, the CAVs are expected to improve the traffic safety due to accurate controls and negligible reaction time. However, there are still many public concerns and uncertain impacts on CAV deployment. According to a recent survey, more than half of the American public is worrying about the driverless vehicles [9]. The concerns include the distrust toward the system reliability, sensor malfunction, and chaotic driving environment.

On the view of the transportation system, the behaviors of CAVs are also very critical to the system efficiency. Automated platooning, or CACC is a method for improving the capacity of freeways. The primary control mechanism of CACC is to have every vehicle in a platoon follow its preceding vehicles with a certain user predefined distance or time headway [12]. The distance between vehicles can be maintained in a very small value so as to allow more sufficient movements and improve safety. However, most of the researchers quantified the benefits of CACC by assuming 100% of market penetration rate (MPR), which needs a few decades to achieve. According to a report from HIS Markit, autonomous vehicle sales will be more than 26% of new car sales in 2040 [7]. This means the mixed traffic flow, where the human drivers drive closely to CAVs on the same roads, will dominate for a long time in the future. Therefore, the impact of CACC in the mixed traffic is as important as the controller itself. Especially in the weaving, merging, or diverging segments of the freeway, the long and dense platoons may impede lane changing of human drivers and bring another challenging issue. It should be noted that the weaving segments are very common and are the bottleneck of the freeways due to the significant lane-changing activity [104]. This indicates that besides the movement or safety performance of CAV itself, the impacts to the mixed traffic should also be evaluated for exploring the pros and cons of the CAVs in various situations.

However, in the most common methods of mixed traffic simulation, the behaviors of CAVs are simplified with strong assumptions. For example, the time-gaps were set for ACC or CACC vehicles, which allows the output of the controllers as the immediate speed change, in [15]. An enhanced car-following model, based on Newell's and Gipps' models, is developed in [105] to simulate the CAVs more realistically. In [18], a car-following model is derived from field test trajectories and used for estimating the capacity of mixed traffic. However, these models are not considering the actual vehicle dynamics so that unrealistic acceleration or deceleration rates appear. Therefore, a simple first-order dynamic is used in [16] for ACC systems in a single lane. Since they are focusing on the steady-state car following behavior, the maximum acceleration and deceleration rates are set for ACC or CACC. For the situations that require the acceleration or deceleration to be out of the range, the CAVs are assumed to turn to human-driven mode, which means vulnerable platooning. The same method is used in MIXIC simulation ([88], [106]). This lacks the consideration of oscillations that is caused by the control mode switch, and the consideration of not all speed or acceleration ranges being covered in the CAV simulation. Especially in the weaving, merging, or diverging segments which related to frequent human-driver cut-in, these limitations should be overcome.

According to [34], incorporating realistic vehicle dynamics allows simulations to be complete and authentic, and is necessary for CAV simulations. Therefore, in the CAV controller developments, various vehicle dynamics models (VDM) are considered. Most ACC or CACC controller studies ([30], [35], [36]) adopt linearized VDM to simplify system analysis ([12]). A generic VDM in [31] and a second-order VDM in [13] are applied, and the results showed consistency between simulation results and actual field results. A relatively complete vehicle dynamics model, which is a nonlinear model with the engine, road, tire and slope resistance, was adopted in the simulation conducted by [37]. Therefore, the purpose of this research is to incorporate controllers and a dedicated VDM for CAV simulation in the traffic flow simulation.

By integrating VDM and controller for CAVs instead of using simplified car-following models, the behaviors of CAVs are expected to have several improvements: 1) allowing realistic acceleration and deceleration behaviors; 2) cover all range of speed; 3) complying with the CAV control mechanism; and 4) in a long-term range, simulating heterogeneous platoon with different VDM parameters is available, and various CAV controllers can be simulated.

With the integrated simulation platform, the mixed traffic on the weaving segment is the exploring point. Most of the research by far is focusing on the capacity improvement with CACC platoons. It has been commonly said that shorter desired gaps and higher MPR would have the higher capacity [15]. However, as mentioned above, the long and dense platoons may block the on- and off- ramp vehicles who are trying to make lane-changing. Therefore, to quantify the impact of mixed traffic on the weaving segment and provide a basement for CACC strategy enhancement or freeway automation operation, the mixed traffic with CAVs forming CACC platoons are tested. Besides, some variables, such as the traffic volume, free flow speed, CACC platoon length, desired gaps of the platoon, and MPR, which may affect the performance of the mixed traffic, are considered as factors in the simulation test. The ultimate goal of the simulation is to answer these questions: with CACC platoons, how will the performance change in weaving segment; what will be the optimal platoon length and inter-platoon gaps for weaving segment; how would other factors, i.e., MPR, speed, and traffic flow rate, affect the performance of weaving segments. It should be noted that further research can adopt more CAV applications, not limited to CACC, under different scenarios with the proposed simulation platform.

This paper is organized as the following sequence. Next part is describing the integration of a microscopic transportation simulation tool (PTV VISSIM, [19]) and a control simulation tool (Matlab SIMULINK, [107]) to simulate the mixed traffic flow more realistically. Then platoon trajectories using different simulation methods are compared to show improvement of the proposed simulation method. Section 4.3 provides detail information about geometry design and test scenarios for the mixed traffic evaluation on the weaving segment, which is followed by the simulation results. In Section 4.4, discussions and future work are presented.

4.2 Simulation platform structure

The integrated simulation platform framework is as Figure 25. The programming language Python is used to access COM (Component Object Model) interface for controlling the microscopic transportation simulation tool VISSIM, where the human driver behaviors are modeled. For CAVs, SIMULINK provides behavior modeling by simulating the controller and vehicle dynamics. TCP/IP connects python and SIMULINK to share the data [108]. The detailed information of each component is to be followed.

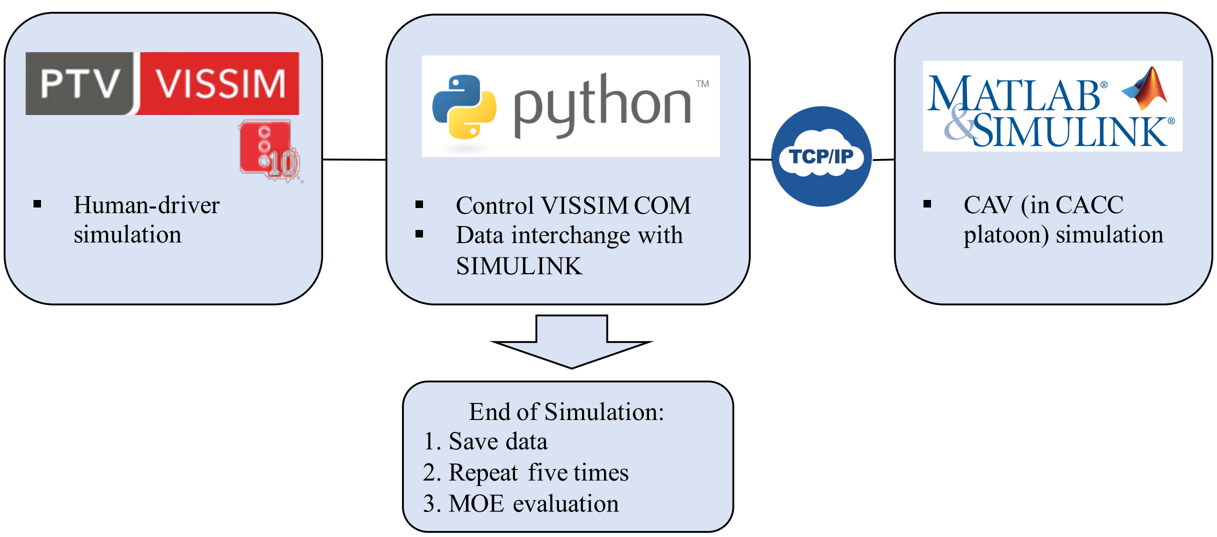

Figure 25 Integrated Simulation Platform Framework Overview

4.2.1 CAV modeling

Control simulation tool Matlab SIMULINK is in charge of the CAV simulations. The simulation mechanism of CAV (Figure 26) is borrowed from Chapter 2, which is designed to fully replicate the real world. The major components are the CAV controller, which is CACC in this paper, and the VDM.

The input is the information of surrounding vehicles, which is sent through TCP/IP. The information, including the distance and relative speed between ego-vehicle and its preceding vehicles, is calculated with python by getting all vehicle attributes from VISSIM. Then it is fed into the CACC controller to calculate the throttle or brake level for feeding the vehicle dynamics model. The controller aims to keep the desired time gap between consecutive vehicles with dynamic weights [109]. The stability and robustness have been validated against unexpected human driver cut-in scenario.

The output of the CACC controller, i.e., the throttle and brake level, goes into the VDM to get the actual acceleration rate. In the VDM, response delay and imperfect executions of vehicle mechanical system are simulated using the model developed by [48]. It incorporates the gear shift, engine model, torque transmission, and chassis model, where the friction of tire and air resistance are considered. The output is the newly updated acceleration rate, speed, and location, which are for the next iteration and also for being sent through TCP/IP.

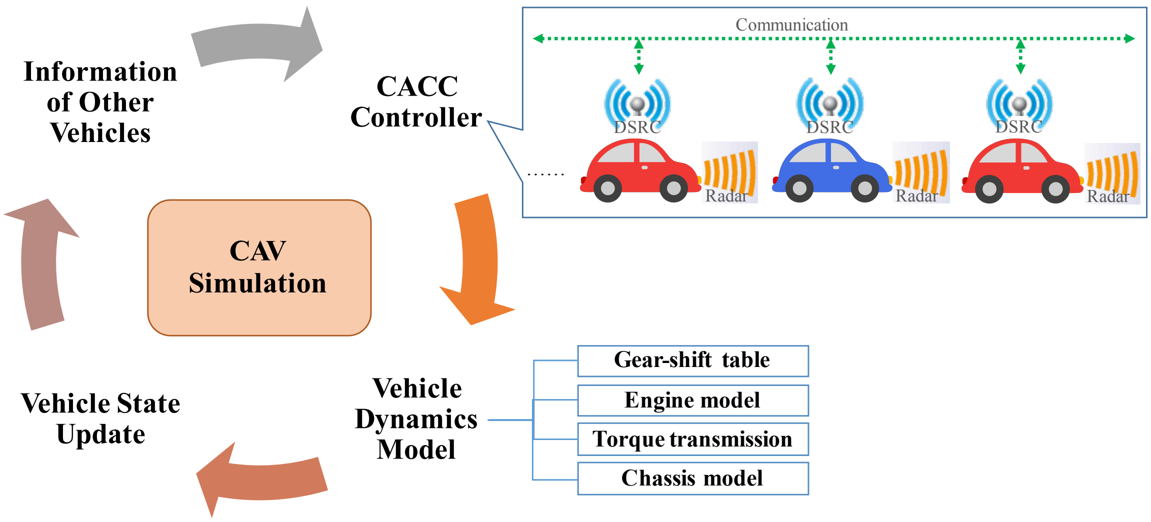

Figure 26 CAV Simulation Structure

4.2.2 Human driver modeling

Microscopic simulation tool VISSIM provides a central space for the simulation platform, including the road network, vehicle generation, route choices, and desired speed distribution of human drivers. It is controlled through VISSIM COM using python programming. For the vehicle models, only human-driven behaviors are simulated with default models in VISSIM. CAVs are also presented on the road of VISSIM to interact with human drivers but not controlled by VISSIM.

The driving behavior models in VISSIM include psycho-physical longitudinal and latitudinal movements to simulate the driver behavior and interaction with other vehicles. The stachasticity of human drivers are considered by using the distributions of reaction time, desired speed, maximum acceleration, and critical gap.

Car-following model: The longitudinal movements are modeled with the Wiedemann

74 car-following model at four different driving modes (Figure 27): free-driving (unconstrained), approaching a vehicle, following a vehicle and breaking for safety ([110], [111]). The dynamic speeds and stochastic car-following models are used and are close to the driving behaviors in the field ([112]). Therefore, it has been widely used for traffic engineering purpose due to the realistic traffic simulation under various scenarios.

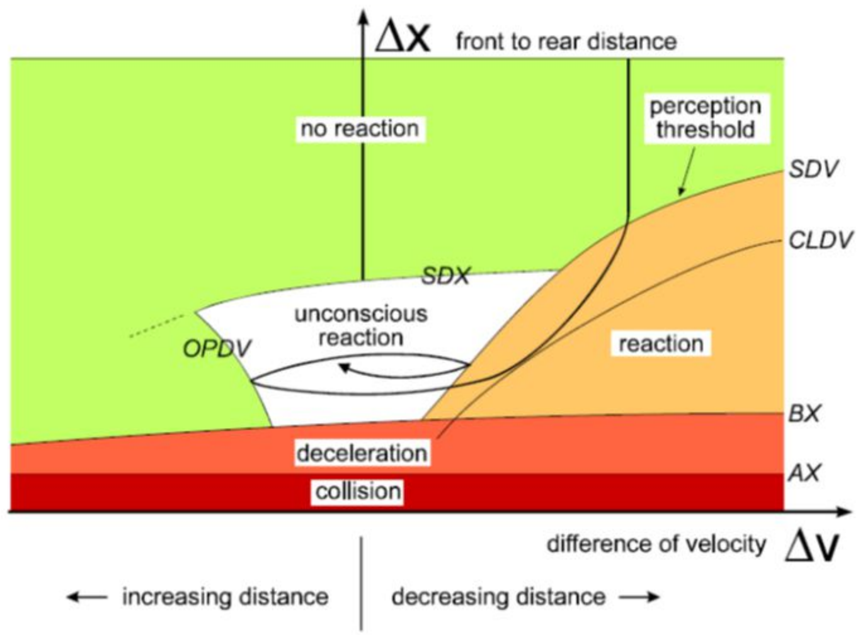

Figure 27 Car-following Logic of Wiedemann 1974 (Copyright to PTV VISSIM)

As an example, the speed and acceleration profiles of one vehicle is shown in Figure 28 (a). The vehicle started from zero speed to the desired speed of 27.8m/s (=100km/h), then at time 80s, the vehicle decelerates to 15.8m/s (=57km/h). Though some rapid changes can be observed in the acceleration profile, the overall performance is reasonable to model a human driver's behavior.

Lane-changing model: For human drivers, the free and mandatory lane changing behaviors are modeled ([19]). The free lane changing occurs when the adjacent lane has faster speed and the driver decide to change the lane to satisfy the desired speed. The mandatory lane changing occurs when the vehicle have to make the lane change because of the routing decision or the lane drops. Both types of lane changing are looking for a suitable gap with gap acceptance model, which is decided by the speeds of the subject vehicle and the lag vehicle (the vehicle after the targeted gap). Since the VISSIM does not specify the gap acceptance model, a model with similar mechanism, which is used in another simulation software MITSIM, is presented for reference ([113]):

$$G^{lead}(t) = \exp[2.72 - 0.055v(t) + \epsilon^{lead}]$$

$$\begin{aligned} G^{lag}(t) = \exp\big[&-9.32 + 0.1170\min(\Delta v^{lag}(t), 10) \\ &+ 0.1174\max(\Delta v^{lag}(t) - 10{,}0) + 1.57\delta(t) + 1.88\ln\,(L^{remain}(t) \\ &- 1.90v(t) + \epsilon^{lag}\big] \end{aligned} \tag{4.1}$$

Where $G^{lead}(t)\ and\ G^{lag}(t)$ are the lead and lag critical gaps (feet), $v(t)$ is the speed of subject vehicle (mph), $\Delta v^{lag}(t)$ is the lag vehicle speed minus subject vehicle speed, $\epsilon^{lead}\ and\ \epsilon^{lag}$ are the random terms for individual drivers, $\delta(t)$ is a dummy variable that equals to 1 if the delay is 0 and 0 for else, and $L^{remain}(t)$ is the remaining distance to the emergency stop point at which lane change must be completed (feet). Based on the estimation, 72% of the acceptable gaps are greater than 0.9s ([113]).

Therefore, it can be seen that the delay time and the remaining distance also affect the gap acceptance, meaning that the aggressiveness of drivers plays an important role in the gap acceptance of the mandatory lane changing. Besides, in VISSIM, once a driver needs to make a mandatory lane changing, he/she would force the lag vehicle to decelerate, and the force on the deceleration rates depends on the distance to the emergency stop point ([114]). This is realistic driving maneuver for the vehicles who are eager to merge.

4.2.3 Integration

TCP/IP is used to share data between two software and realize the integration. Therefore, python and SIMULINK both added connection ports for establishing communication. The contents listed below is the work that is conducted by the programming in python during simulation, which updates every 0.1 seconds.

- To set parameters for VISSIM and SIMULINK (the parameters include the speed limit, traffic volume, and the desired gaps of CACC platoon)
- To get the vehicle attributes (speed and location) from VISSIM, calculate the distance, the relative speed between CAVs and their preceding vehicles
- To send the calculated values through TCP/IP
- To receive data from SIMULINK and control CAVs in VISSIM with the received data

4.2.4 Improvements of the simulation platform

To show the improvement of the simulation platform, three different simulation methods are compared: 1) CACC algorithm with VDM integrated (proposed simulation method), 2)

CACC algorithm without VDM (where the desired speed is assumed to achievable immediately), and 3) CACC car-following model from [18]. In the simulation, the platoons are given with the same reference speed (as Figure 28 (a)), which is the speed profile extracted from VISSIM. This scenario is designed to observe both acceleration and deceleration behaviors.

From the figures, it can be observed that the CACC platoons can follow the reference speed nicely in general. With VDM being considered, which is the proposed simulation platform, the response delays, gradually changing acceleration, and the gear shifts (can be seen from the bumps in the acceleration profile) are observed (Figure 28 (b)). This is as expected because a dedicated VDM is adopted in the simulation platform.

When VDM is left out (Figure 28 (c)), immediate accelerations and decelerations are observed. Especially for the first vehicle, the speed is almost the same as the reference speed, which means the response ideally, but also unrealistically, goes with the reference. Therefore, if the reference is given unrealistically, the simulation is far away from the reality.

For the CACC car-following model (Figure 28 (d)), there are zigzags in speed and acceleration profile. This happens because the acceleration is very sensitive to the spacing error and the acceleration comes into effect in the speed immediately. Besides, the maximum acceleration and deceleration values are set as $2m/s^2$ and $-2.5m/s^2$, respectively, which results in the accelerations fluctuate between $2m/s^2$ and $-2.5m/s^2$. The behaviors are apparently far from reality and need to be improved. The main reason is the limited field test data, which is used for the car-following calibration.

The results from the CACC car-following model are also not suitable for further analysis, such as fuel estimations. For example, the 8^{th} vehicle, in this case, consumes 683.6ml fuel while traveling 3.2km, which equals the fuel efficiency rate of 4.6 km/l. However, the tested fuel efficiency rate usually ranges from 8-20 km/l, depending on the driving scenario ([115]). Therefore, the fuel consumption of CAV that is simulated with CACC car-following model is out of the normal range. On the contrary, the 8^{th} CAV modeled with the proposed simulation platform consumes 195.9ml fuel, leading to the fuel consumption rate of 15.8km/l, which is a reasonable value. It should be noted that VT-CPFM (Virginia Tech Comprehensive Power-based Fuel Consumption Model) is used for calculating the fuel consumption with the input of speed trajectory ([115]).

Furthermore, besides yielding unrealistic acceleration values and instantaneous speeds, car following models, such as intelligent driver model (IDM) and Gipps' model, commonly have fundamental problems in some scenarios ([116]–[118]). For example, they lose realistic properties in the deterministic limit ([118]). Similar issues exist in this CACC car-following model. Firstly, due to the strict acceleration rate range, the CACC platoons cannot maintain the desired headway, and the platoons lose the platooning function when the first vehicle accelerates or decelerates with the maximum value. Secondly, the full range of speed is not able to be covered, especially for the low-speed range. When the cruising speed is low, the desired headway would be very small, and the distances between the adjacent CAVs become more sensitive to the acceleration decisions. Therefore, the fluctuation of the speed control and the limited acceleration rate may cause unstable movements associated with crashes. Finally, the mode switch between CACC and human driver, which is used to avoid crashes that are not included in the CACC control mode, also increases problems. Improper criteria for switching the mode still cannot handle crashes. The issues can be observed when the platoons approach a congested or unstable traffic flow and when frequent human-driver cut-ins happen due to congestion. When this car following model is used for simulating mixed traffic on a weaving segment with high traffic flow, which is the same scenario as in the next section, plenty of over-laps are observed.

For the proposed simulation platform, its process follows the control process of CAVs, i.e., detecting information, making decisions, and then realizing through vehicle dynamics. The CAV behaviors are much more reasonable without constraints. Therefore, the simulation platform can simulate the mixed traffic realistically and is expected to be a powerful and useful tool for mixed traffic evaluation research.

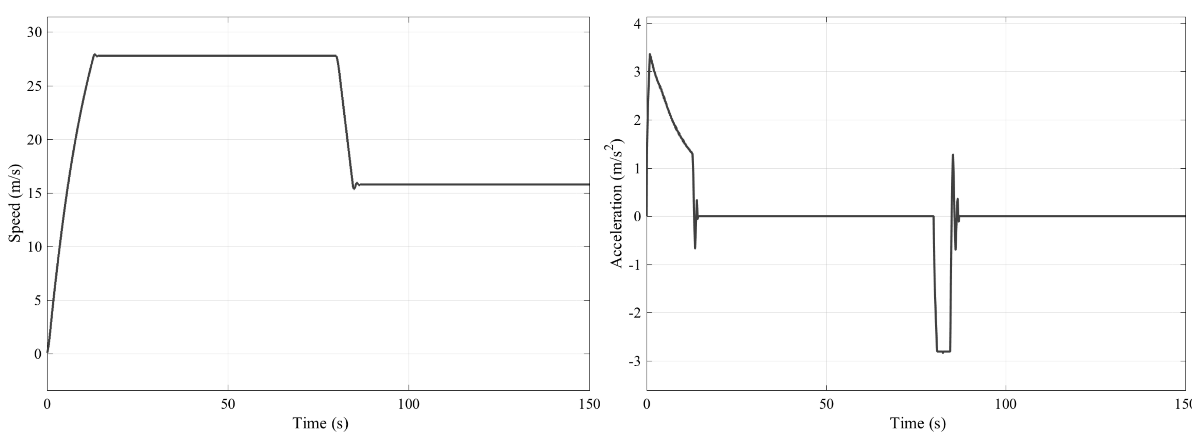

a) Reference speed (left) and acceleration (right)

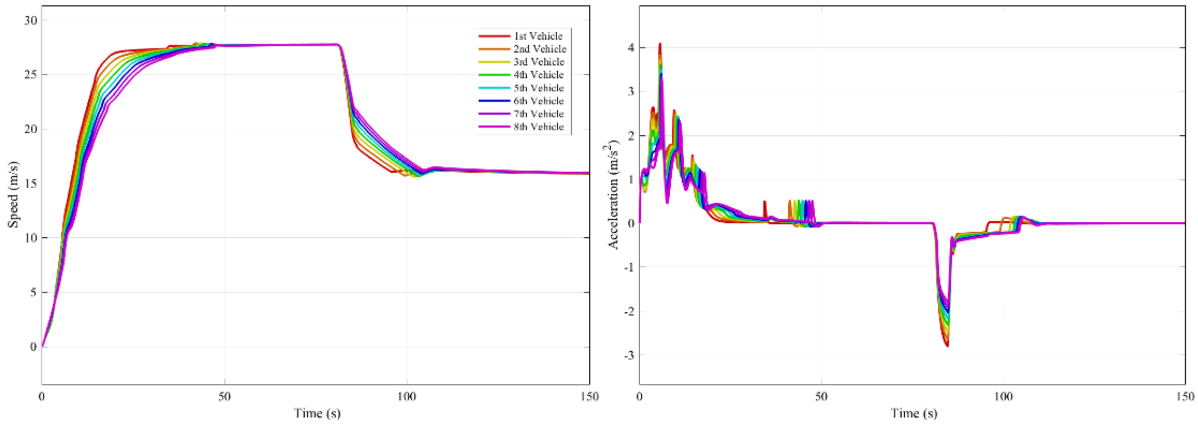

b) CACC platoon with VDM

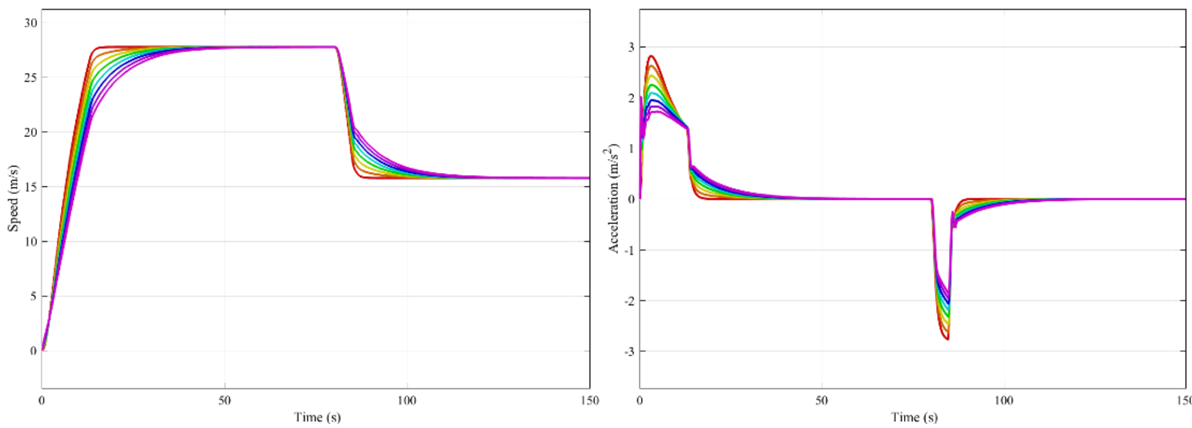

c) CACC platoon without VDM

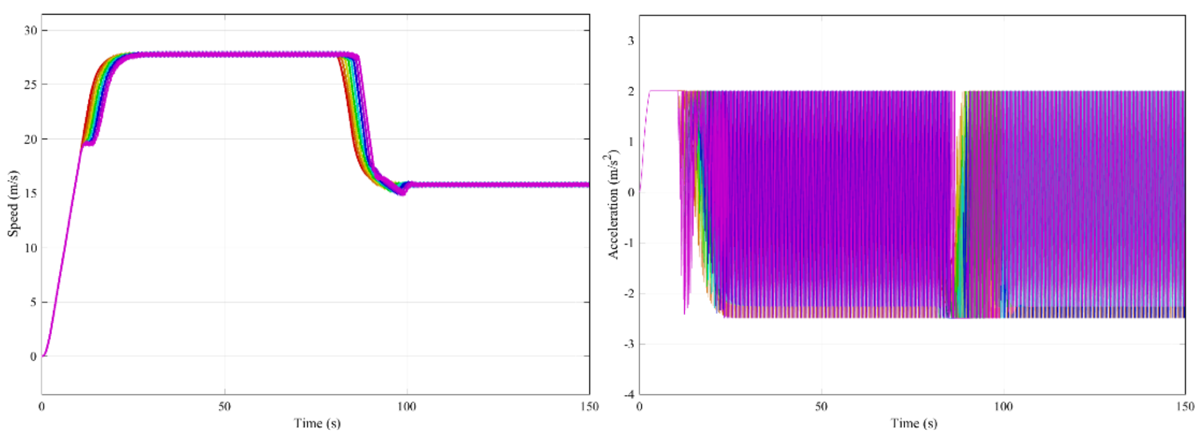

d) CACC platoon with car-following model

Figure 28 Platoon Speed & Acceleration with Different Simulation Mechanisms

4.3 Simulation design and results

4.3.1 Geometry design

As mentioned above, a freeway with a weaving segment is designed for mixed traffic performance evaluation. The road network (Figure 29) is a typical one-sided weaving segment with the length of 500m (= 1640 ft.), which is covered by the typical range of weaving length [119]. Before and after the weaving segment, there are two 800m (= 2625 ft.) basic segments. The basic segments have two lanes, and the weaving segment has three (two plus one auxiliary) lanes. There is no grade on the road. For the convenience of describing the results, the links and lanes are numbered as in Figure 29.

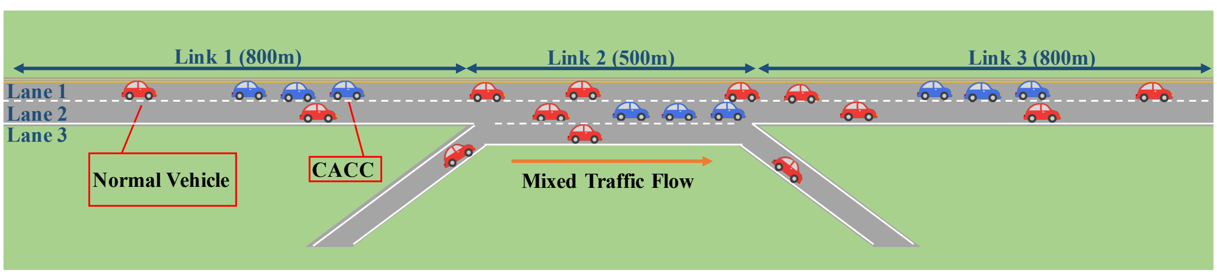

Figure 29 Experiment Design for Evaluating Performance of Mixed Traffic

4.3.2 Test scenarios

Since the focus of this paper is to understand the influence of the CACC platooning in the weaving segment under mixed traffic condition, the scenarios are made to stress out the interactions between CAVs and human drivers. Following assumptions and settings for the traffic flow and CACC platoons are adopted in the simulation:

- The traffic is homogeneous, where no heavy vehicles are included
- CACC platoons have already been formed before the start point of the to-be-tested segment and travel through the freeway section without lane changes
- CACC platoons use the speed limit as the target speed
- CACC platoons are distributed on either lane
- Modeling of CACC platoon and human driver behaviors are as described in the simulation platform introduction part
- On-ramp and off-ramp traffic volume is 500 veh/h
- The time interval for simulation is 0.1s

A set of scenarios is tested in the simulation. The factors, which are commonly expected to influence the mixed traffic performance, include: the traffic volume, free flow speed, CACC platoon length, desired gaps of the platoon, and MPR. Therefore, the following factors are considered:

- Free flow speed: 60 km/h (=37 mi/h), 80 km/h (=50km/h), 100 km/h (=62 mi/h)
- CAV market penetration rate: 0%, 33%, 67%
- The desired time gap of CACC: 0.6s, 0.9s, 1.2s

- CACC platoon length: 4-CAV, 8-CAV, 12-CAV
- Mainstream traffic volume: 1940 veh/h/ln (high) for all platoon sizes, 1500 veh/h/ln (medium) and 1100 veh/h/ln (low) for 8-CAV

The CACC desired time gap and platoon size both decide the degree of blockage on the weaving segment. For example, if the desired time gap is too small, the human driver would have to wait until the platoon passing by to make a lane-changing; and if the platoon is too long, the human driver may wait for the platoon. Therefore, different values from other research are referred. The gaps that had been tested in the field – 0.6s, 0.9s, and 1.2s – are adopted ([13], [120]). For the platoon size, in the SARTRE project, the recommended maximum platoon length is 15, and in the PATH group research, the maximum platoon length is 10 ([18], [121]–[123]). Considering the difficulty in testing every possible platoon length, a long platoon size 12, a medium size 8, and a short size 4 are selected to test.

For the mainstream traffic volume, the high volume is tested for all three kinds of platoon sizes since the high volume would emphasize the interactions between CACC platoons and the human drivers. The medium and low volumes are only tested using 8-CAV case to focus more on the traffic volume factor, rather than making the scenarios more complicated with all different platoon sizes. Besides, each run is replicated five times to consider the effect of stochasticity of traffic and ensure statistically significant results at a 95% confidence level ([124]). Each run is 550s with the first 250s as warm-up time and the rest 300s as the time to be analyzed. Besides, considering the traffic near the weaving segment may change the lanes in advance, the lane change distance, which is the distance that vehicles start to try lane changing caused by route, is lengthen from the default value 200m to 500m.

4.3.3 Results interpretation

As mentioned above, the simulation is to quantify the impact of mixed traffic on the weaving segment and provide a basement for CACC strategy enhancement or freeway automation operation. The questions that are expected to be answered with the simulation are: with CACC platoons, how will the performance change in weaving segment; what will be the optimal platoon length and inter-platoon gaps for weaving segment; how do other factors affect the performance of weaving segments.

The results are going to be presented in three parts. First, the typical performances of the weaving segment with the normal traffic and the mixed traffic are described in the first two parts. Then in the third part, the results with different mainstream volumes are provided, followed by the results with different platoon sizes under high mainstream volume.

4.3.3.1 Performance of weaving segment

Frequent lane changing needs are expected in the weaving segment, which leads to speed drops and capacity drops. In HCM 2010, the capacity, average speed, and density are used as MOEs for weaving segments ([125], [126]).

In the view of drivers, they seek acceptable gaps as soon as arriving at the auxiliary lane to merge into the target lanes. When there are CACC platoons in the traffic flow, it will be difficult to find any acceptable gaps when the human driver occasionally cruises parallel to the platoons due to the short gaps between CAVs. Therefore, the vehicles that are trying to make a lane-changing would slow down near the off-ramp and more speed drops are observed (Figure 30). For this reason, the following results are going to focus on the speed at the end of the auxiliary lane.

Besides, the speed of the middle lane is slightly lower than the others on the upstream of the weaving segment. This is caused by more numbers of vehicles, among whom some vehicles from on-ramp that have already merged into the mainline and some vehicles from the leftmost lane that are trying to drive to the auxiliary lane. It can be easily observed in the real world as well.

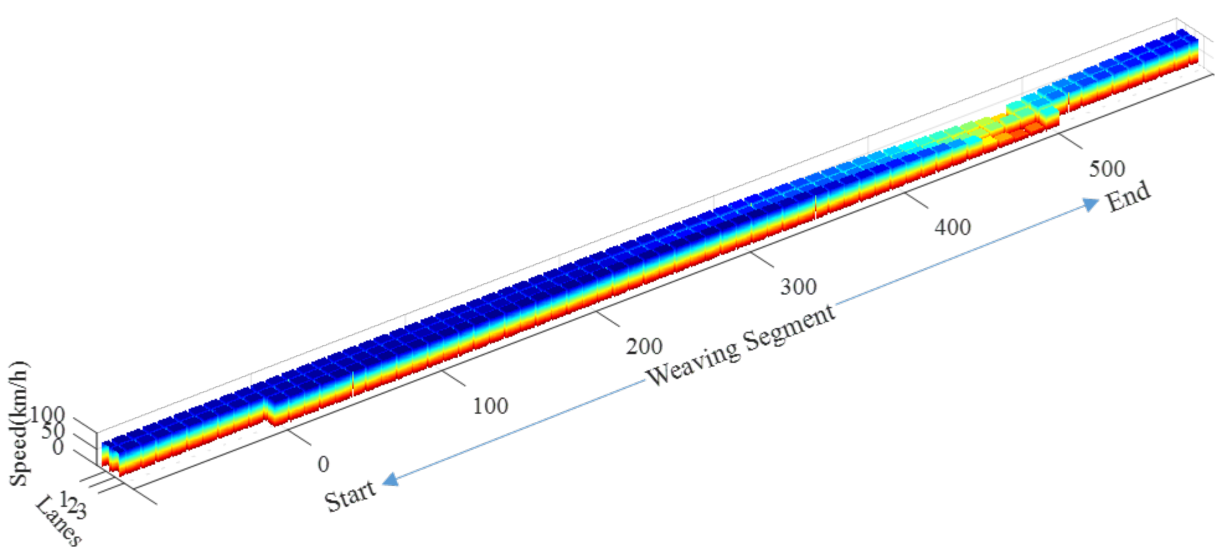

Figure 30 Time Mean Speed Distribution on Weaving Segment

4.3.3.2 Mixed traffic on weaving segment

This section presents the performance of normal traffic vs. mixed traffic. As a demonstration, the high volume case with 8-CAV platoons is selected for discussion. The auxiliary lane and mainline speeds are shown in Figure 31 for comparing the normal traffic and mixed traffic. The significances of speed mean differences are tested with ANOVA single factor test ([127]). The red-bordered bars represent that the speeds are different at the significance level of 95%. The number of vehicles that cut-in the CACC platoons on weaving segment is counted to show how human drivers interact with the platoons (Figure 31). It should be noted that no vehicle can be categorized as cut-in behaviors in normal traffic. Considering that 72% of the acceptable gaps are greater than 0.9s ([113]), these overall values are reasonable, especially for comparing between the different cases.

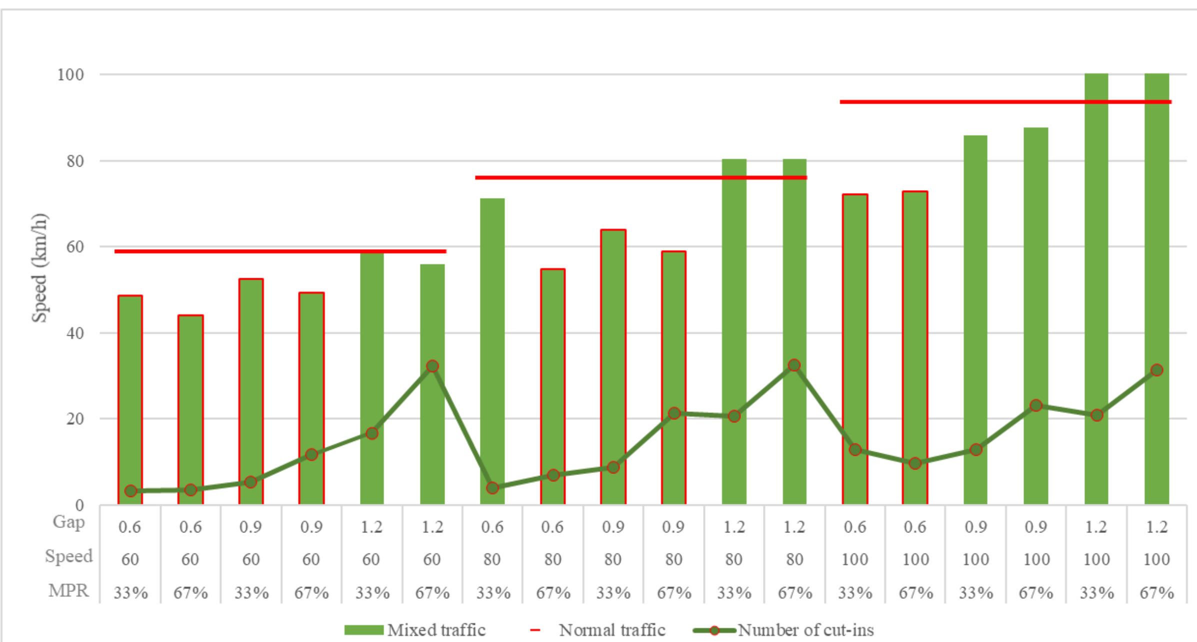

a) Speed on the auxiliary lane

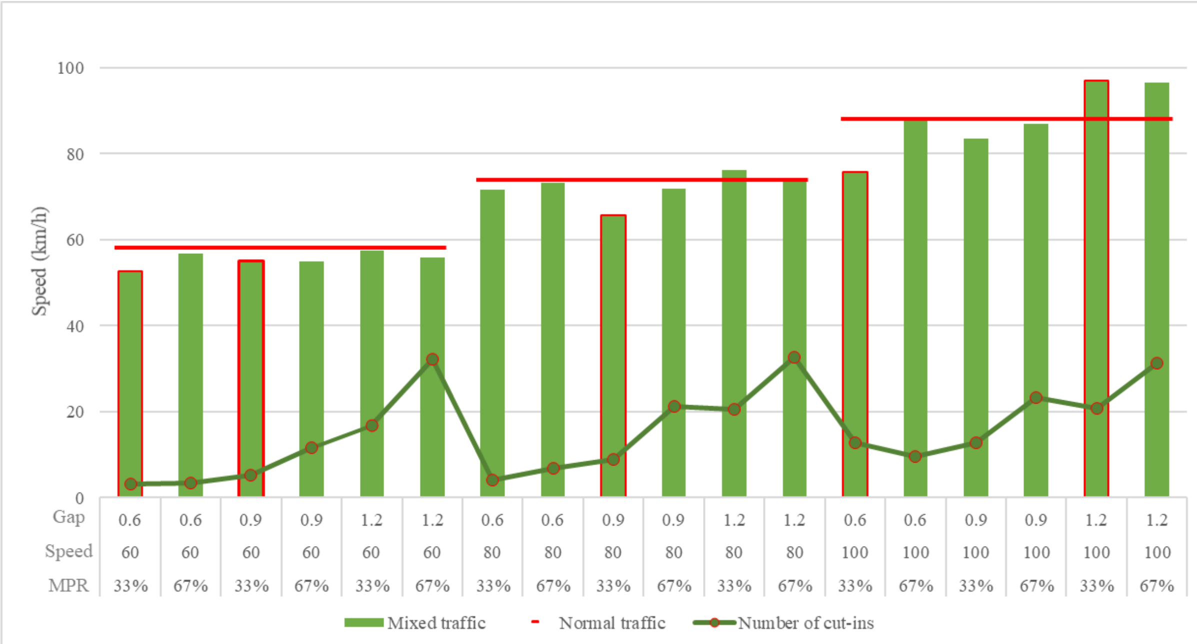

b) Speed on mainline

* Red bordered bars represent significant differences between normal traffic and mixed traffic

Figure 31 Speed of Weaving Segment in Normal Traffic vs. Mixed traffic

From Figure 31 (a), it can be observed that the speed in mixed traffic is lower, in general, than that in the normal traffic. Especially when the desired gap is small, i.e., 0.6s or 0.9s, the speed is significantly low. This is because the short gaps between CAVs block the lane-changing activities of human drivers and lead to more speed drops on the auxiliary lane. The number of cut-ins also supports this phenomenon. Platoons with smaller desired gaps tend to prohibit the cut-ins of human-driven vehicles. On the other hand, higher desired gaps allow more frequent cut-ins, which leads to higher speed on the auxiliary lane. Therefore, with the desired gap of 1.2s, the speed of mixed traffic is similar or even higher than the normal traffic. For the speed as the factor, a higher speed also allows more cut-ins and less speed drops (seen from the cases of speed 100 km/s, desired gap 0.9s). The reason is that the higher speed with the same desired gap would lead to a longer distance headway and may let the human drivers accept the gap. When regarding the MPR, the higher MPR 67% results in more serious speed drops when the desired gap and speed are both small. This is caused by more chances that the vehicles meet the platoons when trying to make lane-changing, thus, more chances of being blocked by the platoons. However, in the higher speed or big desired gap cases, the MPR does not significantly affect the speed on the auxiliary lane. Therefore, the chance of vehicles from on-ramp meeting the platoons, together with the probability of the gaps being taken by the human drivers, decide the efficiency of the auxiliary lane.

For the mainstream speed, the similar trend is shown ((Figure 31 (b)). However, the speed drops are slighter, compared to the auxiliary lane. This is explained by the CACC platoons on the mainline blocking the lane-changing activities of the vehicles from on-ramp and to off-ramp, which on the other side ensures or protect the movement of the mainstream from the auxiliary lane.

4.3.3.3 Impact of traffic volumes

The impacts of mainstream volumes are studied in this section. Three different volumes (1100 veh/h/ln, 1500 veh/h/ln, and 1900 veh/h/ln) are tested with 8-CAV platoons, representing low, medium, and high traffic flow, respectively. The average speeds of the auxiliary lane are presented in Figure 32, the speed values of the auxiliary lane and the numbers of cut-ins are in Table 13. Detail speeds of weaving segment are listed in Appendix A (Table A.1 - Table A.3).

Within the same traffic volume, similar trends in auxiliary lane speed are observed as the previous section. Those are: speeds in mixed traffic are in general lower than normal traffic; smaller gaps lead to more speed drops on the auxiliary lane; higher speed has less speed drops, and higher MPR results in more serious speed drops when the desired gap and speed are both small. Under the same mixed traffic case, the higher volumes decrease the speed of the weaving segment.

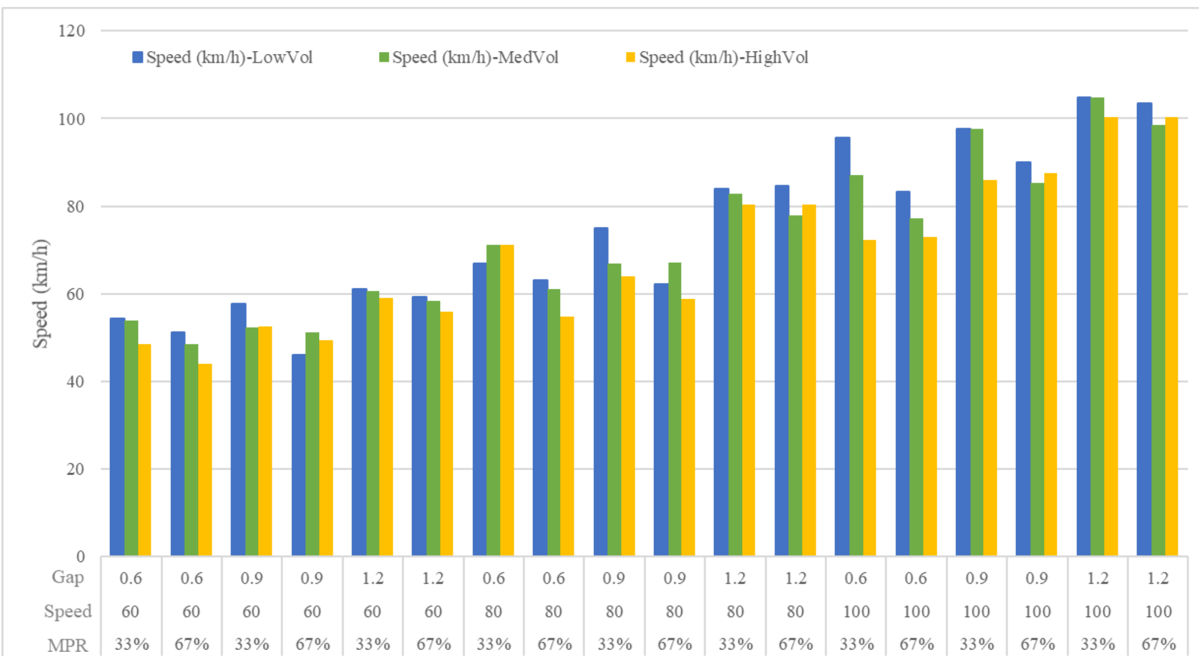

Figure 32 Average Speed of Auxiliary Lane at Different Volumes

For a more intuitive comparison, the relative speeds are shown (Figure 33), which are calculated as the speeds in mixed traffic minus the speeds in normal traffic (MPR = 0%) with corresponding traffic volume. The impact of volumes on the relative speed, ranging from –27 km/h to +8 km/h, are not obvious or consistent. From the figure, the six cases out of eighteen have more speed drops with higher traffic volume (speed 60km/h, desired gap 0.6s, MPR 67%; speed 60km/h, desired gap 1.2s, MPR 33%; speed 80km/h, desired gap 0.6s, MPR 67%; speed 80km/h, desired gap 0.9s, MPR 33%; speed 100km/h, desired gap 0.6s, MPR 33%; and speed 100km/h, desired gap 1.2s, MPR 33%). Some cases (speed 60km/h, desired gap 1.2s, MPR 67%; speed 80km/h, desired gap 1.2s, MPR 33%;) have similar speed drops, and some have irregular relative speeds along the traffic volume. This might be caused by the different average speed of normal traffic. The speeds of auxiliary lane in low volume (61.9 km/h, 84.6 km/h, and 104.4 km/h) are 2.7 km/h, 2.9 km/h, and 11.7 km/h higher than in high volume (Table 13). Therefore, the speed drops in low volume are amplified.

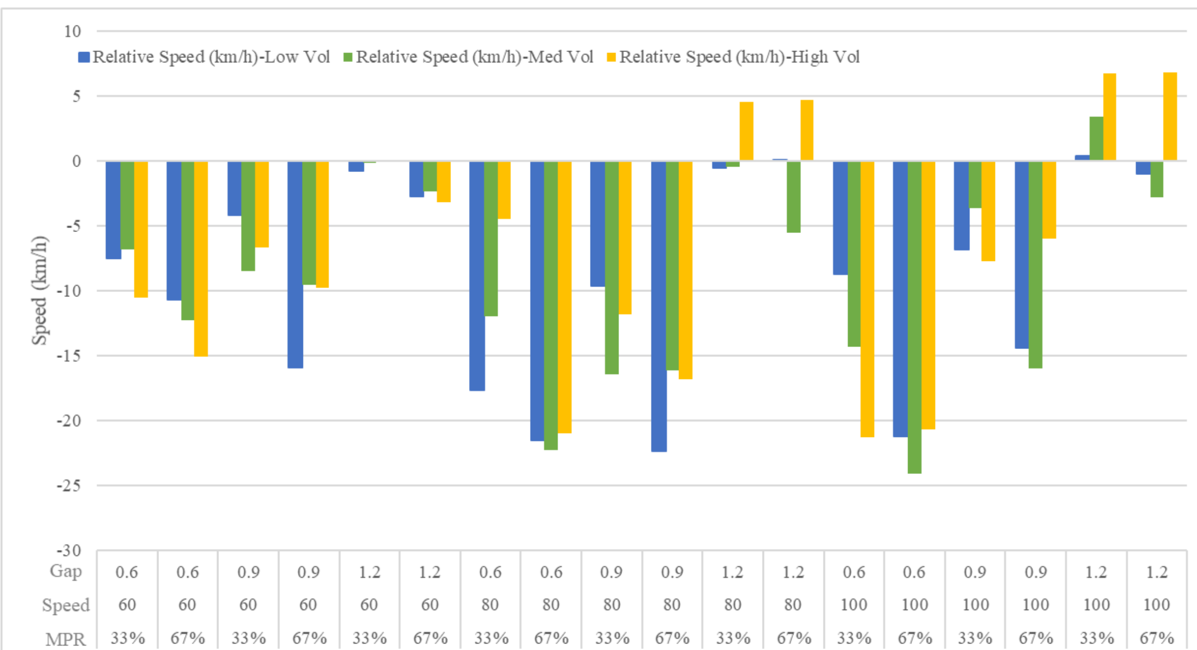

Figure 33 Relative Speed of Auxiliary Lane at Different Volumes

Table 13 Flow Rate and Average Speed of Auxiliary Lane

	60 km/h		80 km/h		100 km/h	
MPR = 0%	Speed (km/h)	Number of cut-in	Speed (km/h)	Number of cut-in	Speed (km/h)	Number of cut-in
Low Vol	61.9	-	84.6	-	104.4	-
Med Vol	60.8	-	83.3	-	101.3	-
High Vol	59.2	-	81.7	-	92.7	-
8-CAV	MPR = 33%; Desired gap = 0.6s					
Low Vol	54.4	0.0	66.9	0.8	95.7	2.2
Med Vol	54.0	1.6	71.3	1.4	87.0	3.2
High Vol	48.6	4.2	71.3	4.4	72.3	14.4
	MPR = 67%; Desired gap = 0.6s					
Low Vol	51.3	0.8	63.0	1.6	83.2	3.0
Med Vol	48.5	0.6	61.0	3.4	77.2	5.8
High Vol	44.1	3.8	54.8	7.6	72.9	11.2
	MPR = 33%; Desired gap = 0.9s					
Low Vol	57.8	3.4	75.0	5.6	97.6	7.0
Med Vol	52.3	5.0	66.9	5.2	97.7	13.2
High Vol	52.5	9.6	63.9	10.0	85.9	17.8
	MPR = 67%; Desired gap = 0.9s					
Low Vol	46.0	3.4	62.2	3.4	90.0	12.6
Med Vol	51.2	9.4	67.1	15.6	85.3	13.6
High Vol	49.4	13.6	58.9	23.8	87.6	27.4
	MPR = 33%; Desired gap = 1.2s					
Low Vol	61.2	8.0	84.0	9.8	104.7	12.4
Med Vol	60.6	10.0	82.8	15.0	104.8	19.0

High Vol	59.1	19.4	80.3	25.4	100.3	29.2
	MPR = 67%; Desired gap = 1.2s					
Low Vol	59.2	15.6	84.6	13.0	103.4	22.8
Med Vol	58.4	19.0	77.8	18.6	98.5	20.8
High Vol	56.0	39.0	80.5	37.6	100.4	40.2

4.3.3.4 Impact of platoon sizes

A long CACC platoon is expected to increase the capacity because with the same number of CAVs, a longer platoon strategy will lead to less number of platoons [18]. However, a too long platoon may have difficulties in stable communication and thus, in string stable [123]. Then the impact of platoon size on the traffic flow on the weaving segment is another exploring spot. With a long platoon, the lane changing of human drivers would be impeded more seriously, or the human drivers may be more aggressive due to long waiting time. The performance of the weaving segment with different platoon sizes is studied in this section. Three platoon sizes (4-CAV, 8-CAV, and 12-CAV) are simulated with high mainstream volume.

The average speeds on the auxiliary lane and the numbers of cut-in vehicles with different platoon sizes in Figure 34 present the performance of the weaving segment with different CACC platoons. The speed values and the numbers of cut-ins can be seen in Table 14, and more detail speed values of weaving segment are attached in Appendix A (Table A.3 - Table A.5).

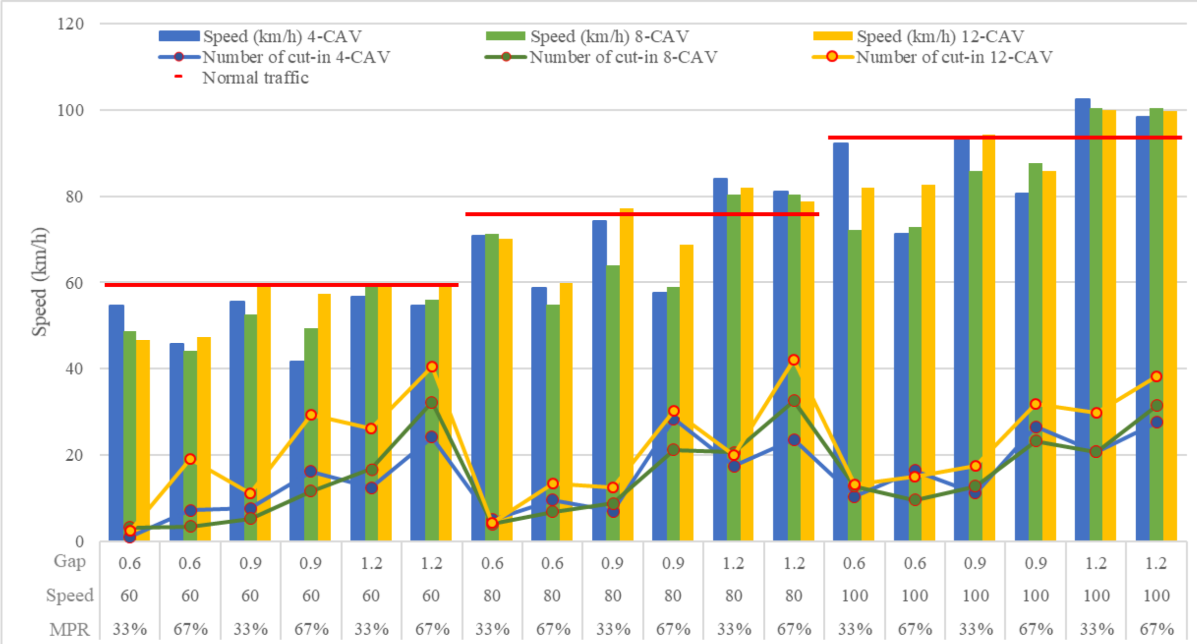

Figure 34 Speed of Auxiliary Lane with Different Platoon Size

In general, the speed drops on the auxiliary lane are worse with smaller gaps of platoons, lower speeds, or higher MPRs. When comparing the speeds with different platoon sizes, the trends are not consistent. However, the number of cut-ins have some obvious consistent changes. The cut-in happens when the gap is acceptable for the driver, and the driver is more close to the emergency stop place. Therefore, congested traffic results in more aggressive behaviors. That means with a longer platoon, the lane changing of human drivers would be impeded more seriously, but at the same time, the human drivers may be more aggressive due to longer waiting time. Therefore, the number of cut-ins increases as the platoon size becomes bigger. This is the reason why there are no consistent changes in the speed drops on the auxiliary lane.

The number of inter-platoon gaps also contributes to cut-ins. With the same number of

CAVs N_{CAV}, the numbers of platoons are different, and the numbers of inter-platoon gaps are as follows:

$$N_i = N_{p\_i} \times (i-1) = N_{CAV} \times \left(1 - \frac{1}{i}\right) \tag{4.2}$$

where, N_i is the number of gaps of the platoon size i, and N_{p_i} is the number of platoons.

For example, if the platoon size is 4 and 12, the total number of gaps are:

$$N_4 = N_{p\_4} \times (4-1) = N_{CAV} \times \frac{3}{4} \tag{4.3}$$

$$N_{12} = N_{p\_12} \times (12-1) = N_{CAV} \times \frac{11}{12} \tag{4.4}$$

There are $\frac{N_{CAV}}{6}$ more gaps in the 12-CAV platoon size than the 4-CAV platoon size. However, the increase rates of cut-in number are much more than that of inter-platoon gap numbers. Therefore, the aggressiveness of human drivers contributes the main part of the number of cut-ins with longer platoons and the probability of cut-ins increases with a longer platoon.

The number of cut-ins indicates that the longer platoons are more easily to be divided by cut-in vehicles on the weaving segment, which means the efficiency of automated platoons would be affected. From the view of human drivers, the driving workload also increases with a longer platoon.

As mentioned to the vehicle cut-in and the driving workload, the safety is assessed in addition. The time-to-collision (TTC), which is the time needed for two vehicles collide assuming no speed or direction changes, is selected and the threshold 1.5s in Surrogate Safety

Assessment Model (SSAM) is used for counting critical cases [128]. The numbers of critical cases in different scenarios are counted (Figure 35). Though TTC is well accepted to indicate the safety of the traffic flow, it is not comprehensive enough, and its absolute value cannot represent a firm meaning. When comparing the TTC counts of mixed traffic and normal traffic, the most obvious rule is that TTC counts in the desired gap 1.2s cases are lower than the normal cases or the smaller desired gaps. The other factors, such as speed, MPR, platoon size, do not have obvious or consistent impacts. This indicates short gaps of CACC platoons cannot stand the cut-ins and would result in relatively dangerous situations compared to the long desired gaps.

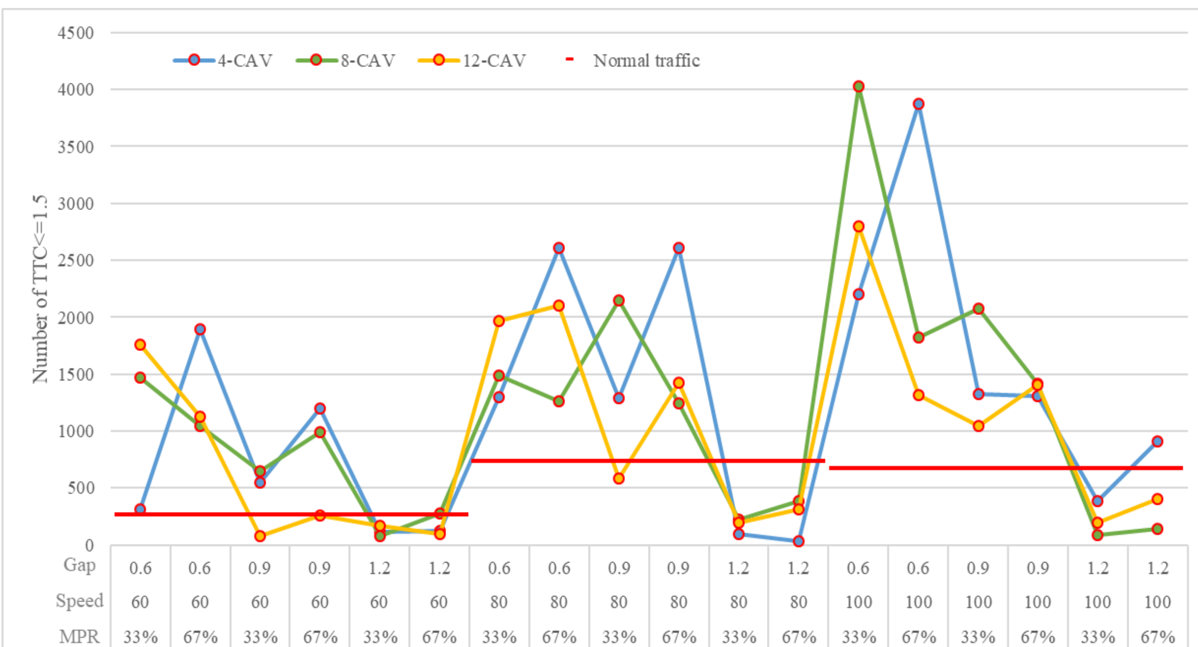

Figure 35 Number of TTC<=1.5s on Weaving Segment with Different Platoon Size

Table 14 Flow Rate and Average Speed of Auxiliary Lane (High Volume)

	60 km/h		80 km/h		100 km/h	
Input: 1900 veh/h/lane	Speed (km/h)	Number of cut-in	Speed (km/h)	Number of cut-in	Speed (km/h)	Number of cut-in
MPR = 0%	59.2	-	81.7	-	92.7	-
	MPR = 33%; Desired gap = 0.6s					
4-CAV	54.7	1.0	70.7	5.0	92.2	10.4
8-CAV	48.6	3.2	71.3	4.0	72.3	12.8
12-CAV	46.6	2.4	70.1	4.2	81.9	13.2
	MPR = 67%; Desired gap = 0.6s					
4-CAV	45.9	7.2	58.8	9.6	71.4	16.4
8-CAV	44.1	3.4	54.8	6.8	72.9	9.6
12-CAV	47.4	19.2	59.8	13.4	82.6	15.0
	MPR = 33%; Desired gap = 0.9s					
4-CAV	55.6	7.6	74.2	7.0	93.8	11.2
8-CAV	52.5	5.2	63.9	8.8	85.9	12.8
12-CAV	59.9	11.2	77.3	12.4	94.2	17.4
	MPR = 67%; Desired gap = 0.9s					
4-CAV	41.7	16.2	57.6	28.4	80.6	26.6
8-CAV	49.4	11.6	58.9	21.2	87.6	23.2
12-CAV	57.4	29.4	68.7	30.2	85.9	31.8
	MPR = 33%; Desired gap = 1.2s					
4-CAV	56.8	12.4	84.0	17.4	102.5	20.8
8-CAV	59.1	16.8	80.3	20.6	100.3	20.8
12-CAV	59.6	26.2	81.9	20.0	99.9	29.8

	MPR = 67%; Desired gap = 1.2s					
4-CAV	54.6	24.2	81.1	23.6	98.3	27.6
8-CAV	56.0	32.2	69.3	32.6	94.8	31.4
12-CAV	59.2	40.4	78.7	42.0	99.7	38.2

4.3.4 Results and discussions

A. Lessons learned

The mixed traffic simulation on the weaving segment is implemented to explore the impacts of CACC platoons, and further, to find advanced CACC strategies for weaving segments.

In general, based on the simulation results, it can be observed that the speed in mixed traffic is lower than that in the normal traffic. It is caused by the long and dense platoons blocking the lane-changing activities of the vehicles from on-ramp or to off-ramp. Especially when the desired gap is small, i.e., 0.6s or 0.9s, the speed is significantly low. However, higher desired gaps allow more frequent cut-ins, which leads to higher speed on the auxiliary lane. Higher speed also allows more cut-ins and results in less speed drops because of the longer distance headway, which has a higher probability of being taken by the human drivers for lane changing. Besides, the higher MPR results in more serious speed drops when the desired gap and speed are both small. It is due to more chances that the vehicles meet the platoons when trying to make lane-changing, and thus, more chances of being blocked by the platoons. However, in the higher speed or big desired gap cases, the MPR does not significantly affect the speed on the auxiliary lane.

Different mainstream volumes have the same trend with the factors of the desired gap, speed, and MPR. One-third of the cases showed more speed drops with higher traffic volume. However, the relative speed drops compared to the normal traffic with the same volume is not obvious or consistent, which is caused by the different average speed of normal traffic.

With different platoon sizes, the speed on the auxiliary lane has no consistent changes. However, the number of cut-ins increases consistently as the platoon size becomes longer. This is because the lane changing of human drivers would be impeded more seriously with a longer platoon, but at the same time, the human drivers may be more aggressive due to longer waiting time. Therefore, there are no consistent changes in the speed drops on the auxiliary lane. On the other hand, the longer platoons are more easily divided by cut-in vehicles on the weaving segment, which may affect the efficiency of the automated platooning.

B. Discussions on the results

The simulation results reveal the following key outcomes:

- In general, the mixed traffic has lower speed on the auxiliary lane.
- Shorter gaps block the lane changing of the human drivers more seriously and make the speed drops even worse.
- Higher MPR also blocks the lane changing more frequently and results in more speed drops.

- On the contrary, high speed (100 km/h) or long gap (1.2s) improves the speed on the auxiliary lane.
- Longer platoons impede the lane changing more seriously and stimulate the aggressiveness of the human drivers, and thus, can be more easily divided by cut-in vehicles.

Therefore, the CACC or automated platooning strategies should be enhanced for improving the weaving segment performance. Firstly, the CACC mode is better to be active at high free-flow speed. Then the desired gaps are suggested to be increased when approaching the weaving segments. Besides, the trade-off between ensuring the efficiency of CACC platoons and minimizing the speed drops of the auxiliary lane should be made.

4.4 Concluding remarks

In this paper, an integrated simulation platform is proposed for realistically simulating the mixed traffic with CAVs and human drivers. A dedicated VDM and controller for CAVs are embedded instead of using simplified car-following models in order to simulate a realistic decision-making process and driving behaviors. Then with the simulation platform, the performance of mixed traffic on the weaving segment is evaluated, where the CAVs are forming CACC platoons on the mainline.

The simulation result shows that the long and dense CACC platoons block the lane changing activities of human drivers from on-ramp and to off-ramp and result in speed drops on the auxiliary lane. As the desired gaps of platoons are shorter or MPR is higher, the speed drops become worse. When the speed is high, and the desired gap is long, the speed on the auxiliary lane is improved. These changes are consistent under different mainstream volumes and with different platoon sizes. Besides, longer platoons are more easily divided by more frequent cut-in vehicles, whose lane changing are blocked worse and try aggressive lane changing.

Based on the simulation results, some suggestions are provided for CACC or automated platooning strategies to improve the weaving segment performance. The CACC mode is recommended to be activated at high free-flow speed, and to adjust the desired gaps with bigger values, e.g., 1.2s, to decrease the speed drops on the auxiliary lane. At the same time, the efficiency of CACC platoons and mainline traffic flow should also be taken into account. That means the impact of increasing the desired gaps to the upstream traffic flow and to the auxiliary lane should be studied to find the optimal control strategy.

This study is expected to extend to the mixed traffic evaluation with more CAV applications, including the lateral control. Besides, CACC algorithms with the heterogeneous platoons should be developed by adding different VDMs, which considers different vehicle types in the platoon. Fuel and safety-related research should also be implemented with the mixed traffic environment to understand the traffic performance comprehensively.

Chapter 5. Conclusions and future research

5.1 Summary and conclusions

With emerging technologies of connected and automated vehicles (CAVs), CAVs will play key roles in the transportation field. Therefore, the potential risks, such as cyber-attack, system malfunction, and interaction between CAVs and human drivers, and the impacts to the transportation field should be explored in advance for further implementation. However, as the most common method of evaluating traffic performance, traffic flow simulation tools usually model the behaviors of CAVs with strong assumptions. Therefore, this dissertation developed an integrated simulation platform to explicitly and realistically model the driving behaviors of CAVs and mixed traffic flow. Then the simulation is used to develop a robust CACC (cooperative adaptive cruise control) algorithm against cyber-attack to create a crash-free environment and to evaluate the performance of the mixed traffic (with CACC platoons) on the freeway weaving segment.

The proposed simulation process follows the control process of CAVs, i.e., detecting information, making decisions, and realizing through vehicle dynamics. Following features are covered and modeled in the platform: i) vehicle dynamics; ii) sensor errors and communication delays; iii) state-of-the-art CACC controller; and iv) ability to quantify crash severity and CACC stability. The vehicle behavior is accurate when being compared with CACC field data. It ensures that stability and severity measurements output from the platform is accurate. Then the safety impact and crash severity of CACC platoon under potential risks, i.e., cyber-attack, in sensors and communications are evaluated.

Considering the potential risks in the traditional CACC, a robust CACC algorithm is developed. The proposed algorithm combines the advantage of APF (all-predecessor following) and PLF (predecessor-leader following) control methods to improve the stability and robustness of the CACC platoon under unexpected cyber-attack. String stability of the proposed CACC algorithm has been theoretically proven, and the performance has been validated with the simulation of various cyber-attack scenarios. Except in the extreme case, the proposed algorithm is capable of ensuring the collision-free environment. Considering the comfortable maximum deceleration rate lies on –2.5~3 m/s^2, this extreme case (–6 m/s^2) rarely happens in the real world. Therefore, the robust CACC outperforms the traditional algorithm in most of the cases.

The CACC platoon simulation is further expanded to the mixed traffic flow simulation by integrating the CAV simulation platform with a microscopic transportation simulation tool VISSIM for human driver behavior modeling. Then the mixed traffic on weaving segment is evaluated to explore the impact of CAVs, provide potential problems of existing algorithms, and propose alternative strategies. The free flow speed, market penetration rate (MPR), the desired gap of the platoon, traffic volume, and mainstream volume are studied as the sensitivity analysis factors.

Key conclusions of this research are listed below:

- The proposed CACC evaluation platform is capable of quantifying the crash severity level. The result shows that the severity output is sensitive to the degree of cyber-attacks. Cyber-attacks do not always result in crashes, but they do create large oscillations. It is relatively dangerous and unstable when both GPS and Radar have the same sign of errors (positive/negative). GPS jamming is the most dangerous cyber-attack and always results in crashes.

- When the emergency braking system (EBS) embedded to CACC algorithm, most of the crashes can be effectively avoided. However, when the radar sensor is attacked with inappropriate information, the crash may not be prevented since EBS relies on radar. EBS trigger determination is a critical issue with CACC. To avoid the frequent mode switches and violent vehicle oscillations, a method to compute the threshold of triggering EBS should be developed.
- Robust CACC algorithm is developed to overcome the shortcoming of the state-of-the-art CACC in dealing with unexpected cyber-attack and to improve the stability and robustness of the CACC platoon. It is theoretically proven to be able to maintain string stability and can effectively react to different situations, except in extreme case, without control jags, which commonly happen in traditional algorithms when switching the control mode between CACC and EBS or transferring the leading vehicles.
- When CAVs are traveling in CACC platoons, the lane changing of the human drivers from the on-ramp and to off-ramp is affected by the long and dense platoons. Therefore, the speed on the auxiliary lane in mixed traffic is lower

than that in the normal traffic. Shorter gaps block the lane changing of the human drivers more seriously and make the speed drops even worse. Higher MPR also blocks the lane changing more frequently and results in more speed drops. On the contrary, high speed (100 km/h) or long gap (1.2s) improves the speed on the auxiliary lane. Longer platoons impede the lane changing more seriously and stimulate the aggressiveness of the human drivers, and thus, can be more easily divided by cut-in vehicles and the efficiency is affected.

- Therefore, the CACC or automated platooning strategies should be enhanced for improving the weaving segment performance. Firstly, the CACC mode is better to be active at high free-flow speed. Then the desired gaps are suggested to be increased when approaching the weaving segments. Besides, the trade-off between ensuring the efficiency of CACC platoons and minimizing the speed drops of the auxiliary lane should be made. For example, the impact of the desired gap adjustment to the upstream and to the auxiliary lane should be studied to find the optimal strategy.

The contributions are as follows:

- The first important contribution of this study is to develop the integrated simulation platform (VISSIM, PreScan, and MADYMO) for simulating mix traffic flow realistically and overcome the shortcomings of traditional simulation tools.

- The simulation platform can carry the most prevailing state-of-the-art CAV controllers and any paroxysmal or extreme events that CAVs may be exposed to evaluate the safety performance. The injury probability quantifies the severity of a crash by reconstructing the crash and using a dedicated mathematical method for injury estimation. It is particularly useful when traditional empirical driver models no longer apply. Such situations include, but are not limited to, cyber-attack, sensor failure, and heterogeneous traffic.
- The mixed traffic simulation can provide the pros and cons of the CAV controllers, CACC in this research, which provided the basis of the robust CACC development. It is expected to help the researchers in the future to improve the algorithms and optimize the controllers for mixed traffic flow before further implementation.

5.2 Future research

Even though many efforts have been made to minimize unrealistic assumptions in the simulation and the evaluation of the mixed traffic, there are still some assumptions adopted, and the research scope is limited in current studies. Therefore, potential future research is proposed to make further efforts, release more assumptions, deal with some details in modeling, and to cover more aspects of mixed traffic for further evaluation and improvement.

Firstly, as mentioned above, CACC algorithm should be enhanced for different types of freeway segments, such as weaving segments. Considering that CACC is quite mature and ready-to-implement technology with field test validation, its adaptability to the transportation system is especially significant. However, traditional algorithms are only focusing on the basic segment efficiency, where not all kinds of freeway segments are considered. If the potential issues of this emerging technology are not clearly addressed, it will cause weak points near non-basic segments along the freeways. Therefore, sufficient simulations should be implemented with different factors to thoroughly understand the mixed traffic performance. For example, the impact of increasing the desired gaps to the upstream traffic flow need to be explored since shockwave can be generated. Then the strategies can be enhanced with optimal parameters, e.g., desired gaps, in order to maximize the freeway efficiencies.

Secondly, various CAV controllers should be incorporated in the future. Current research is focused on the longitudinal movements of CAVs, where only CACC is considered. As the automated levels become higher, the vehicle controls will cover more aspects and combine various driving tasks. For example, merging assistance system can be added for the CAVs to merge into the platoons smoothly; lane change system can help CAVs with lane changing maneuvers, which should be different from human drivers and also differ by the parameter settings. Therefore, the CAV modeling should cover various controllers, not only CACC, to evaluate the performance in network-wide.

Finally, the mode switches between automated control mode and human control mode need to be studied. By far, most of the studies are assuming immediate switches in the simulations. This means that the mode switch process is idealized or ignored. However, the mode switch may contain control jags, cognizance delay, or perception-reaction time. Besides, as more and more automated control functions being available, the human driver may behave differently from traditional driving, such as concentrate less on the driving activity, which leads to longer delay and affects the safety. Therefore, field data or experiments with driving simulators should be used for understanding the realistic human-automation interactions, which can be reflected in the CAV simulation in the future.

References

[1] 2013 Daimler AG Germany, "Welcome to the Mercedes-Benz Tech Center." [Online]. Available: http://techcenter.mercedes-benz.com/en/. [Accessed: 01-Sep-2017].

[2] "Experience automated driving," *Bosch Global*. [Online]. Available: https://www.bosch.com/explore-and-experience/experience-automated-driving/. [Accessed: 10-Sep-2018].

[3] "Volvo Car USA Makes Semi-Autonomous Driving Features Standard on All-New Volvo S90 sedan." [Online]. Available: https://www.media.volvocars.com/us/en-us/media/pressreleases/172317/volvo-car-usa-makes-semi-autonomous-driving-features-standard-on-all-new-volvo-s90-sedan. [Accessed: 10-Sep-2018].

[4] "A New Level of Performance and Sophistication — The Next Generation Lexus ES | Toyota USA Newsroom." [Online]. Available: http://pressroom.lexus.com/releases/new+level+perfor+sophistication+next+generation+lexus+es.htm. [Accessed: 10-Sep-2018].

[5] US DOT, "Critical Reasons for Crashes Investigated in the National Motor Vehicle Crash Causation Survey," US DOT NHTSA, Washington DC, DOT HS 812 115, 2015.

[6] M. Timothy, L. Julie, N. Diane, P. Adrian, and H. Elliot, "Leveraging the Promise of Connected and Autonomous Vehicles to Improve Integrated Corridor Management and Operations: A PRIMER," Primer FHWA-HOP-17-001, Jan. 2017.

[7] "Autonomous Vehicle Sales to Surpass 33 Million Annually in 2040, Enabling New Autonomous Mobility in More Than 26 Percent of New Car Sales, IHS Markit Says |

IHS Online Newsroom.” [Online]. Available: http://news.ihsmarkit.com/press-release/automotive/autonomous-vehicle-sales-surpass-33-million-annually-2040-enabling-new-auto. [Accessed: 06-Jul-2018].

[8] B. Schoettle and M. Sivak, “A Survey of Public Opinion about Autonomous and Self-Driving Vehicles in the U.S., the U.K., and Australia,” p. 42.

[9] A. Smith and M. Anderson, “Automation in everyday life,” Pew Research Center, Oct. 2017.

[10] J. Levenson, “Google’s self-driving car has been involved in its worst crash yet,” *The Next Web*, 26-Sep-2016. [Online]. Available: https://thenextweb.com/google/2016/09/26/googles-self-driving-car-involved-worst-crash-yet/. [Accessed: 21-Sep-2017].

[11] A. Singhvi and K. Russell, “Inside the Self-Driving Tesla Fatal Accident,” *The New York Times*, 01-Jul-2016.

[12] K. C. Dey *et al.*, “A Review of Communication, Driver Characteristics, and Controls Aspects of Cooperative Adaptive Cruise Control (CACC),” *IEEE Transactions on Intelligent Transportation Systems*, vol. 17, no. 2, pp. 491–509, Feb. 2016.

[13] V. Milanes, S. E. Shladover, J. Spring, C. Nowakowski, H. Kawazoe, and M. Nakamura, “Cooperative Adaptive Cruise Control in Real Traffic Situations,” *IEEE Transactions on Intelligent Transportation Systems*, vol. 15, no. 1, pp. 296–305, Feb. 2014.

[14] J. Ploeg, B. T. Scheepers, E. Van Nunen, N. Van de Wouw, and H. Nijmeijer, “Design and experimental evaluation of cooperative adaptive cruise control,” in *Intelligent*

Transportation Systems (ITSC), 2011 14th International IEEE Conference on, 2011, pp. 260–265.

[15] J. Vander Werf, S. Shladover, M. Miller, and N. Kourjanskaia, "Effects of adaptive cruise control systems on highway traffic flow capacity," *Transportation Research Record: Journal of the Transportation Research Board*, no. 1800, pp. 78–84, 2002.

[16] S. Shladover, D. Su, and X.-Y. Lu, "Impacts of Cooperative Adaptive Cruise Control on Freeway Traffic Flow," *Transportation Research Record: Journal of the Transportation Research Board*, vol. 2324, pp. 63–70, Dec. 2012.

[17] L. C. Davis, "Effect of adaptive cruise control systems on mixed traffic flow near an on-ramp," *Physica A: Statistical Mechanics and its Applications*, vol. 379, no. 1, pp. 274–290, Jun. 2007.

[18] H. Liu, X. Kan, S. E. Shladover, X. Y. Lu, and R. A. Ferlis, "Impact of Cooperative Adaptive Cruise Control (CACC) on Multilane Freeway Merge Capacity.pdf," presented at the Transportation Research Board 97th Annual Meeting, Washington, DC, 2018.

[19] PTV Group, "PTV Vissim 10 Manual." 2017.

[20] G. Nelson, "Tesla beams down 'autopilot' mode to Model S," *Automotive News*. [Online]. Available: http://www.autonews.com/article/20151014/oem06/151019938/tesla-beams-down-autopilot-mode-to-model-s. [Accessed: 01-Sep-2017].

[21] "Chapter 8: Advancing Clean Transportation and Vehicle Systems and Technologies," US DOE, Sep. 2015.

[22] J. Lee and B. Park, “Development and Evaluation of a Cooperative Vehicle Intersection Control Algorithm Under the Connected Vehicles Environment,” *IEEE Transactions on Intelligent Transportation Systems*, vol. 13, no. 1, pp. 81–90, Mar. 2012.

[23] H. Jiang, J. Hu, S. An, M. Wang, and B. B. Park, “Eco approaching at an isolated signalized intersection under partially connected and automated vehicles environment,” *Transportation Research Part C: Emerging Technologies*, vol. 79, no. Supplement C, pp. 290–307, Jun. 2017.

[24] J. Ma, X. Li, F. Zhou, J. Hu, and B. Park, *Parsimonious shooting heuristic for trajectory control of connected automated traffic part II: computational issues and optimization*. 2016.

[25] E. Hamida, H. Noura, and W. Znaidi, “Security of Cooperative Intelligent Transport Systems: Standards, Threats Analysis and Cryptographic Countermeasures,” *Electronics*, vol. 4, no. 3, pp. 380–423, Jul. 2015.

[26] D. Dominic, S. Chhawri, R. M. Eustice, D. Ma, and A. Weimerskirch, “Risk Assessment for Cooperative Automated Driving,” 2016, pp. 47–58.

[27] J. Petit and S. E. Shladover, “Potential Cyberattacks on Automated Vehicles,” *IEEE Transactions on Intelligent Transportation Systems*, pp. 1–11, 2014.

[28] L. Xu, L. Y. Wang, G. Yin, and H. Zhang, “Communication Information Structures and Contents for Enhanced Safety of Highway Vehicle Platoons,” *IEEE Transactions on Vehicular Technology*, vol. 63, no. 9, pp. 4206–4220, Nov. 2014.

[29] L. Xu, L. Y. Wang, G. Yin, and H. Zhang, “Impact of Communication Erasure Channels on the Safety of Highway Vehicle Platoons,” *IEEE Transactions on Intelligent Transportation Systems*, vol. 16, no. 3, pp. 1456–1468, Jun. 2015.

[30] A. A. Peters, R. H. Middleton, and O. Mason, “Leader tracking in homogeneous vehicle platoons with broadcast delays,” *Automatica*, vol. 50, no. 1, pp. 64–74, Jan. 2014.

[31] G. Naus, R. Vugts, J. Ploeg, R. van de Molengraft, and M. Steinbuch, “Cooperative adaptive cruise control, design and experiments,” in *American Control Conference (ACC), 2010*, 2010, pp. 6145–6150.

[32] G. Naus, R. Vugts, J. Ploeg, M. Van de Molengraft, and M. Steinbuch, “Towards on-the-road implementation of cooperative adaptive cruise control,” in *Proceedings of the 16th World Congress & Exhibition on Intelligent Transport Systems and Services*, Stockholm, Sweden, 2009.

[33] R. Van den Bleek, “Design of a hybrid adaptive cruise control stop-&-go system,” *Master’s Thesis, INO Science & Industry, Technische Universiteit Eindhoven*, 2007.

[34] D. Ward, T. Bertram, and M. Hiller, “Vehicle dynamics simulation for the development of an extended adaptive cruise control,” in *Advanced Intelligent Mechatronics, 1999. Proceedings. 1999 IEEE/ASME International Conference on*, 1999, pp. 730–735.

[35] S. Oncu, J. Ploeg, N. van de Wouw, and H. Nijmeijer, “Cooperative Adaptive Cruise Control: Network-Aware Analysis of String Stability,” *IEEE Transactions on Intelligent Transportation Systems*, vol. 15, no. 4, pp. 1527–1537, Aug. 2014.

[36] Y. Zheng, S. E. Li, J. Wang, L. Y. Wang, and K. Li, “Influence of information flow topology on closed-loop stability of vehicle platoon with rigid formation,” in *Intelligent Transportation Systems (ITSC), 2014 IEEE 17th International Conference on*, 2014, pp. 2094–2100.

[37] Xiao-Yun Lu, J. K. Hedrick, and M. Drew, “ACC/CACC-control design, stability and robust performance,” 2002, pp. 4327–4332 vol.6.

[38] P. Seiler, A. Pant, and K. Hedrick, “Disturbance propagation in vehicle strings,” *IEEE Transactions on automatic control*, vol. 49, no. 10, pp. 1835–1842, 2004.

[39] S.-B. Choi and J. K. Hedrick, “Vehicle longitudinal control using an adaptive observer for automated highway systems,” in *American Control Conference, Proceedings of the 1995*, 1995, vol. 5, pp. 3106–3110.

[40] “SSAM 2.1.6 Release Notes,” *Federal Highway Administration*. [Online]. Available: http://www.fhwa.dot.gov/downloads/research/safety/ssam/ssam2_1_6_release_notes.cfm. [Accessed: 23-Mar-2016].

[41] R. Zou, R. Grzebieta, and S. Richardson, “Rear seated occupant safety in frontal impacts,” *Department of Civil Engineering, Monash University, Australia*, 2001.

[42] R. Kent, J. Forman, D. Parent, and S. Kuppa, “Rear seat occupant protection in frontal crashes and its feasibility,” in *20th International Conference on the Enhanced Safety of Vehicles*, 2007.

[43] S.-J. Park, S.-W. Chae, and E.-S. Kim, “Analysis of neck fractures from frontal collisions at low speeds,” *International Journal of Automotive Technology*, vol. 11, no. 3, pp. 441–445, Jun. 2010.

[44] M. McGurrin, “Vehicle Information Exchange Needs for Mobility Applications,” Federal Highway Administration, FHWA-JPO-12-021, Feb. 2012.

[45] FAA, “Global Positioning System Standard Positioning Service Performance Standard,” Federal Aviation Administration, 89, Apr. 2015.

[46] US DOT, “SAE J2735 Standard- Applying the Systems Engineering Process,” US DOT, Standard FHWA-JPO-13-046, Jan. 2013.

[47] B. F. La Scala and G. W. Pulford, “An Analysis of Manoeuvring Target Detectors and Trackers for Over-The-Horizon Radar,” CSSIP Report, 1996.

[48] R. N. Jazar, *Vehicle dynamics: theory and applications*, Corrected at 3. printing. New York, NY: Springer, 2009.

[49] K. Abdelgawad, B. Hassan, J. Berssenbrügge, J. Stöcklein, and M. Grafe, “A Modular Architecture of an Interactive Simulation and Training Environment for Advanced Driver Assistance Systems,” p. 16.

[50] S. Samiee, S. Azadi, R. Kazemi, and A. Eichberger, “Towards a Decision-Making Algorithm for Automatic Lane Change Manoeuvre Considering Traffic Dynamics,” *PROMET - Traffic & Transportation*, vol. 28, no. 2, Apr. 2016.

[51] M. Elbanhawi, M. Simic, and R. Jazar, “Improved manoeuvring of autonomous passenger vehicles: Simulations and field results,” *Journal of Vibration and Control*, vol. 23, no. 12, pp. 1954–1983, Jul. 2017.

[52] P. Seiler, B. Song, and J. K. Hedrick, “Development of a collision avoidance system,” SAE Technical Paper, 1998.

[53] O. Ararat, E. Kural, and B. A. Guvenc, “Development of a Collision Warning System for Adaptive Cruise Control Vehicles Using a Comparison Analysis of Recent Algorithms,” in *2006 IEEE Intelligent Vehicles Symposium*, 2006, pp. 194–199.

[54] J. Piao and M. McDonald, “Advanced Driver Assistance Systems from Autonomous to Cooperative Approach,” *Transport Reviews*, vol. 28, no. 5, pp. 659–684, Sep. 2008.

[55] S. Kannan, A. Thangavelu, and R. Kalivaradhan, “An Intelligent Driver Assistance System (I-DAS) for Vehicle Safety Modelling using Ontology Approach,” *International Journal of UbiComp*, vol. 1, no. 3, pp. 15–29, Jul. 2010.

[56] A. Alam, A. Gattami, K. H. Johansson, and C. J. Tomlin, “Guaranteeing safety for heavy duty vehicle platooning: Safe set computations and experimental evaluations,” *Control Engineering Practice*, vol. 24, pp. 33–41, Mar. 2014.

[57] L. Evans, “Driver injury and fatality risk in two-car crashes versus mass ratio inferred using Newtonian mechanics,” *Accident Analysis & Prevention*, vol. 26, no. 5, pp. 609–616, Oct. 1994.

[58] C. Sunnevång, E. Rosén, O. Boström, and U. Lechelt, “Thoracic Injury Risk as a Function of Crash Severity – Car-to-car Side Impact Tests with WorldSID Compared to Real-life Crashes,” *Annals of Advances in Automotive Medicine*, vol. 54, pp. 159–168, Jan. 2010.

[59] S. G. Shelby, “Delta-V as a measure of traffic conflict severity,” in *Transportation Research Board 90th Annual Meeting*, 2011.

[60] C. Jurewicza, A. Sobhania, J. Woolleyb, J. Dutschkeb, and B. Corbenc, "Proposed vehicle impact speed: Severe injury probability relationships for selected crash types," 2015.

[61] G. Y. Martin, *The crash pulse in rear-end car accidents*. Göteborg, Sweden: Chalmers University of Technology, 2002.

[62] TASS TNO, "MADYMO/Exchange 7.1 Superuser Manual." 2009.

[63] L. L. Hershman, "The US new car assessment program (NCAP): Past, present and future," in *International Technical Conference on the Enhanced Safety of Vehicles*, 2001.

[64] D. Bose and J. R. Crandall, "Influence of active muscle contribution on the injury response of restrained car occupants," *Annals of Advances in Automotive Medicine*, vol. 52, pp. 61–72, 2008.

[65] AAAM, *Abbreviated Injury Scale (AIS) 2005 Manual*, 1 edition. Association for the Advancement of Automotive Medicine, 2005.

[66] R. Eppinger *et al.*, "Development of improved injury criteria for the assessment of advanced automotive restraint systems–II," *National Highway Traffic Safety Administration*, pp. 1–70, 1999.

[67] A. C. Kuchar, "A Systems Modeling Methodology for Estimation of Harm in the Automotive Crash Environment," presented at the 17th International Technical Conference on the Enhanced Safety of Vehicles, 2001.

[68] K. Maika, M. Yusuke, P. Jonas, and U. Sadayuki, "Development of Occupant Injury Prediction Algorithms for Advanced Automatic Collision Notification by Numerical

Crash Reconstructions," presented at the 3rd International Technical Conference on the Enhanced Safety of Vehicles, Seoul, Korea, 2013.

[69] K.-U. Schmitt, P. F. Niederer, M. H. Muser, and F. Walz, *Trauma Biomechanics: Accidental injury in traffic and sports*. Springer Science & Business Media, 2009.

[70] C. Bastien, "The Prediction of Kinematics and Injury Criteria of Unbelted Occupants under Autonomous Emergency Braking," p. 401.

[71] M. de Jager, A. Sauren, J. Thunnissen, and J. Wismans, "A Three-Dimensional Head-Neck Model: Validation for Frontal and Lateral Impacts," *SAE Transactions*, vol. 103, pp. 1660–1676, 1994.

[72] A. Kullgren, L. Eriksson, O. Boström, and M. Krafft, "Validation of Neck Injury Criteria using Reconstructed Real-life Rear-end Crashes with Recorded Crash Pulses," p. 14.

[73] R. Happee, M. Rekveldt, and F. Schoenmakers, "Advanced airbag modelling for side airbags and OOP using MADYMO," presented at the VDI BERICHTE, 2003.

[74] N. Praxl, M. Schönpflug, and J. Adamec, "Simulation of Occupant Kinematics in Vehicle Rollover - Dummy Model versus Human Model," p. 8.

[75] B. R. Deshpande, T. J. Gunasekar, V. Gupta, S. Jayaraman, and S. M. Summers, "Development of MADYMO Models of Passenger Vehicles for Simulating Side Impact Crashes," presented at the Future Transportation Technology Conference & Exposition, 1999.

[76] T. Adam and C. D. Untaroiu, “Identification of occupant posture using a Bayesian classification methodology to reduce the risk of injury in a collision,” *Transportation Research Part C: Emerging Technologies*, vol. 19, no. 6, pp. 1078–1094, Dec. 2011.

[77] D. Bose, J. R. Crandall, G. McGwin, J. Goldman, J. Foster, and P. R. Fine, “Computational methodology to predict injury risk for motor vehicle crash victims: A framework for improving Advanced Automatic Crash Notification systems,” *Transportation Research Part C: Emerging Technologies*, vol. 19, no. 6, pp. 1048–1059, Dec. 2011.

[78] X. Luo, W. Du, and J. Zhang, “Safety benefits of motorized seat belt as a component in ADAS in front-end collisions,” in *17th International IEEE Conference on Intelligent Transportation Systems (ITSC)*, 2014, pp. 661–666.

[79] H. HAMDANE, “Improvement of Pedestrian Safety: Response of detection systems to real accident scenarios,” Theses, Aix Marseille Université ; University of Adelaide, 2016.

[80] J. Moon, I. Bae, and S. Kim, “A pre-crash safety system for an occupant sitting on a backward facing seat for fully automated vehicles in frontal crashes,” in *2017 IEEE International Conference on Vehicular Electronics and Safety (ICVES)*, 2017, pp. 168–171.

[81] M. Klotz and H. Rohling, “24 GHz radar sensors for automotive applications,” *Journal of Telecommunications and information Technology*, pp. 11–14, 2001.

[82] TASS TNO, “PreScan R7.2.0 Manual - A Simulation & Verification Environment for Intelligent Vehicle Systems.” 2015.

[83] A. Teixeira, D. Pérez, H. Sandberg, and K. H. Johansson, "Attack Models and Scenarios for Networked Control Systems," in *Proceedings of the 1st International Conference on High Confidence Networked Systems*, New York, NY, USA, 2012, pp. 55–64.

[84] C. Flack and M. J. Atallah, "Better Logging through Formality," in *Recent Advances in Intrusion Detection*, 2000, pp. 1–16.

[85] K. P. Heaslip, K. B. Kelarestaghi, and M. Foruhandeh, *Transportation Cyber-Physical Security: Things We Should Know*. 2018.

[86] "The New Car Assessment Program Suggested Approaches for Future Program Enhancements," US DOT NHTSA, DOT HS 810 698, Jan. 2007.

[87] L. Guvenc *et al.*, "Cooperative Adaptive Cruise Control Implementation of Team Mekar at the Grand Cooperative Driving Challenge," *IEEE Transactions on Intelligent Transportation Systems*, vol. 13, no. 3, pp. 1062–1074, Sep. 2012.

[88] B. van Arem, C. J. G. van Driel, and R. Visser, "The Impact of Cooperative Adaptive Cruise Control on Traffic-Flow Characteristics," *IEEE Transactions on Intelligent Transportation Systems*, vol. 7, no. 4, pp. 429–436, Dec. 2006.

[89] J. Ploeg, A. F. A. Serrarens, and G. J. Heijenk, "Connect & Drive: design and evaluation of cooperative adaptive cruise control for congestion reduction," *Journal of Modern Transportation*, vol. 19, no. 3, pp. 207–213, Sep. 2011.

[90] L. Cui, J. Hu, P. Byungkyu, and B. Pavle, "Development of a Simulation Platform for Safety Impact Analysis Considering Vehicle Dynamics, Sensor Errors, and Communication Latencies: Assessing Cooperative Adaptive Cruise Control under

Cyber Attack," *Accepted by Transportation Research Part C: Emerging Technologies*, 2018.

[91] Y. Lian, Y. Zhao, L. Hu, and Y. Tian, "Longitudinal Collision Avoidance Control of Electric Vehicles Based on a New Safety Distance Model and Constrained-Regenerative-Braking-Strength-Continuity Braking Force Distribution Strategy," *IEEE Transactions on Vehicular Technology*, vol. 65, no. 6, pp. 4079–4094, Jun. 2016.

[92] S. Moon, I. Moon, and K. Yi, "Design, tuning, and evaluation of a full-range adaptive cruise control system with collision avoidance," *Control Engineering Practice*, vol. 17, no. 4, pp. 442–455, Apr. 2009.

[93] R. J. P. de Castro, "Motion control and energy management of electric vehicles," Ph.D. dissertation, Faculdade de Engenharia da Universidade do Port, Porto, Portugal, 2013.

[94] R. W. Rothery, "Car following models," *Trac Flow Theory*, 1992.

[95] C. Satzger and R. de Castro, "Predictive Brake Control for Electric Vehicles," *IEEE Transactions on Vehicular Technology*, pp. 1–1, 2017.

[96] A. Geiger *et al.*, "Team AnnieWAY's Entry to the 2011 Grand Cooperative Driving Challenge," *IEEE Transactions on Intelligent Transportation Systems*, vol. 13, no. 3, pp. 1008–1017, Sep. 2012.

[97] J. Ploeg, D. P. Shukla, N. van de Wouw, and H. Nijmeijer, "Controller Synthesis for String Stability of Vehicle Platoons," *IEEE Transactions on Intelligent Transportation Systems*, vol. 15, no. 2, pp. 854–865, Apr. 2014.

[98] J. I. Ge and G. Orosz, “Dynamics of connected vehicle systems with delayed acceleration feedback,” *Transportation Research Part C: Emerging Technologies*, vol. 46, pp. 46–64, Sep. 2014.

[99] P. Bujanovic, T. Lochrane, J. Hu, T. Bujanovic, and C. M. Walton, “Cooperative Adaptive Cruise Control Algorithm with Priority Weights Assigned to Downstream Vehicles for Increased Safety,” presented at the Transportation Research Board 97th Annual Meeting, 2018.

[100] R. Rajamani, *Vehicle Dynamics and Control*, 2nd ed. Springer US, 2012.

[101] V. Milanés, S. E. Shladover, and J. Spring, “Cooperative Adaptive Cruise Control in Real Traffic Situations,” *IEEE Transaction on intelligent transport systems*, vol. 15, no. 1, pp. 296–305, 2013.

[102] M. Barth, S. Mandava, K. Boriboonsomsin, and H. Xia, “Dynamic ECO-driving for arterial corridors,” in *Integrated and Sustainable Transportation System (FISTS), 2011 IEEE Forum on*, 2011, pp. 182–188.

[103] M. V. Ala, H. Yang, and H. Rakha, “Modeling Evaluation of Eco–Cooperative Adaptive Cruise Control in Vicinity of Signalized Intersections,” *Transportation Research Record: Journal of the Transportation Research Board*, vol. 2559, pp. 108–119, Jan. 2016.

[104] R. P. Roess and E. S. Prassas, “Analysis of Weaving Segments,” in *The Highway Capacity Manual: A Conceptual and Research History: Volume 1: Uninterrupted Flow*, R. . P. Roess and E. . S. Prassas, Eds. Cham: Springer International Publishing, 2014, pp. 249–338.

[105] X.-Y. Lu, X. Kan, S. E. Shladover, D. Wei, and R. A. Ferlis, “An Enhanced Microscopic Traffic Simulation Model for Application to Connected Automated Vehicles,” presented at the Transportation Research Board 96th Annual Meeting, Washington, DC, p. 21.

[106] B. Van Arem, C. M. Tampere, and K. M. Malone, “Modelling traffic flows with intelligent cars and intelligent roads,” in *Intelligent Vehicles Symposium, 2003. Proceedings. IEEE*, 2003, pp. 456–461.

[107] “Simulink - Simulation and Model-Based Design.” [Online]. Available: https://www.mathworks.com/products/simulink.html. [Accessed: 08-Jul-2018].

[108] “The TCP/IP Guide - The TCP/IP Guide.” [Online]. Available: http://www.tcpipguide.com/free/. [Accessed: 08-Jul-2018].

[109] L. Cui, J. Hu, A. Wang, and B. B. Park, “Robust CACC Development Against Unexpected Cyber and Physical Interference,” *unpublished*.

[110] R. Wiedemann, “Simulation of the series of publications of the institute for Transportation,” *University of Karlsruhe*, vol. no. 8, 1974.

[111] F. G. Habtemichael and L. de P. Santos, “Sensitivity Analysis of VISSIM Driver Behavior Parameters on Safety of Simulated Vehicles and Their Interaction with Operations of Simulated Traffic,” presented at the 92nd Annual Meeting of the Transportation Research Board, Washington DC, 2012, p. 18.

[112] B. Park and H. Qi, “Development and Evaluation of a Procedure for the Calibration of Simulation Models.pdf,” *Transportation Research Record: Journal of the Transportation Research Board*, vol. 1934, pp. 208–217, 2005.

[113] K. I. Ahmed, “Modeling Drivers’ Acceleration and Lane Changing Behavior,” Doctor of Philosophy, Massachusetts Institute of Technology, 1999.

[114] M. Fellendorf and P. Vortisch, “Microscopic Traffic Flow Simulator VISSIM,” in *Fundamentals of Traffic Simulation*, vol. 145, J. Barceló, Ed. New York, NY: Springer New York, 2010, pp. 63–93.

[115] H. A. Rakha, K. Ahn, K. Moran, B. Saerens, and E. V. den Bulck, “Virginia Tech Comprehensive Power-Based Fuel Consumption Model: Model development and testing,” *Transportation Research Part D: Transport and Environment*, vol. 16, no. 7, pp. 492–503, Oct. 2011.

[116] A. Kesting, M. Treiber, and D. Helbing, “Enhanced intelligent driver model to access the impact of driving strategies on traffic capacity,” *Philosophical Transactions of the Royal Society of London A: Mathematical, Physical and Engineering Sciences*, vol. 368, no. 1928, pp. 4585–4605, Oct. 2010.

[117] P. G. Gipps, “A behavioural car-following model for computer simulation,” *Transportation Research Part B: Methodological*, vol. 15, no. 2, pp. 105–111, Apr. 1981.

[118] M. Treiber and A. Kesting, *Traffic Flow Dynamics: Data, Models and Simulation*, 2013 edition. Heidelberg ; New York: Springer, 2012.

[119] “Analysis of Freeway Weaving Sections,” NCHRP 3-75 Final Report, Jan. 2008.

[120] C. Nowakowski, J. O’Connell, S. E. Shladover, and D. Cody, “Cooperative Adaptive Cruise Control: Driver Acceptance of Following Gap Settings Less than One Second,” *th ANNUAL MEETING*, p. 5, 2010.

[121] M. Amoozadeh, H. Deng, C.-N. Chuah, H. M. Zhang, and D. Ghosal, “Platoon management with cooperative adaptive cruise control enabled by VANET,” *Vehicular Communications*, vol. 2, no. 2, pp. 110–123, Apr. 2015.

[122] T. Robinson and E. Coelingh, “Operating Platoons On Public Motorways: An Introduction To The SARTRE Platooning Programme,” p. 12.

[123] H. Peng *et al.*, “Performance Analysis of IEEE 802.11 p DCF for Multiplatooning Communications with Autonomous Vehicles,” *IEEE Transactions on Vehicular Technology*, 2016.

[124] VDOT, “VDOT Governance Document Traffic Operations and Safety Analysis Manual (TOSAM).” Nov-2015.

[125] T. R. B. Publications, *Highway Capacity Manual: HCM 2010*, 5th edition. Transportation Research Board, 2010.

[126] N. J. Garber and L. A. Hoel, *Traffic and Highway Engineering*, 5 edition. Stamford, CT, USA: Cengage Learning, 2014.

[127] T. H. Wonnacott and R. J. Wonnacott, *Introductory Statistics, 5th Edition*, 5 edition. New York: Wiley, 1990.

[128] D. Gettman, L. Pu, T. Sayed, and S. G. Shelby, “Surrogate safety assessment model and validation: Final report,” 2008.

Appendix A Flow rate and average speed of weaving segment

Table A.1 Platoon size of 8-CAV with low traffic volume

60 km/h

MPR = 0%	Starting point		Middle point		Ending point		Number of cut-in
Input: 1100 veh/h/lane	Flow rate (veh/h)	Speed (km/h)	Flow rate (veh/h)	Speed (km/h)	Flow rate (veh/h)	Speed (km/h)	
Lane1	1126	61.5	962	61.8	982	61.3	
Lane2	1056	61.5	1217	61.0	1214	60.4	
Auxiliary	480	62.2	463	62.0	444	61.9	
MPR = 33%	Desired gap = 0.6s, distance gap = 10.0m						0.0
Lane1	1049	60.9	950	61.2	1066	58.0	
Lane2	1121	60.7	1375	60.9	1354	58.3	
Auxiliary	514	62.9	367	62.0	329	54.4	
MPR = 67%	Desired gap = 0.6s, distance gap = 10.0m						0.8
Lane1	1022	60.3	924	60.3	905	58.6	
Lane2	1198	60.3	1351	60.4	1358	59.0	
Auxiliary	516	63.0	485	62.0	506	51.3	
MPR = 33%	Desired gap = 0.9s, distance gap = 15.0m						3.4
Lane1	1010	60.9	847	61.2	917	58.5	
Lane2	1217	60.8	1291	60.5	1291	58.7	
Auxiliary	494	62.6	576	62.2	552	57.8	
MPR = 67%	Desired gap = 0.9s, distance gap = 15.0m						3.4
Lane1	1046	60.4	960	60.4	960	59.8	
Lane2	1188	60.3	1334	60.1	1394	58.7	

Auxiliary	540	62.7	516	62.4	514	46.0	
MPR = 33%	Desired gap = 1.2s, distance gap = 20.0m						8.0
Lane1	1018	61.0	946	61.2	1018	59.6	
Lane2	1111	60.8	1373	60.2	1390	59.4	
Auxiliary	494	62.8	326	61.2	269	61.2	
MPR = 67%	Desired gap = 1.2s, distance gap = 20.0m						15.6
Lane1	972	60.2	907	60.2	934	60.2	
Lane2	1157	60.3	1325	59.1	1284	58.8	
Auxiliary	482	62.9	430	62.5	466	59.2	

80 km/h

MPR = 0	Starting point		Middle point		Ending point		Number of cut-in
Input: 1100 veh/h/lane	Flow rate (veh/h)	Speed (km/h)	Flow rate (veh/h)	Speed (km/h)	Flow rate (veh/h)	Speed (km/h)	
Lane1	1022	84.0	862	84.6	919	84.2	
Lane2	1092	85.2	1238	84.2	1174	83.0	
Auxiliary	509	83.5	516	85.2	509	84.6	
MPR = 33%	Desired gap = 0.6s, distance gap = 13.3m						0.8
Lane1	1171	83.0	1010	83.0	974	73.8	
Lane2	1145	82.9	1258	82.8	1258	76.8	
Auxiliary	468	84.4	523	84.3	526	66.9	
MPR = 67%	Desired gap = 0.6s, distance gap = 13.3m						1.6
Lane1	1003	81.0	943	80.7	974	74.2	
Lane2	1190	81.5	1337	81.6	1363	78.0	
Auxiliary	499	84.0	454	85.5	430	63.0	
MPR = 33%	Desired gap = 0.9s, distance gap = 20.0m						5.6

Lane1	1109	82.7	919	82.8	1013	78.6	
Lane2	1159	82.9	1332	82.2	1270	76.9	
Auxiliary	506	83.9	526	85.4	530	75.0	
MPR = 67%	Desired gap = 0.9s, distance gap = 20.0m						3.4
Lane1	1046	80.7	967	80.4	1006	74.4	
Lane2	1142	80.7	1308	81.1	1258	77.8	
Auxiliary	540	84.2	446	84.0	490	62.2	
MPR = 33%	Desired gap = 1.2s, distance gap = 26.7m						9.8
Lane1	1164	82.2	1027	83.3	982	83.5	
Lane2	1159	82.7	1330	81.7	1286	81.1	
Auxiliary	487	83.5	478	84.8	492	84.0	
MPR = 67%	Desired gap = 1.2s, distance gap = 26.7m						13.0
Lane1	1075	80.9	929	80.4	953	80.4	
Lane2	1162	80.7	1294	79.9	1267	79.4	
Auxiliary	480	84.2	487	85.5	509	84.6	

100 km/h

MPR = 0	Starting point		Middle point		Ending point		Number of cut-in
Input: 1100 veh/h/lane	Flow rate (veh/h)	Speed (km/h)	Flow rate (veh/h)	Speed (km/h)	Flow rate (veh/h)	Speed (km/h)	
Lane1	1090	105.4	1015	105.4	1039	106.0	
Lane2	1102	105.9	1258	104.6	1193	104.3	
Auxiliary	523	95.1	468	106.5	499	104.4	
MPR = 33%	Desired gap = 0.6s, distance gap = 16.7m						2.2
Lane1	1022	104.5	871	104.1	967	94.4	
Lane2	1231	103.1	1291	102.6	1270	96.7	
Auxiliary	530	96.3	538	106.3	542	95.7	
MPR = 67%	Desired gap = 0.6s, distance gap = 16.7m						3.0

Lane1	1051	102.6	907	102.0	979	87.2	
Lane2	1193	102.1	1270	101.4	1303	93.3	
Auxiliary	482	93.8	569	105.1	552	83.2	
MPR = 33%	Desired gap = 0.9s, distance gap = 25.0m						7.0
Lane1	1042	104.4	943	104.3	1061	101.7	
Lane2	1128	102.8	1380	102.2	1344	98.5	
Auxiliary	542	95.7	372	105.2	358	97.6	
MPR = 67%	Desired gap = 0.9s, distance gap = 25.0m						12.6
Lane1	1114	101.6	910	100.8	938	95.4	
Lane2	1188	101.7	1337	100.6	1267	96.3	
Auxiliary	473	96.0	526	105.1	526	90.0	
MPR = 33%	Desired gap = 1.2s, distance gap = 33.3m						12.4
Lane1	1015	104.1	850	104.3	967	104.0	
Lane2	1159	103.0	1248	101.8	1253	101.3	
Auxiliary	509	94.5	547	105.3	535	104.7	
MPR = 67%	Desired gap = 1.2s, distance gap = 33.3m						22.8
Lane1	1049	101.8	900	101.1	974	100.7	
Lane2	1193	100.9	1313	98.6	1344	98.3	
Auxiliary	446	96.3	475	104.5	482	103.4	

Table A.2 Platoon size of 8-CAV with medium traffic volume

60 km/h

MPR = 0%	Starting point		Middle point		Ending point		Number of cut-in
Input: 1500 veh/h/lane	Flow rate (veh/h)	Speed (km/h)	Flow rate (veh/h)	Speed (km/h)	Flow rate (veh/h)	Speed (km/h)	
Lane1	1517	60.9	1390	61.2	1438	61.0	
Lane2	1478	60.9	1622	60.2	1577	59.8	
Auxiliary	521	62.1	485	62.5	475	60.8	
MPR = 33%	Desired gap = 0.6s, distance gap = 10.0m						1.6
Lane1	1490	60.6	1306	60.8	1351	57.4	

Lane2	1526	60.9	1639	60.2	1625	56.8	
Auxiliary	487	62.5	610	61.9	557	54.0	
MPR = 67%	Desired gap = 0.6s, distance gap = 10.0m						0.6
Lane1	1457	60.1	1342	60.1	1402	58.4	
Lane2	1639	60.2	1680	60.1	1661	58.4	
Auxiliary	504	62.6	533	62.0	514	48.5	
MPR = 33%	Desired gap = 0.9s, distance gap = 15.0m						5.0
Lane1	1447	60.5	1298	60.5	1368	56.8	
Lane2	1632	60.6	1685	60.0	1716	55.2	
Auxiliary	485	62.6	552	62.1	526	52.3	
MPR = 67%	Desired gap = 0.9s, distance gap = 15.0m						9.4
Lane1	1514	60.0	1366	59.6	1414	56.4	
Lane2	1522	60.0	1670	59.5	1663	57.5	
Auxiliary	526	62.4	528	61.4	554	51.2	
MPR = 33%	Desired gap = 1.2s, distance gap = 20.0m						10.0
Lane1	1548	60.4	1366	60.6	1478	60.3	
Lane2	1536	60.2	1685	59.3	1687	58.2	
Auxiliary	502	62.5	550	62.6	502	60.6	
MPR = 67%	Desired gap = 1.2s, distance gap = 20.0m						19.0
Lane1	1433	59.9	1313	59.9	1342	59.6	
Lane2	1591	59.8	1704	57.6	1644	56.9	
Auxiliary	506	62.6	499	61.6	550	58.4	

80 km/h

MPR = 0	Starting point		Middle point		Ending point		Number of cut-in
Input: 1500 veh/h/lane	Flow rate (veh/h)	Speed (km/h)	Flow rate (veh/h)	Speed (km/h)	Flow rate (veh/h)	Speed (km/h)	
Lane1	1478	83.7	1351	84.1	1385	83.0	
Lane2	1447	83.9	1606	83.0	1562	81.6	
Auxiliary	516	83.5	497	85.6	475	83.3	

MPR = 33%	Desired gap = 0.6s, distance gap = 13.3m						1.4
Lane1	1522	82.5	1454	82.5	1445	76.0	
Lane2	1522	82.6	1630	82.1	1646	76.8	
Auxiliary	473	83.8	494	85.5	514	71.3	
MPR = 67%	Desired gap = 0.6s, distance gap = 13.3m						3.4
Lane1	1493	79.7	1346	79.9	1394	69.5	
Lane2	1500	80.8	1630	81.0	1639	75.5	
Auxiliary	511	83.8	502	85.0	511	61.0	
MPR = 33%	Desired gap = 0.9s, distance gap = 20.0m						5.2
Lane1	1464	81.9	1327	81.8	1361	74.8	
Lane2	1574	82.0	1661	81.1	1733	74.7	
Auxiliary	518	83.6	559	84.7	554	66.9	
MPR = 67%	Desired gap = 0.9s, distance gap = 20.0m						15.6
Lane1	1406	80.8	1322	80.0	1397	77.4	
Lane2	1582	80.6	1733	79.9	1634	75.7	
Auxiliary	492	84.2	427	84.7	475	67.1	
MPR = 33%	Desired gap = 1.2s, distance gap = 26.7m						15.0
Lane1	1517	81.7	1392	81.9	1421	80.9	
Lane2	1562	82.1	1716	80.3	1750	78.8	
Auxiliary	523	83.0	511	84.3	461	82.8	
MPR = 67%	Desired gap = 1.2s, distance gap = 26.7m						18.6
Lane1	1483	80.6	1356	80.5	1361	80.2	
Lane2	1558	80.5	1596	79.0	1642	77.9	
Auxiliary	468	84.2	535	84.1	550	77.8	

100 km/h

MPR = 0	Starting point		Middle point		Ending point		Number of cut-in
Input: 1500 veh/h/lane	Flow rate (veh/h)	Speed (km/h)	Flow rate (veh/h)	Speed (km/h)	Flow rate (veh/h)	Speed (km/h)	
Lane1	1512	103.9	1414	104.6	1452	104.0	

Lane2	1507	103.9	1673	103.0	1589	102.0	
Auxiliary	552	95.0	504	104.9	523	101.3	
MPR = 33%	Desired gap = 0.6s, distance gap = 16.7m						3.2
Lane1	1466	103.5	1342	103.2	1430	89.9	
Lane2	1627	102.8	1699	102.3	1678	88.9	
Auxiliary	547	94.2	528	104.8	511	87.0	
MPR = 67%	Desired gap = 0.6s, distance gap = 16.7m						5.8
Lane1	1464	101.3	1258	100.7	1318	89.8	
Lane2	1565	102.2	1661	101.6	1656	92.3	
Auxiliary	506	95.4	674	104.7	646	77.2	
MPR = 33%	Desired gap = 0.9s, distance gap = 25.0m						13.2
Lane1	1488	102.7	1313	102.7	1366	97.7	
Lane2	1567	102.1	1668	100.3	1656	95.0	
Auxiliary	494	93.3	595	105.3	600	97.7	
MPR = 67%	Desired gap = 0.9s, distance gap = 25.0m						13.6
Lane1	1428	101.6	1260	101.1	1291	97.7	
Lane2	1558	101.7	1685	100.4	1632	96.4	
Auxiliary	509	97.1	583	104.7	550	85.3	
MPR = 33%	Desired gap = 1.2s, distance gap = 33.3m						19.0
Lane1	1445	103.1	1294	103.3	1421	102.6	
Lane2	1570	102.3	1634	100.4	1675	99.4	
Auxiliary	506	96.1	552	105.9	547	104.8	
MPR = 67%	Desired gap = 1.2s, distance gap = 33.3m						20.8
Lane1	1471	101.4	1368	101.3	1404	99.8	
Lane2	1574	101.4	1718	99.2	1745	97.0	
Auxiliary	473	95.1	530	103.5	480	98.5	

Table A.3 Platoon size of 8-CAV with high traffic volume

60 km/h

MPR = 0%	Starting point		Middle point		Ending point		Number of cut-in
Input: 1900 veh/h/lane	Flow rate (veh/h)	Speed (km/h)	Flow rate (veh/h)	Speed (km/h)	Flow rate (veh/h)	Speed (km/h)	
Lane1	1949	60.3	1754	60.4	1817	59.8	
Lane2	1894	60.8	1956	59.5	1961	58.1	
Auxiliary	466	62.4	626	62.3	576	59.2	
MPR = 33%	Desired gap = 0.6s, distance gap = 10.0m						3.2
Lane1	1795	59.8	1613	59.5	1706	53.6	
Lane2	1817	60.1	1867	59.1	1932	52.8	
Auxiliary	487	62.2	595	61.5	550	48.6	
MPR = 67%	Desired gap = 0.6s, distance gap = 10.0m						3.4
Lane1	1970	60.1	1858	60.1	1824	57.5	
Lane2	2004	59.9	2078	60.0	2107	56.8	
Auxiliary	504	62.8	542	62.0	516	44.1	
MPR = 33%	Desired gap = 0.9s, distance gap = 15.0m						5.2
Lane1	1860	60.0	1682	60.1	1730	58.1	
Lane2	1903	60.2	1999	58.7	1966	55.1	
Auxiliary	514	62.3	595	62.0	552	52.5	
MPR = 67%	Desired gap = 0.9s, distance gap = 15.0m						11.6
Lane1	1843	58.8	1656	59.0	1714	56.1	
Lane2	1865	59.4	2030	59.1	2011	55.1	
Auxiliary	511	62.3	511	61.3	530	49.4	
MPR = 33%	Desired gap = 1.2s, distance gap = 20.0m						16.8
Lane1	1865	60.0	1716	60.0	1800	60.1	
Lane2	1817	60.0	1949	57.9	1982	57.5	
Auxiliary	526	62.6	521	61.6	403	59.1	
MPR = 67%	Desired gap = 1.2s, distance gap = 20.0m						32.2
Lane1	1954	59.5	1838	59.6	1874	58.6	
Lane2	1949	59.4	2074	57.5	2040	55.8	
Auxiliary	461	62.1	458	61.0	458	56.0	

80 km/h

MPR = 0	Starting point		Middle point		Ending point		Number of cut-in
Input: 1900 veh/h/lane	Flow rate (veh/h)	Speed (km/h)	Flow rate (veh/h)	Speed (km/h)	Flow rate (veh/h)	Speed (km/h)	
Lane1	1834	80.9	1642	80.6	1627	78.4	
Lane2	1778	82.3	1918	77.6	1831	76.5	
Auxiliary	530	83.1	485	84.8	391	81.7	
MPR = 33%	Desired gap = 0.6s, distance gap = 13.3m						4.0
Lane1	1949	81.4	1812	80.9	1906	72.4	
Lane2	2002	81.8	2093	80.5	2093	71.7	
Auxiliary	535	83.6	569	85.3	540	71.3	
MPR = 67%	Desired gap = 0.6s, distance gap = 13.3m						6.8
Lane1	1822	80.3	1716	79.9	1762	75.2	
Lane2	1807	80.5	1973	80.2	1990	73.2	
Auxiliary	574	83.2	502	84.1	523	54.8	
MPR = 33%	Desired gap = 0.9s, distance gap = 20.0m						8.8
Lane1	1841	81.2	1757	80.5	1812	65.0	
Lane2	2052	81.6	2105	78.5	2112	65.8	
Auxiliary	494	83.2	583	84.3	545	63.9	
MPR = 67%	Desired gap = 0.9s, distance gap = 20.0m						21.2
Lane1	1932	79.7	1807	79.5	1870	76.8	
Lane2	1918	78.5	2016	77.2	1994	71.8	
Auxiliary	487	83.6	509	84.2	482	58.9	
MPR = 33%	Desired gap = 1.2s, distance gap = 26.7m						20.6
Lane1	1934	80.7	1798	80.9	1872	79.4	
Lane2	1961	81.4	2076	78.1	2102	76.3	
Auxiliary	506	83.3	545	85.2	480	80.3	
MPR = 67%	Desired gap = 1.2s, distance gap = 26.7m						32.6
Lane1	1845	80.4	1662	79.8	1689	77.5	

Lane2	1791	79.9	1887	77.0	1905	74.4	
Auxiliary	486	84.1	615	84.2	591	80.5	

100 km/h

MPR = 0	Starting point		Middle point		Ending point		Number of cut-in
Input: 1900 veh/h/lane	Flow rate (veh/h)	Speed (km/h)	Flow rate (veh/h)	Speed (km/h)	Flow rate (veh/h)	Speed (km/h)	
Lane1	1937	100.4	1810	99.6	1910	94.0	
Lane2	1958	101.4	2062	95.9	1879	89.6	
Auxiliary	468	95.1	497	103.9	480	92.7	
MPR = 33%	Desired gap = 0.6s, distance gap = 16.7m						12.8
Lane1	1978	102.0	1877	98.7	1908	75.9	
Lane2	1956	101.4	2086	96.3	2105	75.7	
Auxiliary	499	94.8	514	103.7	506	72.3	
MPR = 67%	Desired gap = 0.6s, distance gap = 16.7m						9.6
Lane1	1798	101.1	1704	99.5	1776	87.1	
Lane2	1930	101.9	1997	100.5	1990	87.9	
Auxiliary	504	94.7	526	104.0	482	72.9	
MPR = 33%	Desired gap = 0.9s, distance gap = 25.0m						12.8
Lane1	1900	101.5	1733	99.7	1853	85.5	
Lane2	1949	101.7	2095	98.4	2050	83.4	
Auxiliary	504	97.9	593	104.0	564	85.9	
MPR = 67%	Desired gap = 0.9s, distance gap = 25.0m						23.2
Lane1	1932	101.5	1764	98.4	1889	88.9	
Lane2	1975	101.2	2052	97.3	2006	87.0	
Auxiliary	490	93.6	528	103.9	497	87.6	
MPR = 33%	Desired gap = 1.2s, distance gap = 33.3m						20.8
Lane1	1795	101.6	1675	101.5	1716	100.3	
Lane2	1882	101.1	1900	99.3	1877	97.0	
Auxiliary	490	94.6	574	103.0	528	100.3	

MPR = 67%	Desired gap = 1.2s, distance gap = 33.3m						31.4
Lane1	1932	101.1	1819	101.0	1848	100.6	
Lane2	1934	101.2	2098	98.7	2119	96.5	
Auxiliary	523	97.1	473	104.2	454	100.4	

Table A.4 Platoon size of 4-CAV with high traffic volume

60 km/h

MPR = 0%	Starting point		Middle point		Ending point		Number of cut-in
Input: 1900 veh/h/lane	Flow rate (veh/h)	Speed (km/h)	Flow rate (veh/h)	Speed (km/h)	Flow rate (veh/h)	Speed (km/h)	
Lane1	1949	60.3	1754	60.4	1817	59.8	
Lane2	1894	60.8	1956	59.5	1961	58.1	
Auxiliary	466	62.4	626	62.3	576	59.2	
MPR = 33%	Desired gap = 0.6s, distance gap = 10.0m						1.0
Lane1	1944	60.1	1810	60.2	1841	59.1	
Lane2	1915	60.2	1982	59.1	2002	56.9	
Auxiliary	475	62.2	559	62.0	502	54.7	
MPR = 67%	Desired gap = 0.6s, distance gap = 10.0m						7.2
Lane1	1802	59.5	1673	59.3	1721	54.6	
Lane2	1812	59.3	2035	59.0	1999	51.6	
Auxiliary	478	62.1	408	61.6	372	45.9	
MPR = 33%	Desired gap = 0.9s, distance gap = 15.0m						7.6
Lane1	1819	58.9	1740	59.6	1800	57.8	
Lane2	1800	59.9	1900	59.3	1898	56.6	
Auxiliary	466	62.2	422	61.8	367	55.6	
MPR = 67%	Desired gap = 0.9s, distance gap = 15.0m						16.2
Lane1	1894	59.4	1814	59.2	1850	55.6	
Lane2	1872	57.3	2011	56.8	1968	52.4	
Auxiliary	494	62.9	470	60.8	434	41.7	
MPR = 33%	Desired gap = 1.2s, distance gap = 20.0m						12.4

Lane1	1903	59.9	1790	59.9	1795	59.6	
Lane2	1889	59.8	2057	58.6	2004	57.7	
Auxiliary	509	62.9	463	62.8	473	56.8	
MPR = 67%	Desired gap = 1.2s, distance gap = 20.0m						24.2
Lane1	1790	59.5	1728	59.5	1670	59.3	
Lane2	1776	58.9	1910	57.4	1908	56.5	
Auxiliary	492	62.2	413	61.7	338	54.6	

80 km/h

MPR = 0	Starting point		Middle point		Ending point		Number of cut-in
Input: 1900 veh/h/lane	Flow rate (veh/h)	Speed (km/h)	Flow rate (veh/h)	Speed (km/h)	Flow rate (veh/h)	Speed (km/h)	
Lane1	1834	80.9	1642	80.6	1627	78.4	
Lane2	1778	82.3	1918	77.6	1831	76.5	
Auxiliary	530	83.1	485	84.8	391	81.7	
MPR = 33%	Desired gap = 0.6s, distance gap = 13.3m						5.0
Lane1	1858	81.4	1769	81.7	1793	74.0	
Lane2	1838	81.6	1968	80.9	1992	72.7	
Auxiliary	516	83.8	437	84.8	338	70.7	
MPR = 67%	Desired gap = 0.6s, distance gap = 13.3m						9.6
Lane1	1906	80.2	1834	79.7	1872	70.0	
Lane2	1997	80.5	2102	79.3	2153	69.3	
Auxiliary	557	84.2	518	83.8	518	58.8	
MPR = 33%	Desired gap = 0.9s, distance gap = 20.0m						7.0
Lane1	2009	81.2	1850	81.2	1906	74.0	
Lane2	1958	81.6	2021	79.9	2038	73.0	
Auxiliary	468	84.4	559	85.0	521	74.2	
MPR = 67%	Desired gap = 0.9s, distance gap = 20.0m						28.4
Lane1	1937	78.5	1853	77.6	1822	74.9	
Lane2	1860	77.2	2021	74.7	2040	67.4	

Auxiliary	526	82.7	470	82.6	475	57.6	
MPR = 33%	Desired gap = 1.2s, distance gap = 26.7m						17.4
Lane1	1937	81.4	1759	81.5	1810	80.4	
Lane2	1946	81.8	2062	79.9	2114	77.8	
Auxiliary	499	83.4	619	85.8	595	84.0	
MPR = 67%	Desired gap = 1.2s, distance gap = 26.7m						23.6
Lane1	1888	78.5	1776	78.4	1836	78.0	
Lane2	1876	78.0	1960	76.0	1984	75.7	
Auxiliary	492	83.8	524	84.4	464	81.1	

100 km/h

MPR = 0	Starting point		Middle point		Ending point		Number of cut-in
Input: 1900 veh/h/lane	Flow rate (veh/h)	Speed (km/h)	Flow rate (veh/h)	Speed (km/h)	Flow rate (veh/h)	Speed (km/h)	
Lane1	1937	100.4	1810	99.6	1910	94.0	
Lane2	1958	101.4	2062	95.9	1879	89.6	
Auxiliary	468	95.1	497	103.9	480	92.7	
MPR = 33%	Desired gap = 0.6s, distance gap = 16.7m						10.4
Lane1	1927	101.6	1793	101.4	1865	84.5	
Lane2	1889	101.4	1990	99.8	1954	85.2	
Auxiliary	475	95.5	499	103.9	468	92.2	
MPR = 67%	Desired gap = 0.6s, distance gap = 16.7m						16.4
Lane1	1978	101.7	1836	100.8	1814	78.0	
Lane2	1949	101.3	1978	100.4	1932	80.0	
Auxiliary	509	92.7	590	104.0	509	71.4	
MPR = 33%	Desired gap = 0.9s, distance gap = 25.0m						11.2
Lane1	1961	102.3	1882	101.7	1934	90.6	
Lane2	1968	101.9	2064	100.2	2141	88.6	
Auxiliary	497	94.8	547	105.2	497	93.8	
MPR = 67%	Desired gap = 0.9s, distance gap = 25.0m						26.6

Lane1	1922	97.9	1805	97.1	1822	89.1	
Lane2	1937	96.4	2059	92.2	1975	82.1	
Auxiliary	521	95.1	482	100.3	454	80.6	
MPR = 33%	Desired gap = 1.2s, distance gap = 33.3m						20.8
Lane1	1826	101.5	1682	101.4	1718	99.3	
Lane2	1898	101.6	1949	99.2	1980	96.9	
Auxiliary	468	95.2	521	104.8	490	102.5	
MPR = 67%	Desired gap = 1.2s, distance gap = 33.3m						27.6
Lane1	1925	99.4	1807	97.2	1860	95.1	
Lane2	1891	95.8	2014	93.4	1994	89.5	
Auxiliary	542	95.7	540	99.5	530	98.3	

Table A.5 Platoon size of 12-CAV with high traffic volume

60 km/h

MPR = 0%	Starting point		Middle point		Ending point		Number of cut-in
Input: 1900 veh/h/lane	Flow rate (veh/h)	Speed (km/h)	Flow rate (veh/h)	Speed (km/h)	Flow rate (veh/h)	Speed (km/h)	
Lane1	1949	60.3	1754	60.4	1817	59.8	
Lane2	1894	60.8	1956	59.5	1961	58.1	
Auxiliary	466	62.4	626	62.3	576	59.2	
MPR = 33%	Desired gap = 0.6s, distance gap = 10.0m						2.4
Lane1	1781	60.0	1690	57.2	1620	52.6	
Lane2	1745	60.4	1942	57.3	1944	50.8	
Auxiliary	545	62.4	398	61.1	324	46.6	
MPR = 67%	Desired gap = 0.6s, distance gap = 10.0m						19.2
Lane1	1853	59.8	1769	59.3	1754	56.7	
Lane2	1982	59.9	2023	58.9	2026	54.4	
Auxiliary	499	62.4	559	61.2	557	47.4	
MPR = 33%	Desired gap = 0.9s, distance gap = 15.0m						11.2
Lane1	1802	60.0	1709	60.3	1764	60.0	

Lane2	1692	60.3	2002	59.0	1966	58.2	
Auxiliary	636	61.8	398	61.7	382	59.9	
MPR = 67%	Desired gap = 0.9s, distance gap = 15.0m						29.4
Lane1	1898	59.5	1766	59.2	1750	58.9	
Lane2	1925	59.0	2038	56.6	2066	55.9	
Auxiliary	470	61.9	490	60.5	480	57.4	
MPR = 33%	Desired gap = 1.2s, distance gap = 20.0m						26.2
Lane1	1884	59.8	1783	59.2	1834	58.6	
Lane2	1896	59.8	2023	56.4	1985	57.4	
Auxiliary	598	61.8	530	61.8	468	59.6	
MPR = 67%	Desired gap = 1.2s, distance gap = 20.0m						40.4
Lane1	1884	59.7	1690	59.9	1637	59.4	
Lane2	1894	58.9	1975	57.2	1956	56.6	
Auxiliary	485	62.1	538	61.1	485	59.2	

80 km/h

MPR = 0	Starting point		Middle point		Ending point		Number of cut-in
Input: 1900 veh/h/lane	Flow rate (veh/h)	Speed (km/h)	Flow rate (veh/h)	Speed (km/h)	Flow rate (veh/h)	Speed (km/h)	
Lane1	1834	80.9	1642	80.6	1627	78.4	
Lane2	1778	82.3	1918	77.6	1831	76.5	
Auxiliary	530	83.1	485	84.8	391	81.7	
MPR = 33%	Desired gap = 0.6s, distance gap = 13.3m						4.2
Lane1	1740	81.5	1486	79.7	1483	68.0	
Lane2	1694	81.8	1858	79.9	1798	69.2	
Auxiliary	523	83.6	629	84.6	614	70.1	
MPR = 67%	Desired gap = 0.6s, distance gap = 13.3m						13.4
Lane1	1860	80.4	1685	76.8	1697	65.9	
Lane2	1949	80.5	2009	78.0	2042	66.7	
Auxiliary	499	83.7	578	83.8	506	59.8	

MPR = 33%	Desired gap = 0.9s, distance gap = 20.0m						12.4
Lane1	1982	81.7	1807	81.5	1855	78.2	
Lane2	1942	81.9	2074	79.6	2052	76.1	
Auxiliary	552	83.6	562	85.9	516	77.3	
MPR = 67%	Desired gap = 0.9s, distance gap = 20.0m						30.2
Lane1	1951	79.4	1872	75.5	1900	69.9	
Lane2	1956	79.8	2129	77.3	2045	72.0	
Auxiliary	511	84.3	418	83.2	406	68.7	
MPR = 33%	Desired gap = 1.2s, distance gap = 26.7m						20.0
Lane1	1838	81.4	1714	81.5	1788	79.2	
Lane2	1901	81.8	2064	79.2	2052	77.4	
Auxiliary	533	83.7	554	84.6	533	81.9	
MPR = 67%	Desired gap = 1.2s, distance gap = 26.7m						42.0
Lane1	1932	77.9	1761	78.3	1797	78.0	
Lane2	1995	79.2	2130	77.7	2097	76.3	
Auxiliary	489	84.2	519	84.2	486	78.7	

100 km/h

MPR = 0	Starting point		Middle point		Ending point		Number of cut-in
Input: 1900 veh/h/lane	Flow rate (veh/h)	Speed (km/h)	Flow rate (veh/h)	Speed (km/h)	Flow rate (veh/h)	Speed (km/h)	
Lane1	1937	100.4	1810	99.6	1910	94.0	
Lane2	1958	101.4	2062	95.9	1879	89.6	
Auxiliary	468	95.1	497	103.9	480	92.7	
MPR = 33%	Desired gap = 0.6s, distance gap = 16.7m						13.2
Lane1	1896	101.7	1817	97.3	1798	81.4	
Lane2	1834	102.1	1908	97.3	1891	81.9	
Auxiliary	569	95.7	605	103.7	566	81.9	
MPR = 67%	Desired gap = 0.6s, distance gap = 16.7m						15.0
Lane1	1826	100.8	1682	99.0	1726	90.6	

Lane2	1848	101.5	2006	100.0	1934	93.4	
Auxiliary	523	97.9	454	104.3	434	82.6	
MPR = 33%	Desired gap = 0.9s, distance gap = 25.0m						17.4
Lane1	1982	101.6	1858	99.7	1774	89.9	
Lane2	1968	101.5	2016	99.2	2023	89.9	
Auxiliary	533	99.7	614	104.8	557	94.2	
MPR = 67%	Desired gap = 0.9s, distance gap = 25.0m						31.8
Lane1	1771	101.0	1661	98.0	1678	89.8	
Lane2	1822	100.2	1934	96.8	1894	89.3	
Auxiliary	506	96.9	449	102.2	406	85.9	
MPR = 33%	Desired gap = 1.2s, distance gap = 33.3m						29.8
Lane1	1870	100.3	1735	100.3	1757	99.0	
Lane2	1769	100.4	1908	97.0	1879	94.6	
Auxiliary	578	97.0	571	102.8	530	99.9	
MPR = 67%	Desired gap = 1.2s, distance gap = 33.3m						38.2
Lane1	1915	100.2	1793	98.5	1841	94.8	
Lane2	1937	99.2	2071	95.5	2016	90.5	
Auxiliary	523	96.4	552	102.6	516	99.7	